ATP Citrate Lyase and mitochondrial membrane potential regulate hematopoietic cell fate and function

By

Dalton Lee Greenwood

Dissertation

Submitted to the Faculty of the

Graduate School of Vanderbilt University

in partial fulfillment of the requirements

for the degree of

DOCTOR OF PHILOSOPHY

in

Molecular Pathology and Immunology

May 12, 2023

Nashville, Tennessee

Approved:

Ken S. Lau, Ph.D.

Oliver McDonald, M.D., Ph.D.

Emily Hodges, Ph.D.

Brent Ferrell, M.D.

Luc Van Kaer, Ph.D.

Jeffrey C. Rathmell, Ph.D.

DEDICATION

In honor of my grandmother, Pauline “Honey” Payne, who lit the spark of curiosity in me and inspired me to pursue my dreams of finding new truths in our world, seeking new frontiers, and helping others all along the way.

ACKNOWLEDGEMENTS

This body of work was advised, guided, and contributed to by many people and institutions. I would first like to acknowledge the coauthors who contributed to the published manuscripts that are part of this dissertation (Chapter 2: Greenwood & Rathmell 2023). For potential coauthors of unpublished works in Chapter 3, Sierra Barone and Caroline Roe provided their computational expertise in analyzing CyTOF profiling of patient tumor immune cells in **Figure 3.3**. Paul Lindau provided his advice on T-cell receptor repertoires and computational experience in analyzing the single-cell RNA-seq and single-cell V(D)J-seq of peripheral CD3+ immune cells. Xiang Ye provided overall programming advice, general aid, and friendship. Kathryn Beckermann, Jonathan Irish, and Jeff Rathmell contributed their overarching guidance, consistent faith, financial support of experiments, and conceptual framework that made the project possible. Funding sources for this work include those acknowledged in the published manuscript including the National Institutes of Health Grants R01DK105550 and R01CA217987 (to J.C.R.), R01DK116005 (to K.E.W.), F31HL152529 (to D.L.G.), F30CA239367 (to M.Z.M.), T32GM007347 (to A.S.), T32DK1011003 (to K.V.), K00CA234920 (to J.E.B.), and K23HL138291 (to P.B.F.), a Blavatnik Family Foundation predoctoral fellowship (to P.T.T.N.), and by a grant from the Vanderbilt–Incyte Alliance (to J.C.R., M.R.S., and P.B.F.). We thank the Vanderbilt Institute for Advanced Genomics (VANTAGE) for library preparation and sequencing of scRNA-seq and scATAC-seq experiments, the Translational Pathology Shared Resource (TPSR) for sample preparation of ccRCC patient FFPE tumors, the Flow Cytometry Shared Resource (FCSR) for facilitating all flow sorting experiments, and the Immunogenomics, Microbial Genetics, and Single-cell Technologies (IMGSCT) core and Rama Gangula for

hashing of ccRCC samples for scRNA-seq and scV(D)J-seq. **Figures 1.1, 1.2, 1.3, 1.4, 2.9A,** and **3.1** were created using Biorender.com.

I would like to deeply thank my thesis committee members for their consistent feedback and encouragement. I would also like to thank Channing Chi for his assistance in experiments that ended in negative results, I will never forget your kindness and eagerness to help others. I would like to acknowledge all graduate students, post-doctoral fellows, medical professionals, and assorted scientific liaisons in the Jeff and Kim Rathmell labs. Their collective enthusiasm, trust, drive, kindness, and joviality made for a fun and motivating lab environment. I would particularly like to thank senior lab members Marc Johnson, Frank Mason, Kelsey Voss, Jackie Bader, Zach Bacigalupa, and Andrew Patterson for their mentorship, technique training, and patience through the years. Thank you to Andrew, Jackie, and Kelsey for their help and guidance in mouse experiments, handling, and husbandry – I would have been lost without you all. Thank you to fellow graduate students Melissa Wolf, Darren Heintzmann, Ayaka Sugiura, Emilie Fisher, Kaylee Steiner, Diana Healey, and Matt Madden for their friendship and many hours of company and conversation during lab work in the tissue culture room spanning countless experiments. Thanks to Debo Dahunsi, Sam Schaefer, and Channing Chi for their constant aid, sanity-preserving conversation, and solidarity through the stress of graduate school. Thanks to Darren for his incredible guide to western blotting and advice around life science investing careers and the CFA I exam. Thanks to David Flaherty in the Flow Cytometry Core for tolerating my lengthy e-mails troubleshooting flow experiments. Many thanks to Roger Chalkley and Jim Patton for their early voice in my graduate career and Vito Quaranta, Scott Hiebert, Ken Lau, and Julie Rhoades for their guidance and direction during my rotations. My never-ending gratitude is extended to Jeff and Kim Rathmell, who truly made my graduate school experience

bountiful in learning, achievement, exploration, and camaraderie and developed my scientific acumen. Jeff put his faith in me, taking me on after a 5th rotation in the Spring of 2018 – I will never forget that, and I will seek to return and multiply that kindness for all my mentees and trainees in the future. Vanderbilt has been a fantastic institution that has pushed me to the limits of what I thought possible and forged me into a fully-fledged *philosophe*. Penultimately, I am forever indebted to my friends Veronika Kondev, Alex Pfannenstein, Justin Critchlow, Jeanette Miller, Brad Pitcher, Lauren Walker, Tiffany and Andrew Walther, Dylan and Sarah Ritter, and others for keeping me sane throughout graduate school. Thanks to my incredible wife Sarah for her encouragement and faith in my abilities that push me to be better every day. Ultimate thanks to my parents, Lee and Kim Greenwood, for providing me with opportunities beyond measure and the self-confidence to pursue my dreams. Thank you all.

TABLE OF CONTENTS

LIST OF FIGURES

LIST OF TABLES

CHAPTER 1: INTRODUCTION

Introduction to the Immune System

As metazoans developed from single-cellular organisms, specialized cells in tissues and organs were eventually organized and sequestered within greater, multicellular organisms spanning trillions of cells. Through this concentration of cells within a greater body, vertebrates no longer required single-cells to be autonomous, independent organisms for nutrient acquisition. Metazoans gained a permissive, homeostatic interior environment that allowed for the specialization of tissues and organs to fit the needs of new, macrobiological niches. Individual cells now had their metabolic needs supplied by the internal multicellular environment, with a greater chance of survival in the context of the collective than alone. While the multicellular organism format came with many advantages, an unescapable challenge arose in the need to patrol and protect the greater organism from opportunistic single-celled and multicellular pathogens, cancer cells derived from mutated somatic and gametic cells, dead and dying cells, and other microscopic threats to the macroscopic body.

Metazoans responded to these challenges with the development of different forms of innate immune systems between species, composed of specialized innate immune cells equipped to repel most pathogens from the body and aid in repairing damaged tissues. Commonalities between innate immune systems include external mucous secretions and specialized skin and mucosa to form a barrier between the interior and the environmental frontier, humoral innate immunity composed of antipathogenic proteins and peptides such as lysozyme, complement, and cytokines, and cell-mediated innate immune cells that will be discussed in greater detail in following sections.

Immune systems range widely in metazoans from relatively simplistic catch-all "innate" systems designed to respond to several hundred common patterns known as damage-associated molecular patterns (DAMPs) and pathogen-associated molecular patterns (PAMPs) to complex systems found only in jawed vertebrates that comprise innate responses and adaptive T and B cell responses. T cell subsets strengthen innate immune responses and perform direct cell killing, while B cells secrete antibodies that bind and opsonize cell surface antigens to facilitate complement activation, engage Fc-receptors on innate immune cells, and potentially neutralize foreign bodies. These adaptive immune cells both hone a custom immune response targeting trillions of potential molecular patterns associated with cellular damage or pathogens (1, 2).

For the remainder of this dissertation, attention will be paid to the innate and adaptive immune systems of *H. sapiens* and its common immune vertebrate model counterpart, *M. musculus*. In chapter 2, *M. musculus* will be discussed, while in chapter 3, *H. sapiens* will be discussed, unless otherwise indicated.

The human immune system comprises adaptive and innate immune responses and has evolved to combat a wide range of pathogens and stressful stimuli (3-5). Functionally and genetically diverse between and within individuals, human immunity spans dozens of distinct types and argued subtypes of innate and adaptive immune cells and leverages its cellular diversity to respond to various pathogens and stresses in the body. Human immune systems vary widely furthermore between individuals based on family, sex, age, and ethnic background. In the largest study of multigenerational heritability of immune variation, the median heritability for immune variation was 37%. This low percentage of heritable immune variation indicates that most genetic drivers of immune variation are not shared between parent and offspring. The human leukocyte antigen (HLA) loci encode peptide-presenting proteins expressed in all cells to

facilitate immune surveillance and are the most polymorphic genes in the human genome, with over 6,400 alleles identified (6). More broadly, over 7,000 distinct loci associated with basic hematologic traits have been identified via genome-wide association studies (GWAS) within the human population that further contribute to population-wide immune diversity (7).

Immune diversity in humans can be also seen between males and females. 47% of HLA class I and II genes are expressed at different levels following stimulation by a common PAMP lipopolysaccharide (LPS), a significantly greater difference than the genomic average. Additionally, immune genes such as the regulatory T-cell transcription factor (TF) *FOXP3* and the pattern recognition receptor (PRR) *TLR7* are both present on the X chromosome. Differences in allosome allocation and hormone activity between sexes thereby result in higher type I interferon induction by innate plasmacytoid dendritic cells and reduced number and suppressive capacity of adaptive regulatory T-cells (Tregs) in females (7, 8).

The immune system is also affected by age, and trends towards systemic inflammation and away from naïve lymphocyte phenotypes as individuals age. Age-associated immunodeficiency is thought to be due to a combination of increased senescence of immune cells, decreased activity of hematopoietic stem cells that repopulated the immune system, altered lineage differentiation, depletion of the thymus, depletion of leukocytes, accumulation of mutations, and mitigated antiviral responses. Postzygotic somatic mutations and age-related chromosomal alterations (mCAs) are enriched at transcriptional regulatory sites for immune cells and have been observed in CD8+ T-cells in elderly people with multiple sclerosis and rheumatoid arthritis (9).

Immunomodulatory gene variants present in ethnic and regional communities globally further result in immune system differences that are relevant to health. Some examples of this

phenomenon include a missense variant in *IL7* present in South Asians that results in increased lymphocyte count (10). In African American men, allelic variants in immune-associated genes such as *IL-12β* and *IFN-γ* can contribute to an immunosuppressive tumor microenvironment, possibly leading to more aggressive prostate cancer progression and poorer disease outcomes vis-à-vis Caucasian Americans that receive the same standard of care therapy (11).

Within individuals, immunity is distributed and diversified between innate cells such as monocytes, macrophages, and neutrophils, adaptive immune cells like T-cells and B cells, and humoral immunity that includes soluble factors contained within the circulating blood and lymph such as complement, antibodies, and lysozyme. In the event of infection by opportunistic pathogens, innate immune cells and baseline humoral immunity serve as front-line sentinels that contain the infection in the short term before the immune response is dominated by the activity of adaptive T and B cells. In most circumstances, immune responses successfully resolve within weeks; however, exceptional pathogens such as human immunodeficiency virus (HIV) may persist for years with a sustained, unresolved immune response that culminates in adaptive immune exhaustion (12, 13).

Innate immune cells circulate within the vasculature or are tissue-resident and respond to tissue damage or infection by opportunistic pathogens and cooperate with adaptive immune cells to resolve immune challenges. Damaged tissue secretes DAMPs while opportunistic pathogens secrete PAMPs into the vasculature. Both DAMPs and PAMPs bind to PRRs on immune cell membranes to activate innate immune cells. Common human PRRs can be divided into thirteen Toll-like receptors (TLRs), two Nucleotide-binding oligomerization domain-like receptors (NLRs), 3 RIG-I-like receptors (RLRs), two C-type lectin receptors (CLRs), and one Absent in melanoma-2-like receptors (ALRs) that bind to PAMPs such as single-stranded RNA, flagellin,

and peptidoglycan that are uniquely associated with opportunistic bacteria, viruses, and fungi. When cognate ligands bind TLRs, NLRs, RLRs, CLRs, and ALRs, these receptors initiate signaling via MyD88 and/or TRIF, RIP2-TAK1-NF-κB, MAVS-TRAF6-NF-κB/TBK1, and the inflammasome-pyroptosis pathways, respectively. PRR activation results in effects that facilitate immune response escalation comprising the release of cytokines, leukotrienes, vasodilating factors, chemokines, hormones, and growth factors. The release of these factors is often accompanied by the induction of chronic or acute inflammatory responses, inflammatory remodeling of local vasculature, initial pathogen killing by innate immune cells, rebalancing of host microbiota, and/or the elimination of dead or mutated cells (14).

Opportunistic pathogens can be intracellular or extracellular in nature, and the methods by which innate immune cells eliminate these pathogens include phagocytosis, bombardment with reactive oxygen and nitrogen species (ROS and RNS), and induced apoptosis of infected cells. The “professional phagocytes”: monocytes, macrophages, neutrophils, dendritic cells, osteoclasts, and eosinophils perform phagocytosis. Phagocytosis is initiated by recognition of pathogens by PRRs and the resulting signaling cascade. Opsonic receptors may also initiate phagocytosis after recognition of host-derived opsonins that include antibodies, complement, fibronectin, mannose-binding lectin, and lactadherin. These opsonins are part of humoral immunity and bind to exterior molecules on the pathogen surface, impede interaction between the pathogen and surrounding host tissue, and can even immobilize and “neutralize” pathogens. Opsonic receptors include fragment crystallizable receptors (FcRs) that recognize constant regions of pathogen-bound antibodies and complement receptors (CRs) that recognize deposited complement factors such as iC3b. The phagocyte remodels its cell membrane and actin cytoskeleton and extends its cell membrane around the offending particle. The particle is then

internalized in the phagocyte within a vacuole known as the phagosome which matures over time in a process mediated by Rab5, Rab7, SNARE proteins, VAMP7, VAMP8, V-ATPases, and other factors. Maturation of the phagosome results in the formation of the phagolysosome which degrades the internalized particle by low pH ~4.5, hydrolytic enzymes like cathepsins, scavenger molecules like lactoferrin, and superoxides and ROS generated by NADP oxidase (15). Nonself-peptides derived from the phagolysosome may also be processed by factors associated with the endoplasmic reticulum (ER) including class II-associated invariant chain peptide (CLIP), HLA-DO, and HLA-DM and presented on antigen-presenting cell (APC) membranes in combination with major histocompatibility complex II (MHC-II). Antigens presented by professional APCs such as dendritic cells, B cells, macrophages, and thymic epithelial cells are presented to antigen-specific CD4+ T-cells that eventually result in CD4+ T-cell clonal expansion and refinement of B cell-mediated humoral immunity that is crucial to adaptive immune response and resolution (16). Similarly, MHC-I is expressed on all nucleated vertebrate cells and indicate the health status of the presenting cell to surveilling CD8+ cytotoxic T-cells. If a peptide corresponding to a normally occurring endogenous protein ("self") is presented to CD8+ T-cells via MHC-I, the cell is treated as healthy. However, if a nonself-peptide is presented via MHC-I, surveilling CD8+ T-cells may initiate cell killing via Fas ligand (FasL), perforin, granzymes, and other effector molecules to eliminate the infected, mutated, or otherwise damaged cell (17, 18). T-cell clonal expansion will be discussed in greater detail in a later section. In addition to phagocytosis, the immune system may employ ROS/RNS and antimicrobial peptides in the extracellular environment to clear opportunistic pathogens.

In addition to these immune effector mechanisms, specific classes of immune cells have unique traits that enhance the immune system's ability to clear pathogens. Neutrophils, as well as

other select immune cells, may undergo neutrophil extracellular trap (NET) formation, also known as NETosis, to kill and slow the spread of extracellular pathogens. NETs consist of modified chromatin studded with bactericidal proteins from the cytoplasm and cellular granules and can be produced by "classical" NETosis in which the cell undergoes programmed cell death (PCD) or by "vital" NETosis after which the cell retains its effector ability and viability (19).

Mast cells, basophils, and eosinophils have unique roles to play in anti-parasitic immunity and allergic response. Mast cells and basophils store and release basophilic granules and eosinophils store and release eosinophilic granules in response to parasitic helminth infection (20-22). Each of these cell types releases its granules in abundance to combat helminth infection. Eosinophilic granules contain major basic protein (MBP), ribonuclease cationic protein (RCP), and eosinophil-derived neurotoxin (21). Basophilic granules contain many of the same effector molecules but contain uniquely high levels of serine proteases in the same family as trypsin/chymotrypsin-related serine proteases, heparin, and histamine (23). All three types of cells also express Fcε receptors, with the high-affinity FcεRI expressed on Mast cells and basophils and the low-affinity FcεRII expressed on eosinophils. These receptors bind to the Fc regions on IgE class-switched antibodies, the lowest-concentrated immunoglobulin subtype, which is closely associated with the allergic response in addition to parasitic infections like schistosomiasis (24). These three cell types are thereby uniquely active in the "Type 2" immune response against parasites and the propagation of an allergic response.

The immune system coordinates which responses to mobilize and where to mobilize them through molecules secreted into the vasculature including cytokines, chemokines, and hormones. These immune communication molecules may act on the cell that secreted them in an autocrine fashion, on cells purely in the local vicinity in a paracrine fashion, or on distant, nonself cells

within reach of the circulatory system in an endocrine fashion. Cytokines encompass many soluble proteins with molecular weights between 6 and 70 kDa and are secreted by lymphocytes, macrophages, natural killer cells, Mast cells, stromal cells, and more. Similarly, cytokines act on many target cells to promote macrobiological programs and induce individual cells to alter intracellular processes that promote or inhibit immune responses. Cytokines may be classified as pro-inflammatory, anti-inflammatory, or both, but cytokines also can be classified by their cellular source. Type 1, 2, and 3 cytokines are secreted by cells including adaptive immune CD4+ Th1 cells, CD4+ Th2 cells, and CD4+ Th17 cells, respectively, and promote immune programs for specific pathogenic contexts (25).

Type 1 cytokines include IL-2, IL-12, IL-18, IFN-γ, and TNF-β and promote the inflammatory response to clear intracellular pathogenic stimuli. Type 2 cytokines include IL-4, IL-5, IL-6, IL-10, and IL-13, IL-33 among others, and they decrease the inflammatory response after pathogen clearance and can initiate tissue repair (26). Tissue repair is mediated by tissue macrophages, tissue stem cells, CD4+ Th2 cells, anti-inflammatory + anti-fibrotic macrophages (M(IL-10)-like), pericytes, dendritic cells, neutrophils, and Mast cells and is promoted by IL-4, IL-10, and IL-13. These cells collectively phagocytose cellular debris, close the wound if open to the frontier, and remodel the extracellular matrix to heal the wound (27).

Type 2 cytokines, as mentioned before, may also potentiate the immune response against extracellular parasites and allergic stimuli (28, 29). Type 2 cytokine release also improves barrier defenses by promoting mucus production, smooth muscle contractility, and intestinal epithelium turnover (29). Type 3 cytokines can also be produced by Th17/Th22 cells and include IL-17A, IL-17F, IL-22, and IL-26 and accelerate extracellular bacterial clearance and promote tissue and microbiome homeostasis (30, 31).

Adaptive CD4+ T-cells are prominent sources of cytokines, and innate cells are just as important for cytokine production. Inflammatory macrophages, NK cells, and group 1 innate lymphoid cells (ILC1) frequently secrete type 1 cytokines (32, 33). Type 2 cytokines may be produced by basophils, Mast cells, eosinophils, and group 2 innate lymphoid cells (ILC2) (29). Type 3 cytokines are commonly secreted by neutrophils, Mast cells, and group 3 innate lymphoid cells (ILC3). Innate immune cells release cytokines upon PRR stimulation by pathogens to improve the function of innate cells and adaptive cells in the site of inflammation to quicken the clearance of the inflammatory stimulus (or tamp it down for inhibitory Type 2 cytokines). The interaction between innate and adaptive immune cells that both produce inflammatory or anti-inflammatory cytokines may lead to a feed-*forward* loop that intensifies or a feed-*back* loop that diminishes an immune response. Th1 cells and macrophages both secrete IFN-γ in inflammatory contexts, and IFN-γ acts on both cell types to increase IFN-γ secretion and impact them and their neighbors in other ways. IFN-γ increases the cell membrane expression of MHC-II on APCs and MHC-I on non-APCs while perpetuating Th1 lineage commitment and intensifying the pathogenic killing capacity of macrophages. This is accomplished through the activation of the NADPH-dependent phagocyte oxidase system, nitric oxide production, and upregulation of lysosomal enzymes (34). While other immune contexts have different propagating effects, this innate-adaptive immune coordination through cytokines can also be seen in Type 2 immunity between Th2 cells and eosinophils, basophils, and Mast cells through IL-4 and in Type 3 immunity between Th17 and neutrophils through IL-17A (35, 36). In extreme cases, inflammatory feed-forward loops may bloom into cytokine release syndrome (CRS), in which site-specific inflammation spreads system-wide and leads to ever-

increasing cytokine release, inflammation, vascular endothelium breakdown, organ failure, and eventual death if left untreated (37).

While T-cells mediate cell-mediated immunity against pathogens, B cells that produce antigen-specific antibodies in mass quantities enervate immune effector cells via humoral immunity. B cells, T follicular helper (T_{fh}) cells, follicular dendritic cells (FDCs), and other APCs and stromal cells cooperate within the lymph node to hone and refine humoral immunity in a process known as somatic hypermutation (SHM). Tfh differentiation is promoted early on by IL-6 and the costimulatory molecule ICOSL which among other signals activates lineage-committing transcriptional programs driven by the TF BCL6. Tfh differentiation typically requires priming by both DC and B cell APCs and is inhibited by IL-2/IL-2R signaling that activates Blimp-1 and STAT5-mediated transcriptional programs. T-cells that are primed to become Tfh cells up-regulate CXCR5 and downregulate CCR7. This altered expression of chemokine receptors allows for T-cell migration to the T-B border. At the T-B border, Tfh-primed T-cells interact with B cells through ICOS-ICOSL and pMHC-II interactions to promote the formation of germinal centers (GCs). Tfh cells will eventually localize beyond the T-B border into GCs (GC-T_{fh}) by repressing PSGL1 and the chemotaxis-mediating receptor Ebi2. These changes are accompanied by altered S1P receptor expression patterns, SLAM family receptors, and integrins (38).

Specialized cells with dendritic morphology that reside in the light zone of the lymph node GC are known as FDCs. FDCs uptake nonself antigens in their *native* form and present them to B cells via complement receptor 1 (CR1) in combination with survival signals. B cells also interact with nonself pMHC-II on lymph node APCs via their surface B cell receptors (BCRs), upon which interaction they may localize to the T-B border, interact with Tfh cells, and

migrate into GCs of lymph nodes to undergo SHM. SHM improves the specificity of secreted B cell receptors (i.e., antibodies) for their cognate nonself antigen as well as class-switch antibody production to optimize the innate immune response triggered by interaction with Fc-regions of antigen-bound antibodies.

During SHM, B cells oscillate between the "light" zone and the "dark" zone of a lymph node GC, as specificity for native-conformation nonself antigens is refined. The light zone contains FDCs and GC-Tfh cells that present native antigens and monitor pMHC-II presentation via surface-expressed TCRs, respectively; both cells provide survival signals to those B cells which best bind native antigens *and* present that antigen-derived peptides in abundance on MHC-II. Those B cells bind and present antigens less competently will not receive survival signals and will be outcompeted and perish. After competent B cells in the light zone receive survival signals, they migrate into the dark zone which induces the processive enzyme activation-induced cytidine deaminase (AID). AID deaminates cytosines in B cell immunoglobulin (Ig) genes which encode for antigen-specificity-determining regions of the B cell receptor.

AID activity is necessary for the initiation of SHM and class switch recombination (CSR), the process by which rearrangement within the Ig heavy constant region allows isotype changes to B cell clonotypic antibodies to change the antibodies' effector functions and tissue distribution (39). The different types of antibody classes include those associated with naïve B cells, IgM and IgD, and those associated with activated, mature B cells: IgG, IgE, and IgA (40). Over time, GC B cells differentiate into long-lived plasma cells which secrete great amounts of class-switched antibodies and memory B cells to respond to future antigenic stimulation. Plasma cells reside primarily in the bone marrow while memory B cells are localized to secondary

lymphoid organs (SLOs) (41). Successful SHM and CSR in GC B cells will produce cells that secrete antibodies that effectively bind to nonself antigens to coat, or opsonize, pathogens to tag them for elimination by phagocytes through engagement with FcRs through the Fc region of the bound antibody. Secreted antibodies may also "neutralize" pathogens, in which pathogens have severe difficulty in spreading or are completely unable to interact with the surrounding tissue (42).

Chemokines allow immune cells to localize to sites of inflammation to overwhelm pathogens and accelerate the immune response. Classified into four main subfamilies, CXC, CC, CX3C, and C, chemokines interact with G protein-linked transmembrane receptors known as chemokine receptors and induce transcriptional programs to remodel cellular membrane composition and intracellular cytoskeletal elements to promote cell trafficking to sites of inflammation (43, 44). The multitude of chemokines allows for the precise tuning of immune cells recruited to an inflammatory site, among other functions. To name a few examples, CXCR4 acts to retain marginated neutrophils within the lung vasculature, CCL11 acts on eosinophils and basophils to promote their migration from the embryonic gastrointestinal (GI) tract into the periphery, CXCR2 promotes intestinal Mast cell localization and residence in the intestine, tissue-resident macrophages associate closely with CXCL14-producing fibroblasts in the skin and lamina propria, and CCL20 promotes migration of CD14+ dendritic cells (45). Immune cells follow the molecular "signal flare" of chemokines to go where they are most needed. Localized cytokine milieus present at inflammatory sites then help program the exact type of immune response needed from those localized cells.

Hormones complement cytokines and chemokines as another humoral regulator of immune outcomes. Hormones are secreted locally but permeate into the bloodstream to act on

local and distant cell populations. Classic examples of immunomodulatory hormones include immunosuppressive testosterone and immunoenhancing estrogen. Estrogen impairs autoreactive B cell negative selection and promotes CD4+ Th2 responses. Testosterone on the other hand can promote CD4+ Th1 responses, CD8+ cytotoxic T-cell responses, and anti-inflammatory IL-10 while tamping down NK cell responses and TNF-α secretion. The effects of testosterone/estrogenic impacts on sex-based immune differences can be seen in the higher Th1:Th2 ratio found in men compared to women (46).

The introduction of major components of the immune system now will allow the basic overview of an immune response from initiation to resolution using an idealized example of a cut in the skin that permits invasion and infection by an opportunistic, extracellular bacterium followed by successful clearance and resolution. In the first minutes of the infection, secreted humoral factors such as lysozyme, complement, and antibodies may opsonize, neutralize, and/or kill the infiltrating pathogen. Assuming the pathogen survives this phase, its secreted PAMPs will trigger PRR activation on tissue-resident macrophages, dendritic cells, and other innate immune cells. During this phase, nucleated cells will begin the presentation of bacterial nonself-peptides on MHC-I for surveillance by antigen-specific CD8+ cytotoxic T-cells.

Driven by PRR activation, innate immune cells release inflammatory cytokines, chemokines, and other factors to recruit circulating immune cells to the site of inflammation. These secreted factors facilitate extravasation into the inflamed site by loosening the endothelial cell-cell adhesion and intensify the inflammatory functions of immune cells in the inflammatory site. Resident and recruited phagocytes will phagocytose the offending live pathogen, dead fragments of the pathogen, and dead or dying infected cells. Phagocytotic APCs will lyse phagocytosed pathogens and present their nonself-peptides on their MHC-II molecules for

surveillance by antigen-specific CD4+ T-cells. Upon presentation of nonself-peptides on MHC-II (nonself pMHC-II), dendritic cells will then traffic to the nearest draining lymph node through afferent lymphatic vessels, allowing the billions of clonal T-cells to examine the DC's nonself pMHC-II (47). Once an antigen-specific T-cell binds to the nonself pMHC-II through interactions with an antigen-specific T-cell receptor (TCR) and CD4, that T-cell will undergo activation, clonal expansion, and differentiation over days into billions of antigen-specific T-cell subsets depending on the cytokine milieu and localize to the site of inflammation.

Upon interaction with a myeloid professional APC that presents nonself pMHC-II, T-cells may differentiate into the previously mentioned T effector cells such as Th1, Th2, and Th17 or into Tfh cells to promote GC formation and assist B cells in SHM (48). Antigen-specific Tfh cells will then assist GC B cells in SHM and CSR and eventually differentiate into plasma cells and memory B cells. Plasma cells will then produce vast quantities of class-switched antibodies that will seek out and opsonize the pathogen. Pathogen-bound antibodies then alert local phagocytes via FcR signaling and possibly neutralize the pathogen entirely. Production of B and T lymphocytes results in the characteristic swelling of lymph nodes over 3-4 days, after which T-cells relocate to the periphery, plasma cells to the bone marrow, and memory B cells to SLOs (49). After immune cells cooperate to eradicate the opportunistic pathogen and inflammatory stimuli disappear, the immune response shifts to tamp down the inflammatory response through CD4+ Treg cells, CD4+ Th2 cells, M(IL-10)-like macrophages, and other effector cells which secrete growth factors, lay down ECM, and contribute to wound healing. Simultaneously, the mobilized B and T lymphocytes deplete over time or form their memory B and T counterparts as inflammatory stimuli and antigen-specific innervation wane (50). In most cases, immune responses resolve over 14 days post-infection (51).

Introduction to Hematopoiesis

Hematopoiesis is the process that allows an organism to produce and maintain key populations of immune and blood cells throughout its life. In a single day, adult humans produce on average ~4-5 × 10^{11} hematopoietic cells comprising innate immune cells, adaptive immune cell precursors, and other blood cells. The hematopoietic cell types include but are not limited to osteoblasts, osteoclasts, macrophages, monocytes, dendritic cells, neutrophils, basophils, eosinophils, Mast cells, thrombocytes, erythrocytes, platelets, and common lymphoid progenitors which further develop into natural killer, T, and B cells (52, 53). While a portion of tissue-resident immune cells including select Mast cell and macrophage populations is fetal-derived and self-maintains separate from hematopoiesis, the vast majority of immune cells and blood cells originate from hematopoiesis (54).

Hematopoietic cells stem from a small population of long-term hematopoietic stem cells (LT-HSCs) with the ability to self-renew asymmetrically. LT-HSC asymmetric self-renewal replenishes the LT-HSC in cell division and simultaneously produces a daughter cell which differentiates into a mature hematopoietic cell itself or further begets progenitors with more limited asymmetrical self-renewal characteristics such as multi-potent progenitors (MPPs). In classical models of hematopoiesis, investigators envisioned a hierarchical process with LT-HSC giving rise to MPPs, then to common myeloid progenitors (CMPs) and multi-lineage progenitors (MLPs) which bifurcated the fate decision between myelo-erythroid and lymphoid, respectively. CMPs were seen to differentiate into megakaryocyte-erythroid progenitors (MEPs) and granulocyte-macrophage progenitors (GMPs). MLPs were postulated to give rise to mature DCs, pre-B cell/Natural Killer (PreB/NK) progenitors, and early T-cell precursors (ETPs). MEPs,

GMPs, PreB/NK, and ETPs would then differentiate into mature hematopoietic cells in an irreversible and non-overlapping fashion (55).

However, research published over the last decade has challenged this simplistic "family tree" of hematopoiesis. For example, it has been shown that lineage choice occurs in the primitive HSC compartment rather than further down a differentiation hierarchy (56, 57). Additionally, MPPs which were formerly seen as distinct from HSCs have been shown to share similar HOXB6/HOXA2/PRDM16-driven gene modules but differ in metabolic characteristics. Whereas HSCs are more metabolically quiescent, MPPs have greater cell cycle activation, gene expression, protein biosynthesis, and increased cell respiration (58). A more detailed vision of metabolic influences on hematopoiesis will be discussed in a later section.

Newer models of hematopoiesis mitigate the former unidirectional hierarchy in the self-renewing HSCs and MPPs and reveal new connections between progenitor groups in more mature descendant populations. For example, lymphoid-myeloid primed progenitor cells (LMPPs) denoted by Lin-CD34+CD38-CD90-/loCD45RA+CD10- are a recent addition to the model that are distinct from MPPs and MLPs with both myeloid and lymphoid potential. In previous models, unless an MPP had committed to myeloid lineage through CMP, there was no hematopoietic route to generate polymorphonuclear leukocytes (PMNs) such as neutrophils, eosinophils, basophils, and Mast cells (57). Hematopoietic progenitor groups are also now presented as less monolithic and more heterogeneous than in previous models with the aid of new single-cell sequencing techniques. HSCs and MPPs appear not to be limited to "vertical" hierarchical transitions through hematopoiesis but are capable of lineage bias in which the pool of HSCs and MPPs may express gene programs driven by TFs associated with certain lineages.

These include GATA2 and MESP1, which are correlated with erythroid and lymphoid trajectories, respectively (56).

Certain "master regulator" TFs have been identified that drive the production of hematopoietic precursors, regardless of those precursors' heterogeneity. These TFs include those which help determine initial fate choices in the HSC/MPP compartment: NFE2, GATA2, FLT3, CBPE, STAT1, and TCF4. NFE2/GATA2 induction contributes to MK/erythrocyte fate, FLT3 to myeloid fates through CMPs, and CBPE/STAT1/TCF4 induction may route HSCs/MPPs into LMPP, DC, and/or MLP fates. To briefly illustrate the diversity of hematopoietic transcriptional programs, I will examine several major TFs and how they contribute to lineage specification. The MK lineage requires PBX1/VWF induction, the erythrocyte lineage requires GATA1/KLF1 induction, the macrophage lineage requires CEBPD/IRF8 induction, the PMN lineage requires sequential CEBPD/CEBPE/CEBPD induction, the DC lineage requires STAT1/IRF8 induction, and T-cells, B cells, and NK cells require TCF4/ID3 induction. A more detailed list of TFs required for T-cell differentiation will follow in a later section and reviewed (58).

Hematopoiesis requires high throughput to maintain homeostasis while retaining dynamic regulation of dozens of hematopoietic differentiation pathways. Mammalian systems accomplish this through spatial and metabolic characteristics of the hematopoietic niche combined with a diverse set of stromal cells that facilitate maintenance, retention, and proliferation of HSCs through secreted factors, direct cell contact, and indirect action on neighboring stromal cells. Thought to localize to the endosteal layer of bone that divides central bone marrow (BM) from outer bone, HSCs are regulated by endothelial cells, perivascular mesenchymal stem cells (MSCs), adipolineage cells, MKs, macrophages, osteoblasts, sympathetic nervous system (SNS) nerves, and Treg cells (59).

A variety of cells regulate HSCs. First among these stromal cells are nestin (*Nes)*-GFP+ perivascular cells which express CXCL12 and SCF which bind to CXCR4 and KIT, respectively. These cells also express regulatory factors like ANGPT1, OPN, IL-7, and VCAM1, and similar populations can be isolated from non-transgenic mouse BM and human fetal BM via the surface markers PDGFRα and CD51. Hematopoietic-lineage cells like macrophages, MKs, neutrophils, and Tregs also act to regulate HSCs. Macrophages may secrete DARC and TGF-β to directly impact HSCs and OSM to indirectly regulate HSCs through *Nes*-GFP^{low} cells, LEPR+ cells, or CXCL12-associated reticulocytes (CAR cells) which are closely associated with BM sinusoids and arterioles. These vasculature-associated cells can also secrete CXCL12 and SCF to provide survival and maintenance signals to HSCs and IL-7 to promote lymphoid progenitor, T-cell, and B cell maintenance. MKs are also potent regulators of HSC quiescence and secrete CXCL4, TGF-β, and THPO. While depletion of MKs from transgenic mice does not affect overall HSC abundance in the BM, *Vwf*-GFP+ HSCs which are myeloid lineage-primed to become platelets closely associated with MKs and selectively expand upon MK depletion in mice. Neutrophils may also impact HSCs indirectly through the secretion of TNF into the vasculature, which accelerates vascular recovery following BM niche stressors such as irradiation. Treg cells can endow the BM niche with a degree of immune privilege through the secretion of immunomodulatory IL-10. Transplanted allogeneic HSCs were shown to colocalize with FOXP3+ Tregs in mice which further promotes allo-HSC longevity through CD39-catalyzed production of adenosine in the HSC niche. The absence of Tregs leads to rapid loss of allo-HSCs.

Osteolineage cells, endothelial cells, nonmyelinating Schwann cells, SNS nerves, and adipocytes also regulate HSC maintenance. Osteoblasts secrete molecules associated with

hematopoietic maintenance: osteopontin (OPN), CXCL12, thrombopoietin (TPO), and angiopoietin 1 (ANGPT1). However, 3D-imaging studies have demonstrated that osteoblasts and HSCs do not closely associate. Furthermore, other cell types have been shown to produce greater amounts of these molecules, suggesting that osteoblasts do not directly regulate HSC activity (60). Endothelial cells lining BM sinusoids and arterioles may secrete CXCL12, Notch ligands, pleiotrophin, and SCF to regulate HSCs. Nonmyelinating Schwann cells are glial cells that insulate artery-tracing nerves and promote HSC quiescence through TGF-β and SMAD signaling. SNS signals can stimulate the release of the neurotransmitter noradrenaline into the HSC niche, which facilitates the establishment of a CXCL12 gradient in the BM to facilitate progenitor egress into peripheral organs. SNS signals are also crucial for an intact osteocyte network and repopulation of the hematopoietic compartment following genotoxic stress. Finally, adipocytes may also negatively impact HSC maintenance. In humans, BM adiposity increases with age while HSCs become less abundant. Adipocyte-secreted adiponectin impairs progenitor proliferation *in vitro*, HSC engraftment in A-ZIP/F1 "fatless" mice is faster than WT counterparts, and antagonism of peroxisome proliferator-activated receptor γ (PPARγ) in mice to inhibit adipogenesis further accelerates BM recovery following transplantation or chemotherapy (60).

Osteoblasts, MSCs, and endothelial cells further enable HSC maintenance and differentiation via JAGGED-NOTCH interactions in mice and humans. It has been suggested that NOTCH signaling is especially important for lymphoid differentiation; *Notch1* is expressed at much higher levels in committed lymphoid progenitors than in purified murine HSCs. Also, inhibited NOTCH signaling in xeno-HSC-engrafted mice results in reduced engraftment and human HSC frequency. The exact function of this interaction is still debated (61). HSCs have

also been shown to change localization patterns with age. In mice, HSCs were shown to localize close to Cxcl12+ stromal cells and further from sinusoids and megakaryocytes at 3 weeks than HSCs *and* progenitor cells at 5 weeks and older (62).

Mutations acquired at any stage in hematopoiesis can lead to impaired differentiation, accelerated self-renewal, and resulting hematologic malignancies and leukemias. Leukemia accounts for ~309,000 annual deaths globally as the 15th most diagnosed cancer and the 11th greatest cause of global cancer mortality (63). More minor malignancies such as myelodysplastic syndrome (MDS) can occur which is a chronic health burden that can devolve into leukemia. Both are severe health outcomes that can occur when hematopoiesis goes awry (64). The ultimate triggers of genetic mutations that cause leukemias such as acute myeloid leukemia (AML) are unknown, but risk factors include radiation therapy, chemotherapy, smoking, and pollutants (63). Common mutations that underlie AML include many of the same genes that transduce signaling to regulate hematopoietic differentiation and proliferation such as *FLT3, KRAS, NRAS, PTPN11*, *NF1,* and *KIT.* Collectively, these genes are mutated in roughly two-thirds of AML cases. Other major gene groups represented in recurrent AML mutations are epigenetic modifiers like *DNMT3A*, nucleophosmin (*NPM1*), TF gatekeepers of lineage like *CEBPA* and *RUNX1*, tumor suppressors like *TP53*, spliceosome complex members like *SRSF2*, and cohesin complex genes like *RAD21* (65).

Steady-state vs. Emergency Hematopoiesis

In addition to steady-state homeostatic functions, hematopoiesis can dynamically respond to secreted cytokines, chemokines, and metabolites to supply cell types that are urgently needed through stressed or “emergency” hematopoiesis. Infection, irradiation, and chemical stress leads

to inflammation that can trigger emergency hematopoietic processes to facilitate immune responses to clear the inflammatory stimuli. The dearth of a given hematopoietic cell type may also trigger emergency production of that cell type until the need is met.

Infection by opportunistic pathogens can trigger emergency myelopoiesis and/or granulopoiesis that generates a greater number of innate immune monocytes and neutrophils to respond to the pathogen. Bacterial challenges may trigger endothelial cell secretion of granulocyte-colony stimulating factor (GCSF). Stromal cells and hematopoietic stem and progenitor cells (HSPCs) within the BM respond to GCSF binding to its receptor GCSFR. GCSF acts on the BM stroma to reduce the number of osteoblasts and macrophages which results in increased mobilization of murine and human HSCs and progenitors into the periphery. Human HSPCs proliferate and activate TLR signaling in response to GCSF to increase neutrophilic differentiation. In addition to pathogenic stimuli, emergency myelopoiesis can be artificially triggered by the administration of PAMPs like LPS, polyI:polyC (pIpC), and others (61). Production of cytokines like TNF-α may boost myelopoiesis through inhibiting other hematopoietic pathways like erythropoiesis. TNF-α also blocks HIF1α signaling that could promote erythropoiesis by activation of NFκB and Gata2-mediated transcriptional programs (66).

Viral infections are also likely to trigger emergency myelopoiesis. In the case of SARS-CoV-2 (COVID-19) infection, human patients with severe disease have characteristically elevated inflammatory markers IL-6 and c-reactive protein (CRP) and increased emergency myelopoiesis compared to patients with more favorable outcomes. This emergency myelopoiesis produces primarily monocytes and neutrophils which may or may not be fully mature and functional. Neutrophils profiled from patients with severe COVID-19 tended to be more

immature than other contexts, indicated by lower expression of CD10 and CD16. Monocytes from severe COVID-19 patients expressed less HLA-DR, with both neutrophils and monocytes positively correlated with each other. A potential mechanism to promote immature populations could be a response to monocyte pyroptosis following COVID-19-mediated inflammasome activation (67).

Irradiation and chemical stressors can also initiate emergency hematopoiesis. Administration of ionizing radiation or chemotherapy increases expression of fibroblast growth factor 2 (FGF2) in the BM which can expand *Nestin*$^{+}$ and other stromal cells that produce increased HSPC-expanding. At higher doses at ~2 Gy for human total body irradiation (TBI), irradiation is capable of devastating hematopoietic stem cells, progenitors, and stromal cells, though stromal cells can recover rapidly via expanded osteoblast-lineage cells and megakaryocytes at the bone endosteal surface. Removal of host HSPCs allows for repopulation with autologous and allogeneic hematopoietic stem cell transplants for the treatment of hematologic malignancies, certain immune disorders, and more (61). Treatment with chemical stressors like 5-fluorouracil (5-FU) targets cells in S-phase to induce HSPC cycling and differentiation via MEK/ERK, PI3K, and AKT/mTORC1 signaling, among other pathways (66).

Aside from infection, irradiation, and chemical stressors, steady-state hematopoiesis may be pushed into a stressed state to compensate for a rapid loss of cells. For example, acute or excessive blood loss and the resulting loss of erythrocytes needed to supply oxygen to peripheral tissues can induce stress erythropoiesis. Hypoxia in the bone marrow can activate hypoxia-inducible genes mediated by VHL repression and resulting stabilized HIF1α. These include BMP, GDF15, glucocorticoid receptor, and erythropoietin (EPO). These factors act on HSPCs and stromal cells to dramatically promote the production of erythroid-restricted stress erythroid

progenitors (SEPs) that rapidly repopulate erythroid populations. While both rely on inflammatory signals to activate, emergency myelopoiesis is promoted over emergency erythropoiesis after induction of TLR signaling that signals through MyD88 to NFκB to increase inflammatory cytokine production (66).

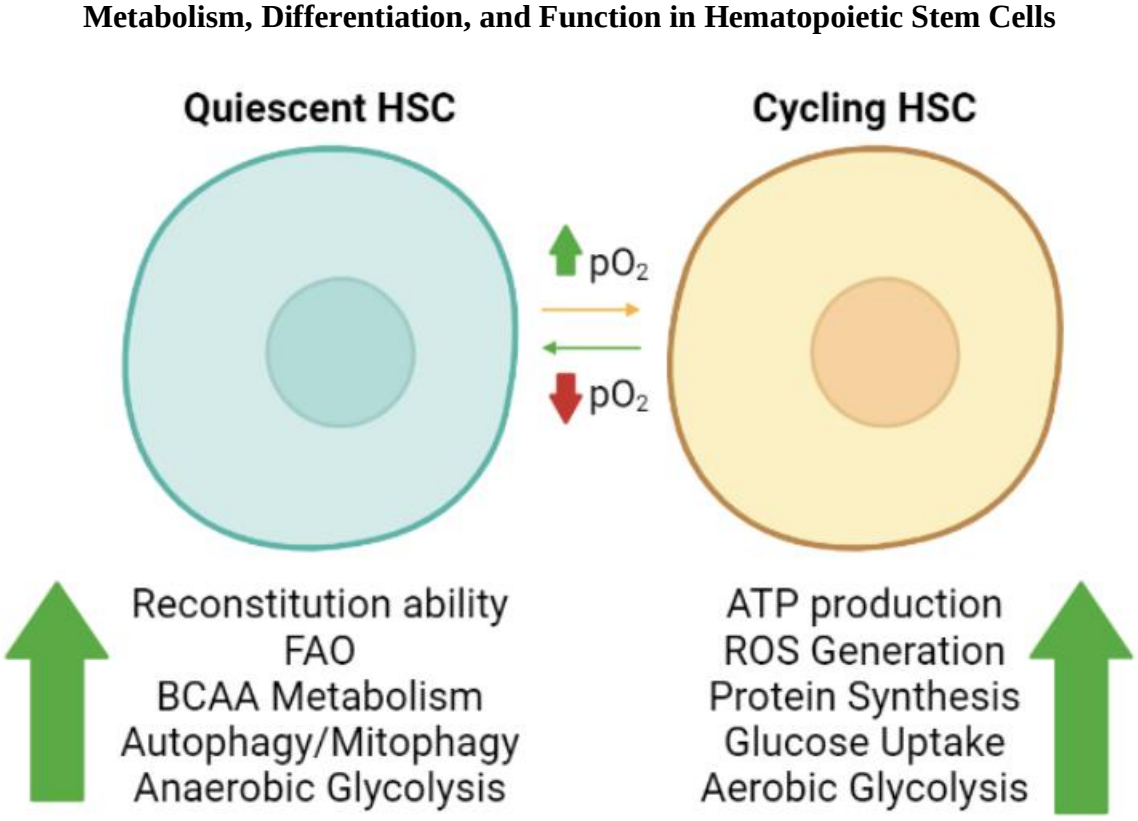

Figure 1.1. Metabolic Requirements of Quiescent and Cycling Hematopoietic Stem Cells. To preserve stemness, quiescent HSCs upregulate fatty acid oxidation (FAO), branched-chain amino acid (BCAA) metabolism, autophagy/mitophagy, and anaerobic glycolysis. Conversely, cycling HSCs that are primed for differentiation may be activated following increased oxygen concentration or inflammatory cytokines. This activation then leads to greater OXPHOS, ATP and ROS production, protein synthesis, and more aerobic glycolytic metabolism.

In addition to cytokines, chemokines, and other secreted factors that influence HSC behavior and fate, cellular metabolism is also an important regulator of hematopoietic "stemness" and differentiation potential. "Stemness," or the ability of HSCs and certain

progenitor cells to self-renew over a given time frame, indeed requires tight regulation of cellular metabolic processes for lifelong maintenance. While metabolic changes in HSCs may be induced by cytokine, chemokine, and other secreted factor-induced signaling, fluctuation to HSC microenvironmental nutrients and O_2 can potently alter HSC behavior and function. Overall, HSCs utilize and regulate anaerobic glycolysis, ROS, mitophagy, electron transport chain management, amino acid metabolism, and lipid metabolism to preserve quiescence and "stemness".

Due to their residence in the hypoxic bone marrow niche, with an estimated 32 mm Hg pO_2 in live mice, HSCs mainly derive energy production from anaerobic glycolysis. Low pO_2 allows for the repression of the E3 ligase Von Hippel-Lindau (VHL) and stabilization of hypoxia-inducible factors HIF-1α and HIF-2α, which then heterodimerize to promote transcription of genes like *Epo*, *Vegfa*, and *Glut1* that promote glycolytic metabolism. HIF-signaling has also been shown to promote GLUT1 localization to the cell membrane (68-70). While *Hif-1α* and *Hif-1β* are dispensable for HSC self-renewal in some genetic mouse model studies, loss of their transcriptional activator *Meis Homeobox 1* (*Meis1*) results in increased mitochondrial metabolism, increased ROS levels, and loss of quiescence and repopulation potential after transplantation. HSCs also exhibit high expression of pyruvate dehydrogenase kinase (*Pdk*) which inhibits pyruvate dehydrogenase (PDH)-mediated conversion of pyruvate to acetyl-CoA to down-regulate aerobic glycolysis. Glucose uptake levels are lower in HSCs than in subsequent progenitors and more mature hematopoietic cells in the BM. Proliferative HSCs display greater glucose uptake, however, than quiescent HSCs. Furthermore, inhibition of V-ATPase, an enzyme required for the establishment of proton gradients across the electron

transport chain, results in increased HSC quiescence, *ex vivo* maintenance of HSCs, and competitive repopulation ability upon transplantation (71).

ROS are a consequence of high metabolic activity and can also trigger HSC entry into the cell cycle and exit quiescence if not properly controlled. HSCs exhibit reduced function in genetic mouse models with increased ROS production resulting from deletions in *Ataxia telangiectasia mutated*, *Tuberous sclerosis complex subunit 1*, or *Forkhead box* (*FoxO*). To scavenge and limit ROS and to preserve quiescence, HSCs utilize antioxidant enzymes such as superoxide dismutase (SOD) and tamp down on mitochondrial oxidative phosphorylation (OXPHOS). HSCs prioritize shunting glycolytic intermediates into the pentose phosphate pathway (PPP) and away from the TCA cycle to avoid excessive OXPHOS, which converts roughly 0.1-0.2% of oxygen processed in the electron transport chain (ETC) into ROS (71).

Though HSCs utilize minimal OXPHOS for their bioenergetic needs, recent evidence has demonstrated that HSCs possess high mitochondrial content, high mitochondrial membrane potential ($\Delta\Psi_m$), and high mitochondrial turnover. Contradicting conclusions from older studies, recent staining of HSCs with tetramethylrhodamine methyl ester perchlorate (TMRM) has revealed that HSCs have the greatest $\Delta\Psi_m$ among hematopoietic populations, after correcting for xenobiotic transporter activity which exports TMRM out of the cell. Xenobiotic efflux pump is higher expressed in HSCs than in mature hematopoietic populations, and the lack of control for that variable had led to biased results in the past when assessing HSC $\Delta\Psi_m$. Using similar xenobiotic efflux correction in measuring mitochondrial mass, HSC mitochondrial mass was shown to be as great or greater than other hematopoietic cells by mitotracker green (MTG) staining and corroborated by 3D image-based assessment of mitochondrial structure in HSCs (72, 73).

HSCs regulate mitochondrial turnover, fusion, and fission to maintain the balance between quiescent self-renewal and metabolically active differentiation. Mitochondria dynamically divide (fission) and combine (fusion) to respond to metabolic and environmental cell stressors to create new mitochondria and partition off damaged or defective mitochondria (74). In HSCs, the mitochondrial fusion-promoting protein Mitofusin 2 (Mfn2) is required for lymphoid-primed HSC maintenance while myeloid-primed HSCs do not require it. HSC mitochondrial fission-promoting Dynamin-related protein 1 (Drp1) is important for HSC quiescence. Loss of *Drp1* results in loss of HSC self-renewal potential but retention of HSC quiescence. Furthermore, the clearance of damaged or defective mitochondria through mitophagy is needed to maintain HSC self-renewal capacity. Recruitment and inhibition of Parkin, a key promoter of mitophagy, results in increased HSC expansion and limited HSC self-renewal, respectively. Without these mitochondrial quality control mechanisms to ensure healthy mitochondria for HSC daughter cells, HSC self-renewal potential erodes (71).

Although HSCs primarily rely on anaerobic glycolysis, they possess high mitochondrial mass and high $\Delta\Psi_m$ that is facilitated by unique regulation of HSC ETC components, and low-level OXPHOS is required for their normal function. For example, HSPCs exhibit greater expression and activity of ETC complex II compared to ETC complex V in most mature cell types. Increased proton pumping into the mitochondria by ETC complex II and decreased proton flux by complex V can explain this heightened $\Delta\Psi_m$. When this $\Delta\Psi_m$ is lowered by deficiencies in subunits of complex III and complex II, HSCs experience loss of quiescence, long-term repopulating capability, or decreased myeloid progenitors (71).

HSCs also make selective use of amino acid metabolism to facilitate homeostasis, primarily glutamine and branched-chain amino acids (BCAAs). Glutamine is the most prevalent

amino acid in mice and humans by concentration and is a critical fuel for the TCA cycle. The enzyme glutaminase (Gls) catalyzes its conversion into glutamate, and subsequently, glutamate dehydrogenase (Gdh) catalyzes glutamate into α-ketoglutarate (α-KG) for entry into the TCA cycle (75). Switching of glutaminase (Gls) isoforms promotes HSC cell cycle activation, and glutamine-dependent de novo nucleotide biosynthesis is required for HSC erythroid specification. BCAAs are also important for normal HSC function. HSC proliferation and maintenance rely on the BCAA valine, and BCAA metabolism is an important regulator of HSC proliferation. Mutations in the BCAA-associated enzymes IDH1 and IDH2 that catalyze isocitrate into α-KG can lead instead to the production of the oncometabolite 2-hydroxyglutarate (2-HG). 2-HG can induce accelerated HSC self-renewal and leukemogenesis partially through inhibition of TET2, a key demethylation enzyme that will be discussed in more detail in a later section. Other BCAAs like purine, aspartate, and asparagine are also capable of regulating hematopoietic self-renewal capacity.

HSCs also utilize fatty acid oxidation (FAO) to regulate self-renewal and differentiation. FAO involves the breakdown of long-chain fatty acids in a process that ranges from activation in the cytosol, transport via the carnitine shuttle system into the mitochondria, and the progressive cleavage from the fatty acid of two carbons at a time to produce acetyl-CoA, NADH, $FADH_2$, and ATP. Deletion of a regulator of fatty acid transport, peroxisome-proliferator activated receptor (Ppar) delta in HSCs impairs HSC reconstitution capability. The PPAR-FAO pathway also promotes Parkin recruitment to the mitochondria, and Parkin promotes mitophagy that is needed to preserve HSC quiescence. Other members of the PPAR family regulate HSC and progenitor behavior; Ppar γ inhibition results in increased expansion of HSPCs derived from human cord blood. Furthermore, stromal cells that store fatty acids in the bone marrow called

bone marrow adipocytes (BMA) are a major source of Scf secreted in the bone marrow after irradiation and are important for the engraftment of HSC transplants (71).

De novo fatty acid synthesis supplies cells with fatty acids, with the first synthetic step performed by the enzyme fatty acid synthase (FASN) that uses acetyl-CoA as a substrate. Acetyl-CoA can be derived from glycolysis, and the enzymes ATP citrate lyase (ACLY) and acyl-CoA synthetase short-chain family member 2 (ACSS2) are major acetyl-CoA suppliers through citrate and acetate catalysis, respectively. While there are no studies that examine the role of ACSS2 on hematopoietic stem cell differentiation, ACSS2 has been shown to regulate adipocyte and neuronal differentiation through its supply of acetyl-CoA to histone acetylation (76). Supply of acetyl-CoA from ACLY is crucial for *de novo* fatty acid synthesis and histone acetylation in HSCs, and ACLY is dynamically regulated throughout myeloid differentiation. *Acly* expression decreases during macrophage differentiation from bone marrow precursors and is one of the primary subjects of this dissertation (77).

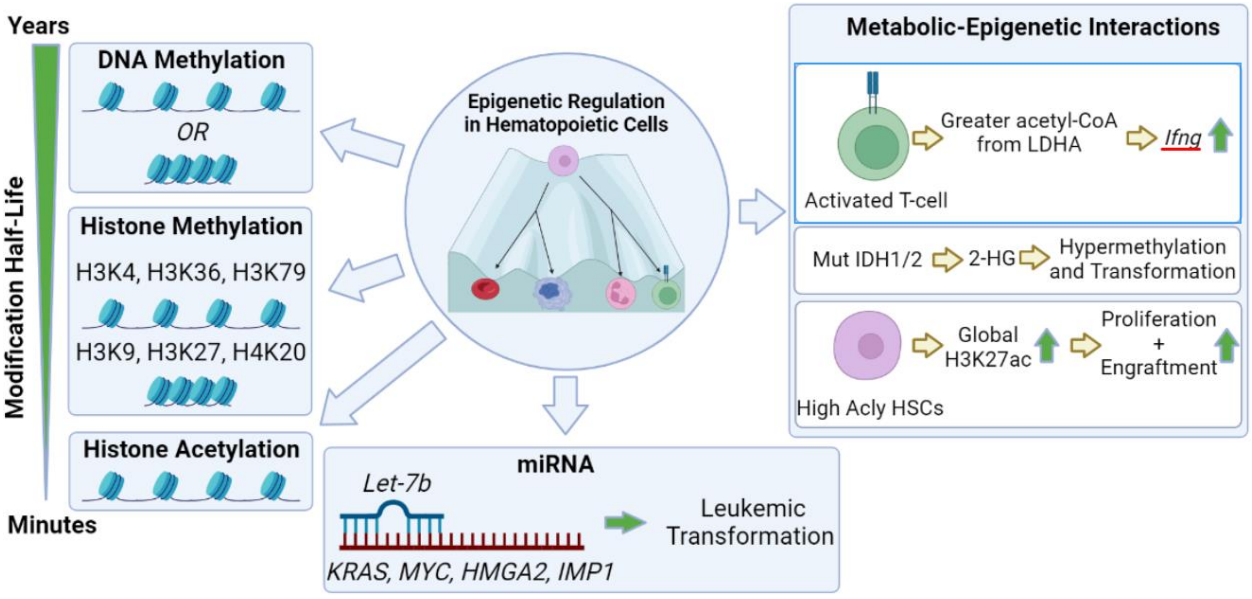

Figure 1.2. Overview of Epigenetic Regulation of Gene Expression in Hematopoietic Cells. Hematopoietic cells undergo epigenetic regulation of gene expression via DNA methylation, histone methylation, histone acetylation, miRNA-mediated degradation of mRNA transcripts, and more. While DNA methylation may open or close chromatin accessibility depending on the locus and type of modification, histone acetylation promotes chromatin accessibility. Histone methylation marks on H3K4, H3K36, and H3K79 are associated with open chromatin while H3K9, H3K27, and H4K20 modifications are associated with closed chromatin structures. Interactions between metabolites and epigenetic enzymes may lead to changes in hematopoietic cell fate and function.

Hematopoiesis relies on epigenetic regulation to dynamically modify cell gene expression programs and respond to stimuli including cytokines, chemokines, hormones, and metabolic changes. “Epigenetics” encompasses all cellular heritable features that result in phenotypic alterations that are non-genetic. Through the main epigenetic mechanisms modification of DNA, modification of histones, and microRNA (miRNA), cells are both able to restrict the expression of genes to specialize their type and to alter gene expression to respond to environmental stimuli. DNA and histones may be modified to alter the transcriptional activity of genes proximal in space to the modification. While DNA modification is limited to methylation at the 5’-position

of cytosine residues, histones may be modified through numerous processes that include acetylation, methylation, ubiquitination, phosphorylation, and sumoylation which commonly target conserved lysine residues on histone tails (78). There are many different epigenetic regulatory processes; however, this introduction will focus on miRNA, DNA methylation, histone acetylation, and histone methylation.

miRNAs are small, non-coding RNA molecules that primarily bind to mRNA molecules through complementary base pairing to mediate translational inhibition and mRNA decay (79). While not a direct focus of this dissertation, miRNA also regulates hematopoietic stem cell behavior and can trigger leukemogenesis when improperly active. For instance, the miRNA Let-7 acts as a tumor suppressor targeting *KRAS, HMGA2, MYC, IMP1*, and other transcripts for degradation. Let-7b expression is decreased in pediatric AML patients and is associated with c-Myc dysregulation (78). Degradation of miRNA-bound mRNAs is mediated by the RNA-induced silencing complex (RISC) primarily composed of members AGO, DICER, TRBP, PACT, and GW182 (80).

Collective epigenetic processes allow for short-term responses to stimuli and can be interpreted as a cellular "memory" of stimuli that a cell and its predecessors experienced. Modifications to histones and DNA are constantly updated by "writers" and "erasers" to respond to stimuli in the short-term. However, certain modifications have longer half-lives than others, meaning that they remain in place longer after deposition. While histone lysine methylation has half-lives in the order of hours to days, histone acetylation and phosphorylation may only last minutes (81). Longer still, DNA methylation may be stable for months to years. In a clinically relevant example, individuals prenatally exposed to the Dutch Hunger Winter famine in 1944-45 had less DNA methylation at the *IGF2* gene compared to their unexposed same-sex siblings

which contributed to their heightened disease risk. These DNA methylation changes were observable *six decades* post-exposure, demonstrating the potential longevity of DNA methylation. The different timescales of epigenetic half-lives illustrate several epigenetic short, medium, and long-term tools that cells possess to respond to their environment (82).

In eukaryotes, DNA methylation most commonly appears as 5'-methylcytosines present at cytosine-guanine (CpG) dinucleotides on both DNA strands and is associated with transcriptional repression and activation depending on the modified locus. When clustered in gene promoters, methylated CpG dinucleotides are associated with transcriptional repression. Conversely, DNA methylation is associated with actively transcribed genes when enriched in the gene body. DNA methylation represents a common method by which gene transcription can be repressed when one considers the prevalence of CpG islands (CGIs) as a gene regulatory element. CGIs are clusters of CpG dinucleotides that measure ~1 kb that are enriched at gene promoters; more than two-thirds of promoters in mammals are CGIs while nearly all housekeeping genes have CGIs. CGIs are generally unmethylated and correspond to actively transcribed genes; however, methyltransferases such as DNMT3B perform *de novo* methylation at CGIs that may allow for transient or durable repression of corresponding genes. In the case of germline genes, 5% of all genes which are sequentially activated or deactivated during organismal development, DNA methylation is required for lifelong somatic silencing through methylation of CGIs at gene promoters. The precise mechanism by which DNA methylation results in transcriptional inhibition is not agreed upon, though it is known that DNA methyl marks may be bound by writers and erasers of other epigenetic marks like histone methylation and acetylation to cooperatively promote or activate transcription (83).

Epigenetic modifications may result in transcriptional activation or repression depending on the nature and site of the modification. While histone acetylation is typically associated with transcriptional activation through charge-based conformational changes, histone methylation may activate or repress transcription depending on the nature of the methylation (84). For example, while modifications to H3K4 (histone 3, lysine residue 4), H3K36, and H3K79 may be associated with active, open chromatin, methylation at H3K9, H3K27, and/or H4K20 is commonly associated with repressed, closed chromatin. Histone lysine tails may also be mono-, di-, or tri-methylated with each variant possessing different regulatory attributes (85). Epigenetic regulation of gene expression is particularly consequential for hematopoietic stem and progenitor cells, as it is the primary means by which cells specialize phenotypically from monolithic hematopoietic stem cells into the panoply of mature hematopoietic populations. Indeed, save for a select few mechanisms that modify germline DNA such as V(D)J-recombination in T-cells and SHM in B-cells, epigenetic regulation of gene expression is the main method available to permit the specialization of cells in the body.

Trained immunity, the process by which innate immune cells like macrophages, monocytes, natural killer cells, and their BM progenitors produce enhanced responses to secondary immune challenges, makes use of epigenetic changes to record the “memory” of initial stimulation. Innate immune cells and progenitors durably regulate chromatin accessibility to facilitate trained immunity through deposition of new histone modifications at H3K4me3 to mark active promoters, H3K4me1 to denote distal enhancers, and H3K27ac that indicate both active promoters and enhancers (86). For example, vaccination with the Bacillus Calmette-Guérin (BCG) vaccine in mice induced trained immunity in HSPCs partially through epigenetic modifications. Post-vaccination, HSPCs exhibit H3K27ac and H3K4me1 deposition which

"prime" enhancers of genes involved in protection against *Mycobacterium tuberculosis*. This priming following BCG-induced IFN-γ stimulation predilected HSPCs to myelopoiesis and macrophage differentiation (87). A similar epigenetic priming effect can also be observed in human responses to BCG vaccination (88). Epigenetic processes have also been implicated in trained immunity priming in response to β-glucan, which can potentiate increased granulopoiesis through increased accessibility at genes implicated in IFN-I signaling in BM granulocyte-macrophage progenitors (GMPs). Furthermore, HSCs appear to accumulate epigenetic marks throughout an organism's life to potentiate HSCs to express genes regulated by inflammatory signaling-related transcription factors like the ATF family, STAT family, and CNC family TFs. Deposition of H3K4me1/H3K27ac at active enhancers, H3K4me1 at primed enhancers, and absence of either mark at inactive enhancers produce differentially accessible regions (DARs) of chromatin that enhance the response to secondary immune challenge compared to young HSCs. While remaining inconclusive, there is speculation that transcriptional dysregulation resulting from these accumulated epigenetic changes could be linked to stress-induced HSC depletion and/or leukemogenesis in older individuals (89).

Epigenetic regulation cooperates with extraneous stimuli-induced signaling and internal metabolic processes to potentiate enhanced immune responses through altered HSPC gene regulation. In a response to IFN-γ signaling, for instance, regulatory elements of genes implicated in *M. tuberculosis* immune response are modified in HSPCs following BCG vaccination through the action of epigenetic writer and eraser enzymes to enhance future responses. Many of these writer and eraser enzymes utilize substrates or are regulated by small-molecule metabolites derived from the TCA cycle, one-carbon metabolism, NAD metabolism, and/or acetate and citrate metabolism. While histone acetyltransferases use acetyl-CoA derived

from glucose, fatty acids, and amino acid metabolism as an acetyl donor substrate, histone and DNA methyltransferases use S-adenosylmethionine (SAM) as a methyl donor substrate (90, 91). Eraser enzymes also are regulated by metabolites; α-KG promotes histone demethylase activity while succinate and fumarate inhibit demethylase activity. Meanwhile, histone deacetylases are promoted by high NAD+ to NADH ratios and are inhibited by β-hydroxybutyrate. The availability of these substrates and regulatory metabolites within the cell can dictate the velocity of these enzymes with consequences for epigenetic homeostasis and overall gene expression regulation.

Referring to Michaelis-Menten enzyme kinetics, the turnover rate for an enzyme (velocity: V), representing the rate of reaction catalysis, increases in response to increased substrate concentration, [S]. K_m is a standardized constant representing the enzyme-specific affinity for its substrate and is the value of [S] that corresponds to half of the maximum velocity of the enzyme (1/2 V_{max}). Idealized enzyme velocity can increase as [S] increases, albeit with diminishing returns, to the enzyme's maximum velocity, V_{max}, after which velocity no longer increases with [S] (92). While enzyme classes like kinases and E3 ligases possess intracellular [S] ranges that maintain constant enzyme velocity at or near V_{max}, DNA methyltransferases, histone methyltransferases, and histone acetyltransferases, and other classes of epigenetic writer enzymes may have their velocities limited by low substrate availability. HATs, for instance, possess K_m values between 0.0002-0.046 mM with acetyl-CoA intracellular concentrations that range from 0.002-0.013 mM. While these ranges overlap, high enzyme K_m value combined with low substrate concentration can result in reduced enzyme velocity with consequences for epigenetic homeostasis (91).

In Treg cells, increased glycolysis experienced during immune activation results in greater acetyl-CoA production and altered histone acetylation. Elevated lactate dehydrogenase (LDHA) activity results in high acetyl-CoA concentration that facilitates transcription of *Ifng*. The deficiency of LDHA in Scurfy mice compensates for the Scurfy phenotype to foster reduced systemic inflammation through altered H3K9ac and H3K27ac modifications (93).

While not hematopoietic cells, embryonic stem cells (ESCs) can be forced into differentiation through the manipulation of metabolic-epigenetic interactions. Short-term deprivation of methionine in human primed ESCs results in the depletion of SAM pools that serve as the substrate for methyltransferases. This deprivation resulted in the activation of differentiation. Alternatively, *naïve* ESCs' self-renewal capability is preserved by the upregulation of nicotinamide *N*-methyltransferase which also depletes SAM pools (94).

ACLY/Acly and ACSS2/Acss2 are major sources of acetyl-CoA and link metabolism and epigenetic processes. Activity of these enzymes is also consequential for HSC self-renewal and priming. In the context of hematopoietic reconstitution following 5-FU treatment, high Acly expression enhanced HSC proliferation and engraftment via the promotion of global H3K27ac levels. $EPCR^{High}$CD150+CD48−c-Kit+Sca1+lineage− (ESLAM KSL) HSCs possess greater Acly activity than $EPCR^{Low}$ counterparts which promoted differentiation into CD48+ progenitor cells while steady-state HSCs suppress Acly expression and have greater potential to differentiate into progenitors (95). ACLY activity that generates acetyl-CoA from mitochondrial-derived citrate is also crucial for H3K9/K27 acetylation increases that delay early differentiation in human pluripotent stem cells (hPSCs) and murine ESCs (mESCs) (96). Though fewer studies connect ACSS2 to changes in hematopoietic cell fate and function, ACSS2 localization to the nucleus has been implicated in promoting lysosomal biogenesis and autophagy in a human

glioblastoma (GBM) cell line that correlates with AMPK activity (97). ACSS2's role in autophagy promotion could thus be important for HSC self-renewal maintenance. However, $Acss2^{-/-}$ ESCs do not display altered differentiation patterns compared to $Acss2^{WT}$ counterparts (98).

One of the most clinically relevant examples of epigenetic-metabolic interaction is 2-HG, an oncometabolite that may be produced from isocitrate by mutated isocitrate dehydrogenase 1 or 2 (IDH1/2). Common mutations that lead to D-2-HG production are IDH1 R132 and IDH2 R172 and are oncogenic, with especially high mutation rates in GBM and AML. 2-HG is thought to trigger oncogenesis through the inhibition of DNA and histone demethylases containing α-KG-dependent domains such as TET2 and Jumonji-C (JmjC). Other enzymes containing Jumonji domains and other domains that utilize α-KG for regulation or substrate are also affected by 2-HG. Examples of IC50 values of 2-HG for enzymes include 79 ± 7 μM for the histone demethylase JMJD2C and 1500 ± 400 μM, demonstrating that 2-HG is a weak antagonist of α-KG at steady-state and does not significantly inhibit α-KG-dependent enzymes. However, mutant IDH1/2 can produce 3-35 mM of D-2-HG and potently inhibits relevant enzymes. 2-HG production from mutant IDH1/2 results in hypermethylation with consequences that can exacerbate genotoxic stress. For example, 2-HG can inhibit the histone demethylase KDM4B that results in hypermethylated DNA break loci, which prevents proper recognition of H3K9me3 signals that enable homology-driven repair (HDR) complex recruitment. 2-HG inhibition of DNA repair could thus explain the hypersensitivity of IDH1/2-mutant colorectal carcinoma and astrocyte cell lines to genotoxic ionizing radiation or H_2O_2 compared to IDH1/2-wt counterparts. 2-HG treatment by itself can recapitulate hematopoietic stem cell differentiation block and cytokine-independent proliferation caused by IDH1/2 mutation. While 2-HG-induced DNA

hypermethylation is known to trigger oncogenesis and cause sensitivity to DNA damage, more research is required to identify the precise mechanism by which IDH1/2 mutations reliably transform hematopoietic and glial populations (99).

Epigenetic processes, metabolism, cytokines, chemokines, PAMPs, DAMPs, and other sources of external stimuli collectively influence cells to establish and regulate cell identity. While long-term chromatin accessibility regulation facilitates cell type specialization, short-term changes in chromatin accessibility mediated by modifications like histone methylation and acetylation promote rapid gene regulation to respond to hematopoietic cell type needs for HSCs, developmental constraints for ESCs, or immune-challenge related differentiation in T-cells.

Introduction to T-cells and V(D)J Recombination

Hematopoiesis is responsible for the population of B- and T-lineage lymphoid cells that comprise adaptive immunity. While B cells are responsible for the production of secreted, circulating immunoglobulins (antibodies) that bind to, opsonize, and potentially neutralize specific peptide sequences, T-cells mobilize cell-based immunity through T-cell receptor (TCR) interactions with pMHC-I or pMHC-II mediated by CD8 or CD4, respectively. As stated in a previous section, T-cell adaptive immunity is relevant for Type 1 immune responses against intracellular pathogens (Th1), type 2 immune responses against extracellular parasites and helminths, and allergic response and tissue repair (Th2), and type 3 responses against extracellular bacteria (Th17). T cells also facilitate refined humoral immunity through B cell cooperation in lymphoid germinal centers (Tfh) (100). Regulatory T-cells (Tregs) also act to terminate immune responses through the secretion of immunomodulatory cytokines like IL-10, among other mechanisms (8). Naïve CD4+ T-cells may differentiate into Th1, Th2, Th17, Treg,

or Tfh cells through the induction of transcriptional programs mediated by the transcription factors T-bet, Gata3, Rorgt, Foxp3, and Bcl6, respectively, following activation by an APC in the periphery (101, 102). While numerous T-cell subsets have been examined in recent years (e.g. Th22) and non-conventional T-cells such as invariant NKT (iNKT) and γδ T-cells, the discussion here will be limited to CD8+ T-cells and CD4+ Th cells Th1, Th2, Th17, Treg, and Tfh (102, 103).

APC activation of naïve CD4+ T-cells in the periphery results in differentiation into subsets which amplify the cytokine regime in the site of inflammation and can secrete additional cytokines to potentiate or circumscribe immune responses. In general, exposure to IL-12 and IFN-γ during APC activation may potentiate naïve CD4+ T-cells into Th1 cells, IL-4 to Th2, TGF-β, IL-6, IL-21, and IL-23 to Th17, IL-6 and IL-21 to Tfh, and TGF-β and IL-2 to Tregs. Th1 cells produce IFN-γ, Th2 produce IL-4, IL-5, and IL-13, Th17 produce IL-17A, IL-17F, IL-21, and IL-22, Tfh produce IL-21, whereas Tregs produce IL-10 and TGF-β. While this is true in the ideal sense, *in vivo* conditions may produce a range of T-cell subsets. The composition of the T cell response depends on the total composition of the cytokine milieu. For example, TGF-β can induce both Th17 and Treg differentiation depending on the nature of the cytokine milieu. In the presence of other inflammatory cytokines IL-6 and IL-21, Th17 differentiation is promoted while in the absence of inflammatory cytokines, Treg differentiation prevails (104).

CD8+ T-cells have distinct transcriptional programs and immune surveillance roles that promote direct T-cell killing of cells expressing nonself pMHC-I when activated in an inflammatory context. Upon activation, CD8+ T-cells expand and differentiate into cytotoxic effector T-cells that mediate target cell death. Cell death can be initiated via death receptor-ligand interactions through FAS and TRAIL, inflammatory IFN-γ and TNF cytokine production,

exocytosis of cytotoxic granules, and/or cytotoxic enzymes contained within granules such as perforin and granzymes (105). Transcription factors that are consequential for CD8+ T-cell function include inhibitory/repressive factors which promote exhaustion or limit effector differentiation like T-cell factor 1 (TCF1) and thymocyte selection-associated high mobility group box protein (TOX). Inflammatory transcription factors NFAT and FOS-JUN dimers (AP-1) allow for the production of cytokines like IL-2 and IFN-γ in CD8+ T-cells (105).

In αβ T-cells, the TCR is composed of an α and β subunit that each have three portions: a cytoplasmic, transmembrane, and cytoplasmic. The extracellular component of the TCR contains a variable immunoglobulin-like (V) domain that confers sequence-specific antigen recognition to the TCR via a complementarity-determining region (CDR) (106). A constant immunoglobulin-like (C) domain and connecting peptides in the extracellular TCR are common features among all TCRs (107).

The TCR interacts with cofactors that enable rapid signal transduction of APC activation through pMHC-I or pMHC-II interactions with the TCR. CD3 is the primary non-covalently associated cofactor of TCRs that form various heterodimers and homodimers to recruit other factors and transduce TCR signaling. CD3εδ and CD3εγ heterodimers associate with the TCR and span the cellular membrane with extracellular regions and intracellular regions with one immunoreceptor tyrosine-based activation motif (ITAM) on each subunit that recruits other transducing factors. CD3ζζ homodimers contain a transmembrane region and an intracellular region with *three* ITAMs. Upon antigen binding to αβ TCR, these ITAM domains are phosphorylated by the kinase Lck. The kinase ZAP-70 then binds phosphorylated ITAMs via its SH2 domains and is also phosphorylated and activated by Lck. ZAP-70 and Lck then phosphorylate additional signaling proteins to activate TCR-CD3-mediated signaling cascades

(108). Distal signaling pathways activated by TCR-CD3 complex signaling include the Ca^{2+}–calcineurin–NFAT pathway, the PKCθ–IKK–NF-κβ pathway, the RASGRP1–RAS–ERK1/2–AP1 pathway, p38, and JNK pathways, and the TSC1/2–mTOR pathway (107). TCR-CD3 complex activation after antigen binding also recruits Nck SH3.1 domains to the proline-rich sequence (PRS) in CD3ε. This interaction is not completely understood, but mutations in Nck that prevent the interaction result in impaired CD3ζ phosphorylation and reduced ZAP-70 binding and subsequent phosphorylation. Nck is also recruited to SLP-76 where it facilitates actin rearrangement, a necessary step in the formation of the immunological synapse. Nck also cooperates with its cofactor WASP in an interaction that is not well understood. TCR-CD3 signaling can be impeded by its cofactor Numb, which interacts with the E3 ligase Cbl and a site on CD3ε which crowds out Nck binding and facilitates internalization and degradation (108).

T-cell activation and differentiation also require the engagement of costimulatory molecules on T-cells with their corresponding ligands on APCs and unhealthy cells like tumor cells. These can be broadly classified as costimulatory molecules which promote T-cell activation and inhibitory molecules which inhibit activation or diminish active immune responses. Costimulatory-axis interactions like CD80/86-CD28, OX40-OX40L, 4-1BB-4-1BBL, GITR-GITRL, and CD40-CD40L cooperate with TCR signaling to potentiate T-cell response and survival. Inhibitory-axis interactions including PD-1-PD-L1, Tim-3-Galectin-9, CEACAM-1-CEACAM-1, and BTLA-HVEM, and CTLA4-CD80/CD86 impede T-cell activation when triggered. The balance between co-stimulatory and co-inhibitory molecules on T-cells ensures appropriate activation and eventual resolution of immune responses (109).

T-cell development begins with hematopoietic production of Lin^- c-Kit^{lo} Sca-1^{lo} $CD127^{hi}$ IL-$7R\alpha^{hi}$ $Flt3^{hi}$ common lymphoid progenitor (CLP) cells and Lin^- c-Kit^{hi} Sca-1^{hi} $Flt3^{hi}$ $CD127^-$

LMPPs which localize into the thymus via CCR9-mediated chemotaxis (110). Once in the thymus, interactions with thymic epithelial cells (TECs) and other stromal cells guide T-cell development through multiple stages. Immature T-cells, known as thymocytes, proceed through several stages of thymic differentiation (thymopoiesis) during which they express different canonical surface surrogate markers and are exposed to different microenvironments. αβ thymocytes proceed from double negative 1 (DN1) to DN3, over which time thymocytes modulate CD25 and CD44 expression from CD44+ CD25- "DN1", CD44+ CD25+ "DN2", to CD44- CD25+ DN3. DN1-DN3 thymocytes undergo V(D)J recombination at TCRβ chain genes that form half of the TCR. After TCRβ chain formation, thymocytes proceed to CD25- CD44- DN4, CD8+ CD4- ISP8, and to CD4+ CD8+ double positive (DP) stages. Over this period, TCRα chain genes recombine via V(D)J recombination. Combined TCRα and TCRβ chains are then tested for recognition of pMHC molecules; if assembled αβ TCRs fail to recognize pMHC molecules with high affinity, cells undergo apoptosis in a process deemed positive selection. Assembled TCRs are also tested for reactions against MHC molecules that present *self*-peptides. If TCRs are reactive against self-MHC, T-cells bearing those TCRs are removed via apoptosis through negative selection. Cells undergo positive and negative selection until they transition from DP to single-positive (SP) CD4+ or CD8+ T-cells (111). There is disagreement about the precise mechanism by which T-cells' CD4+ or CD8+ fate decision is regulated. There are two overall classes of models; the first model paints CD4/CD8 choice as dependent on instructive signals from MHC-I or MHC-II interactions with CD8 or CD4 coreceptors *or* as a random, stochastic choice between SP CD4+ or CD8+ (112). The second model postulates that DP thymocytes will downregulate *Cd8* only if CD8-dependent TCR signaling is lost, upon which *Cd4* will be upregulated to facilitate SP CD4+ T-cell development (113).

Promiscuous gene expression (pGE) of antigens associated with most tissues and cell types in the body by TECs allows for the establishment of central tolerance that eliminates self-reactive T-cells through negative selection and retains T-cells with TCRs reactive against nonself-peptides (114). Mediated by Aire and Fezf2, pGE-mediated presentation by TECs and thymic DCs offers a wide selection of self-antigens that if selectively bound by thymocyte TCRs cause autoreactive thymocytes to undergo apoptosis and be removed by thymic phagocytes following rapid calcium flux, migratory arrest, and Caspase 3 activation (115).

In V(D)J recombination, novel TCRα and TCRβ chains are generated that confer antigen specificity for T-cells through TCR-pMHC interactions. While TCRα chains are composed of variable (V) and joining (J) genes like antibody light chains, TCRβ chains are composed of V, J, and diversity (D) gene segment products in a structure analogous to antibody heavy chain construction (106). Catalytic action by recombination activating genes (RAG) 1 and 2 mediate DNA cleavage at recombination signal sequences (RSSs) that flank V(D)J regions on the chromosome. DNA breaks then recruit non-homologous end-joining (NHEJ) DNA repair machinery. Ku heterodimer binding to double-strand breaks (DSBs) precedes and enables DNA-PKcs, XRCC4, and XLF binding which help align DNA ends. However, due to the nature of the DSB, reconstitution of the original sequence is not possible. Artemis and TdT polymerase activity that elongates 3’ overhangs offer additional opportunities for diversity at V(D)J junctions. The final ligation of DSBs is performed by DNA ligase IV (116). T-cells that exit the thymus following V(D)J recombination of TCRα and TCRβ make up the T-cell pool with a diversity estimated to exceed 10^6 TCR sequences in humans (113).

T-cell Clonality, Diversity, and TIL-Peripheral Overlap in Antitumor Immune Response

T-cell responses play a key role in antitumor immunity by CD4+ T-cell amplifying inflammatory signaling to enervate innate immune tumor cell killing and CD8+ T-cell direct tumor cell lysis. Through V(D)J recombination, the endogenous T-cell pool consists of many unique "clonotypes" that each possesses a TCR that recognizes a unique peptide sequence that could correspond to any nonself-peptide presented on an MHC molecule. These TCR ligand peptides may be expressed in tumors and trigger immune responses that attempt to eliminate the tumor. Tumors may exclusively present antigens via MHC-I called tumor-specific antigens (TSAs) or present antigens that may also be presented on non-malignant tissue known as tumor-associated antigens (TAAs). Antigens may be wild-type sequences or possess non-synonymous amino acid substitutions resulting from somatic mutations including single-nucleotide variants (SNVs), nucleotide insertions and/or deletions (indels), and/or frameshift mutations. T-cells may recognize wild-type or mutant TSAs and TAAs as pathogenic and initiate immune responses against presenting cells.

While wild-type TSAs and TAAs have unaltered amino acid sequences, their corresponding proteins may still be unknown to the immune system and trigger nonself immune reactions. Tumor cell mutations and/or chromatin remodeling may lead to the reactivation of ontogenic expression that had been silenced since early organismal development. Mutant TSAs, also known as neoantigens, are also novel to the immune system and can similarly trigger T-cell immune responses. However, expression of co-inhibitory molecules such as PD-L1 on tumor cells may inhibit T-cell activation and allow tumor cells to elude T-cell-mediated cell killing. Furthermore, immune cell killing of tumor cells presenting TSAs, known as immune surveillance, may select for tumor mutations that confer resistance to T-cell immunity. These

adaptations include the downregulation or complete loss of expression of the TSA that drove the initial immune response and the downregulation of MHC molecules. Tumor cells that develop these adaptations may “escape” immune surveillance and proliferate with less or no immune impediments (117, 118).

T-cell antitumor responses are mediated through the clonal expansion of T-cells that recognize novel TSAs/TAAs, and the diversity of clonal responses represents a prognostic factor for cancer patients. T-cell TCR repertoires possess diversity and clonality, which are understood as the number of unique T-cell clones and the degree to which T-cell clones expand, respectively (119). The clonality and diversity of T-cell clonal responses can be assessed using single-cell resolution sequencing with cell barcodes, and single-rearrangement resolution sequencing with UMI barcodes for each primed gene, among other methods (120, 121). T-cell responses that are dominated by a single expanded clone are monoclonal and can be observed in T-cell responses in OT-I and OT-II mouse models which generate CD8+ and CD4+ T-cells, respectively. OT-I and OT-II cells overwhelmingly recognize the ovalbumin-derived peptide sequences SIINFEKL and ISQAVHAAHAEINEAGR, respectively (122). These monoclonal T-cell models represent the greatest clonality in T-cell responses. At the other extreme, idealized polyclonal T-cell responses have evenly distributed T-cell clonal expansion among all clonotypes. Idealized polyclonal T cell responses represent the T-cell response with the least clonality. In the clinic, T-cell antitumor clonal responses lie in between monoclonal and polyclonal expansion with the nature of the expansion suggesting the tumor antigenic profile and patient prognosis (118).

There is great diversity in potential TAAs/TSAs, but common, “public” TAAs/TSAs may be shared between patients. For example, chronic cytomegalovirus (CMV) and Epstein-Barr Virus (EBV) may lie dormant within cells for years and emerge during times of stress,

compromised immunity, and/or throughout aging. Through their onco-modulatory properties, CMV and EBV can directly contribute to oncogenesis (123). CMV and EBV-associated antigens are capable of mounting profound oligoclonal T-cell responses (124). For instance, T-cell responses against CMV and EBV may expand specific CD8+ T-cell clones to up to 40% of the peripheral repertoire (124).

In a 2020 study that examined T-cell clonal responses in ovarian cancer patients, the Odunsi group determined that tumor-infiltrating lymphocyte (TIL) clonality helps predict patient outcomes. For patients with a detectable immune response, represented by TAA-specific T-cell clonal expansion and TAA-specific antibody seropositivity, against the known TAA NY-ESO-1, greater TIL clonality conferred a favorable prognosis. However, without a detectable immune response against NY-ESO-1, greater TIL clonality was associated with negative outcomes. TILs may be retained in the periphery; the degree of overlap between TILs and peripheral T-cell clones may also serve as a prognostic factor. For NY-ESO-1 seropositive patients, greater overlap of TIL and peripheral T-cell clones is associated with a favorable prognosis while the opposite is true in seronegative patients (118). Greater expansion of tumor-periphery overlapping clones in response to immune checkpoint blockade (ICB) appears to correlate with favorable patient outcomes (119).

However, due to factors including differing analytical techniques, variation in T-cell repertoires between individuals, and diversity in tumor pathology, there is no consensus opinion about the prognostic potential of peripheral T-cell repertoire clonality and diversity. Contrasting with the Odunsi group's ovarian cancer findings, the Lawrence Fong group observed greater diversity and lesser clonality in peripheral TCR repertoires in non-small-cell lung cancer (NSCLC) patient responders to anti-PD-1 therapy (125). In clear cell renal cell carcinoma

(ccRCC), examined in Chapter 3 of this dissertation, the Leibowitz group determined that cancer recurrence was correlated with lower intratumoral T-cell clonality but made no claims on overlap with the periphery (126). While there is variability in interpretations, T-cell clonality and diversity play a role in determining the success of antitumor immune responses.

T-cell Metabolism in Immune Checkpoint Blockade

Upon T-cell antigen recognition, T-cells activate metabolic pathways that enable accelerated proliferation and increased immune effector molecule production. Activated T-cells transition from naïve to effector cells and shift from catabolic to anabolic metabolism to supply their bioenergetic needs. Upregulation of aerobic glycolysis and glutaminolysis supplies activated T-cells with a greater carbon pool to fuel the synthesis of complex biomolecules needed for the proliferation and fulfillment of effector programs. These pathways experience increased flux via increased expression of the glucose transporter GLUT1 and the glutamine transporter ASCT2 combined with upregulation of pathway catalytic enzymes HK2, PDK1, and LDHA among others (127). Activated T-cells also increase mitochondrial membrane potential ($\Delta\Psi_m$) in part to facilitate the production of inflammatory cytokines like IFN-γ and granzyme B by CD8+ T-cells, though activated CD4+ T-cells have been shown to increase $\Delta\Psi m$ to a greater degree than activated CD8+ T-cells (128, 129).

Activated T-cells share metabolic reprogramming aspects with cancer cells and compete for biosynthetic precursors to enable proliferation in the nutrient-deficient tumor microenvironment (TME). Indeed, T-cell activation is constrained by the lack of nutrients in the TME that results in antitumor immune suppression, metabolic reprogramming, and T-cell exhaustion. CD8+ T-cells in the TME are impacted by oxygen and nutrient scarcity and may

become exhausted, switching from glycolysis to FAO. Exhausted CD8+ T-cells also downregulate glutaminolysis and mitochondrial biogenesis while increasing ROS production (127).

Metabolic reprogramming of T-cells in the TME also alters lipid metabolism. Increases in lipid uptake and production of lipid and cholesterol pathway metabolic enzymes may even result in cell death. Upregulation of acyl-CoA synthetase long-chain family member 4 (ACSL4) may lead to ferroptosis because of lipid peroxide buildup (130). Furthermore, cholesterol metabolism modulation in TME T-cells through cholesterol acyltransferase (ACAT) and 3-hydroxy-3-methylglutaryl-coenzyme A reductase (HMGCR) has been implicated in T-cell exhaustion (131, 132). Metabolic limitations in the TME thus represent a major challenge to the effectiveness of T-cell immunotherapies that are intended to amplify T-cell antitumor responses such as immune checkpoint blockade (ICB).

ICB immunotherapy attempts to increase the antitumor potential of the immune system by abrogating or mitigating inhibitory signaling that tumor cells employ that allows them to escape immune surveillance. Common immunotherapies used in the clinic in patients with various advanced solid cancers include anti-PD-1, anti-PD-L1, and anti-CTLA4 monoclonal antibodies. These mAbs may be used in conjunction with traditional chemotherapies or with each other, and they act by binding immunosuppressive molecules on immune cells and tumor cells. By competing with the immunosuppressive intended ligands, ICB allows the immune system to ignore, to some extent, PD-1/PD-L1 and CLTA4-mediated immunosuppression. While ICB is a promising tool to treat cancer, the overall response rate of treated patients remains ~15-30%. Some molecules such as mismatch repair deficiency (dMMR) are used to predict patient response to ICB, but currently used biomarkers are relatively inaccurate and unreliable. The lack

of biomarkers that can *reliably* predict patient response to ICB represents a major unmet need in ICB therapy. Potential biomarker candidates may be found in T-cell metabolism, and the reversal of metabolic reprogramming of TME T-cells may be the key to increasing the effectiveness of ICB (127).

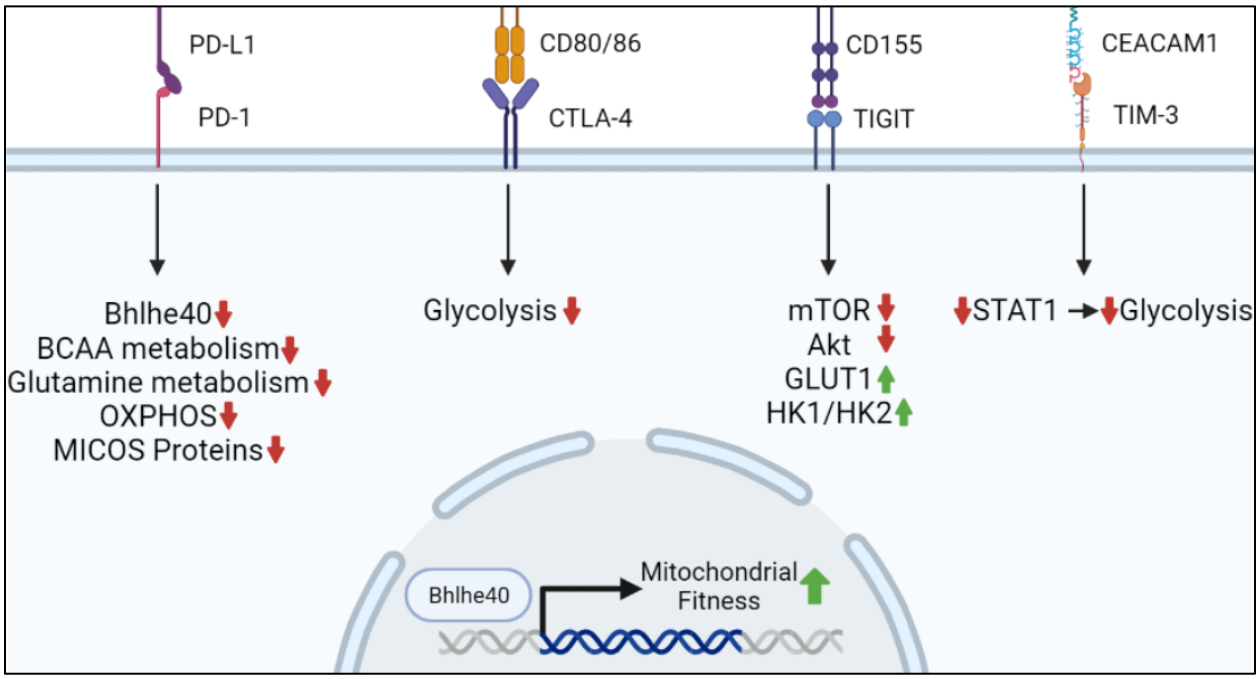

Figure 1.3. Metabolic Consequences of Select Co-Inhibitory Signaling Cascades in T-cells. Signaling through PD-1, CTLA-4, TIGIT, and TIM-3 generally results in decreased metabolic activity and reduced mitochondrial fitness. However, TIGIT signaling has been shown to increase GLUT1 and hexokinase expression. Treatment with α-CTLA-4/α-PD-1 ICB abrogates signaling through PD-1 and CTLA-4.

During immune checkpoint signaling, T-cell antitumor immune responses are undermined in part through changes to cellular metabolism. PD-1 signaling results in reduced OXPHOS and mitochondrial fitness through reduced expression of cristae junction-stabilizing MICOS-associated proteins. PD-1 binding also results in decreased expression of Bhlhe40, a TF that maintains the fitness of mitochondria in B16 melanoma model TILs (133). T-cells also rely less on branched-chain amino acids (BCAAs) and glutamine and elevate FAO metabolism in response to PD-1 signaling (134, 135). Signaling through another immune checkpoint, CTLA4,

similarly decreases glycolytic activity without affecting FAO (134). Immune checkpoints TIGIT and Tim3 also modulate T-cell metabolism to impair antitumor activity. TIGIT receptor-ligand interactions with CD155 reduce mTOR and Akt signaling and result in glycolytic enzyme expression, including GLUT1 and hexokinase (HK1/HK2) (136). Tim3-mediated signaling inhibits glycolytic activity via the STAT1 pathway and could also modify mTOR activity (137). The amplitude of immune checkpoint expression on T-cell membranes can be influenced by the metabolic characteristics of the TME beyond the aspects of hypoxia and nutrient deficit. High concentrations of cholesterol, lactate, and tryptophan and its metabolites in the TME promote the expression of T-cell PD-1 that abrogates antitumor responses (131, 138, 139).

While ICB alters T cell metabolism, metabolic biomarkers that accurately correlate with positive patient responses to ICB remain elusive. However, as more prospective studies are performed that examine new patient characteristics in new cancers, a paradigm of metabolic biomarkers for ICB response is emerging. In ICB-responding melanoma patients, peripheral blood mononuclear cells (PBMCs) exhibited greater glycolysis, FAO, tryptophan, and BCAA metabolism that serves to strengthen mitochondria in stressful environments, such as the TME. Those patients' CD8+ T-cells upregulated the glucose transporter 14 (SLC2A14) and lactate dehydrogenase C (LDHC), enzymes that both support greater glycolytic activity. Conversely, another study monitored overall LDH expression in melanoma patients receiving α-PD1 therapy and identified an association between higher LDH expression and mitigated patient survival. These contrasting results on the role of LDH as a prognostic factor indicate that care must be taken in future studies to isolate metabolic characteristics associated with specific immune subsets, such as the CD8+ T-cells in the former study. Additionally, urological cancer patients with elevated serum long-chain fatty acids and increased very long-chain acyl-CoA synthetase

(SLC27A2) expression responded more favorably to nivolumab. This is hypothesized to be due to VLC fatty acid-induced peroxisomal signaling that induces fatty acid catabolism. VLCFA supplementation therefore could be used in the future to potentiate urological cancer patients with more favorable ICB responses (140).

Beyond biomarkers that can be used to predict response to ICB, metabolism in T-cells has been targeted in preclinical studies to enhance the effectiveness of ICB. Metabolic areas of interest that have been examined include lipid, glucose, amino acid, and adenosine-implicated metabolic pathways. Inhibition of the human cholesterol esterifying enzyme ACAT results in the reversal of T-cell exhaustion and enhanced patient response to PD-1 blockade in hepatocellular carcinoma (141). Glucose-derived lactate also impacts ICB response; inhibition of the lactate transporter monocarboxylate transporter 1 (MCT1) results in greater antitumor activity resulting from ICB resulting from decreased Treg activity in the TME (138). Another avenue available to augment antitumor activity is through amino acid metabolism modulation; deficiency in tumor methionine transporter SLC43A2 increases antitumor efficacy by T-cells. A final example of successful metabolic modulation that unlocks greater ICB antitumor potential is adenosine metabolism. Primarily derived from adenosine triphosphate (ATP) catabolism, adenosine is enriched in the TME and inhibits T-cell antitumor activity in part through an intracellular buildup of cAMP. Inhibitors of the adenosine catabolizing enzymes CD73 and CD39 have shown perhaps the greatest potential of metabolic modulation to increase ICB-related outcomes. Inhibition of CD73 in advanced colorectal or pancreatic cancer patients combined with α-PD-L1 therapy durvalumab achieved clinical efficacy. Similarly, the anti-CD73 mAb BMS-986179 combined with nivolumab has shown efficacy in the treatment of advanced solid tumors, with 7 patients out of 59 achieving a partial response and 10 patients achieving stable disease (142). In

summary, many ongoing studies are attempting to identify potential biomarkers and metabolic interventions to respectively predict and amplify responses to ICB.

T-cell-Based Therapies for Clear Cell Renal Cell Carcinoma (ccRCC)

Renal cell carcinoma (RCC) is the 3rd most common global urological cancer, representing 3% of all female cancers and 5% of all male cancers with an incidence of ~400,000 new global cases annually. The most common subtype of RCC is clear cell renal cell carcinoma (ccRCC) which makes up 75% of all RCC cases, with the other major subtypes being papillary (20%) and chromophobe (5%) RCC (143). ccRCC is frequently associated with loss-of-function driver mutations in *VHL*, found in 82% of patients, which result in the accumulation of HIF-2α and constitutive hypoxic signaling and transcriptional programs in the absence of hypoxia (144). HIF activation leads to characteristically high angiogenesis and tumor vascularity through increased expression of anti-hypoxic genes such as *VEGF* (145). 3-6% of patients may also have mutations in *MTOR*, *PTEN*, or *PIK3CA* that informs the pursuit of mTOR inhibitors for the treatment of ccRCC (146). ccRCC also is associated with a high 40% mutational rate of Polybromo 1 (PRBM1), which encodes for the chromatin remodeler BAF180 that stabilizes SWI/SNF chromatin remodeling complex SWI/SNF-B (PBAF) (147). ccRCC tumors are characteristically immunogenic (“hot”) and contain a large amount of infiltrating immune cells including TILs that can be harnessed to enhance antitumor immune responses against ccRCC tumors (148).

The standard of care for ccRCC has evolved, with new biologic monotherapies and combination therapies approved by the FDA for first-line and second-line-plus treatment of ccRCC. VEGF-pathway tyrosine kinase inhibitors (TKIs) sunitinib, pazopanib, and cabozantinib

have been approved as monotherapies or combinations from the sunitinib approval for first-line therapy in January 2006 to combination cabozantinib/nivolumab approved in January 2021 (149). Given that 23-56% of ccRCC tumors express PD-L1, depending on assay type, there is potential benefit from ICB therapies as monotherapies or in combinations such as axitinib/pembrolizumab for all-risk patients that was approved for treatment of advanced RCC in April 2019 (150-152). Nivolumab (α-PD-1) monotherapy has been approved for second-line monotherapy, while nivolumab/ipilimumab (α-CTLA4) combination therapy (Ipi/Nivo) serves as the standard first-line treatment for intermediate/poor risk disease ccRCC patients (153, 154). Sunitinib may be preferable as a first-line therapy for patients with less aggressive disease, however (155). Other variations of ICB therapy combinations have also been approved for ccRCC therapy; pembrolizumab (α-PD-1) / nivolumab combination therapy is one such example.

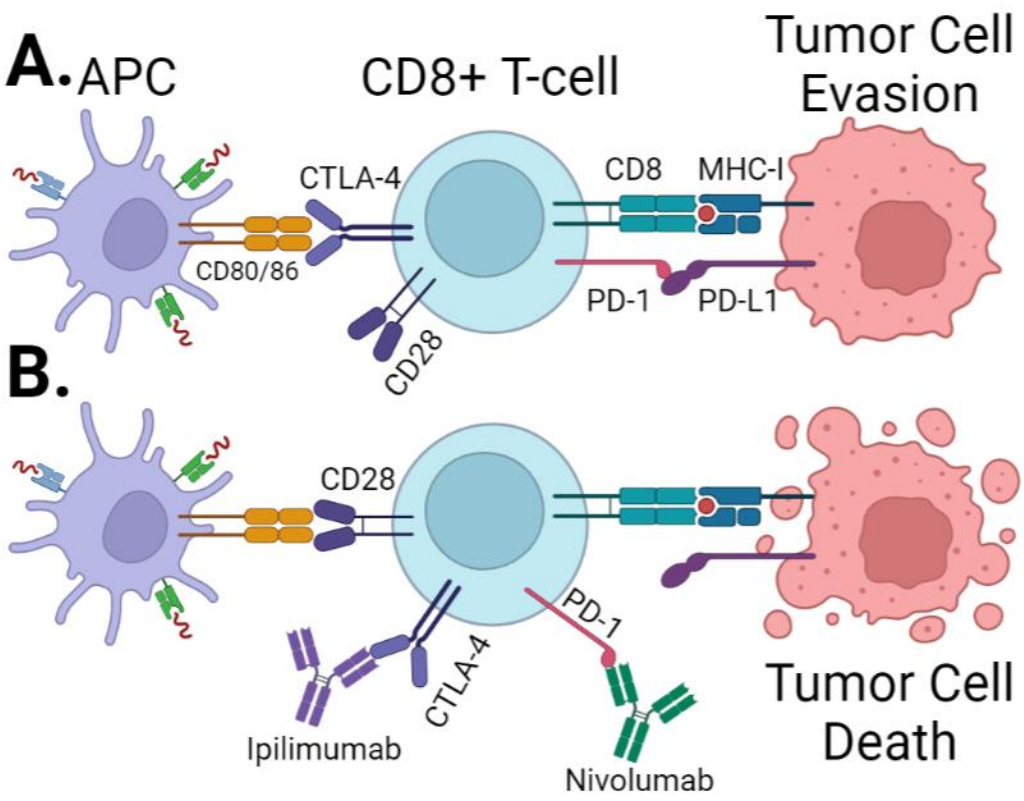

Figure 1.4. Ipilimumab/Nivolumab Immune Checkpoint Blockade Increases Intratumoral T-cell activation. (A) Tumor cells may upregulate PD-L1 to inhibit CD8+ T-cell

activation through binding to PD-1 that triggers immunoinhibitory signaling. CD80/86 expressed on antigen presenting cells (APCs) then preferentially binds to CTLA-4 which similarly inhibits CD8+ T-cell activation. **(B)** Treatment with α-CTLA-4 (Ipilimumab) and α-PD-1 (Nivolumab) binds to CTLA-4 and PD-1, idealistically preventing their binding to their usual ligands. The resulting lack of inhibitory signaling and the added co-activation signal from CD28 binding to CD80/86 increases CD8+ T-cell activation and cytotoxic capability.

For patients with relevant mTOR-pathway RCC driver mutations, the mTOR inhibitor temsirolimus was approved for first-line therapy in intermediate/poor-risk RCC patients (156). Also, while not approved for first-line treatment, the 2nd generation VEGFR TKIs tivozanib and axitinib were approved for the second-line-plus treatment of ccRCC patients (157, 158). Finally, combined therapy with axitinib/avelumab (α-PD-L1) was approved for all-risk patients with advanced RCC in May 2019 (159). While many options are available for ccRCC treatment, ccRCC has an overall poor prognosis with a high risk of metastasis; 30% of RCC patients have metastases when diagnosed while another 30% of RCC patients will develop metastatic disease during follow-up visits (143). While strictly localized RCC has high five-year survival rates between 70-90% dictated by disease stage, metastatic disease has an all-time five-year survival rate of 15.3% (160). New therapies are currently being assessed in clinical trials that harness T-cell antitumor potential against ccRCC to improve clinical patient disease outcomes.

The development of chimeric antigen receptor (CAR) T-cells may yield an effective therapy to treat ccRCC and improve patient outcomes. CAR-T-cells are engineered to directly recognize cell surface antigens and do not require MHC peptide presentation or costimulation to induce T-cell activation. While four generations of CAR-T-cells have been developed, CARs generally are composed of an extracellular single-chain variable fragment (scFv) that confers antigen specificity, an extracellular linking region, a membrane-spanning region, and a signaling domain within the cell. The CAR signaling domain contains ITAMs and other elements such as 1+ costimulatory molecules or cytokine inducers depending on the CAR generation that

increases the depth of T-cell activation. CAR-T-cells specific for CD19 are FDA approved for the treatment of hematological cancers with an impressive 90% CR rate in patients with CD19-positive B-acute lymphoblastic leukemia. However, exhaustion of CAR-T-cells may result in sub-optimal outcomes in certain cancers following CAR-T upregulation of coinhibitory receptors like PD-1, T-cell immunoglobulin, mucin domain-3, and LAG3. Furthermore, toxicities associated with CAR-T-cell therapy remain to be resolved in the clinic, comprising cytokine release syndrome (CRS), tumor lysis syndrome (TLS), neurological toxicity, off-target effects, and anaphylaxis (153, 161-163).

CAR-T-cell candidates for RCC therapy target tumor cells expressing ROR2, VEGFR2, CD70, c-MET, CalX, and Mucin 1 cell surface-associated C-terminal and are all either Phase I or Phase II clinical trial stage in development. The rationale behind these targets is usually based on antigenic targets that are highly expressed in ccRCC or are associated with negative outcomes in ccRCC. While no data is available yet relating to ccRCC patient response rate to CAR-T-cell therapy, trials examining the products P-MUC1C-ALLO1, CCT301 ROR2 CAR-T, COBALT-RCC CD70 CAR-T, TRAVERSE CD70 CAR-T, CalX CAR-T, Anti-VEGFR2 CAR-T will have endpoints that will provide some level of patient response documentation in the coming years (153).

Introduction to Single-cell Resolution Sequencing Techniques

Invented in 2009, single-cell resolution RNA sequencing (scRNA-seq) captures gene expression on a single-cell level, allowing for the discovery and interrogation of rare populations that may be consequential for disease pathogenesis (164). scRNA-seq involves the procedural isolation of individual cells or nuclei from a suspension, lysis of those individual cells, reverse

transcription of single-cell transcriptomes into cDNA, amplification of cDNA, library preparation, and finally deep sequencing of the library. Library preparation steps may vary between scRNA-seq modalities while cells may be isolated through microfluidics, microwell, or droplet-based technology. Individual RNA molecules can be traced back using random n-mer adaptors called unique molecular identifiers (UMIs) introduced during the reverse transcription (RT) step. Similarly, all RNA molecules captured from a single-cell may be barcoded back to that individual cell. By using UMI barcodes associated with individual RNA molecules and origin single-cells, scRNA-seq is now able to compensate for amplification-associated bias that formerly arose in poly(A)/poly(C) 5' DNA end ligation to provide common amplification adaptors as well as IVT as used in CEL-seq, MARS-seq, and inDrop-seq. The formerly most common method of cDNA amplification method relies on SMART technology based on Moloney Murine Leukemia Virus reverse transcriptase to introduce template-switching oligos during RT for future PCR amplification. During RT, the introduction of universal PCR amplification adaptors allows for less biased and more easily normalized cDNA amplification (165).

Data obtained from scRNA-seq experiments are high-dimensional, and analysis of that data is computationally expensive. Assuming a general yield of ~10K cells with thousands of genes quantified per cell, data can easily consist of millions of individual datapoints that must be quality-controlled, normalized, and dimensionally reduced to be comprehensible. While standards differ between groups, general guidelines for scRNA-seq quality control (QC) include percent mitochondrial gene filtering, number of detected genes (nGenes) filtering, and number of UMIs (nUMIs) filtering. QC parameters may need to be adjusted from defaults depending on the experiment-specific or cell type-specific gene and UMI distribution. Example parameters for QC

from a 2018 *Nature Methods* paper by Lambrechts *et al.* are 100 ≤ nGenes ≤ 6000, ≤ 200 UMIs, and ≥ 10% mitochondrial genes (166). While nGenes and nUMI cutoffs are intended to remove low-quality cells with inefficient overall gene capture, percent mitochondrial gene content is limited to eliminate cells from the analysis that are dead or dying. Enrichment of mitochondrial transcripts is associated with cell stress, apoptotic, and/or low-quality cells (167). However, attention must be paid to the specific cell type being examined, as certain cells like cardiomyocytes may naturally express higher mitochondrial gene content ranging from 58-86% of total transcripts that does not necessarily indicate cell stress (168).

After initial QC, scRNA-seq is often normalized to mitigate technical noise and dimensionally reduced using a combination of principal component analysis (PCA) followed by either t-distributed stochastic neighbor embedding (t-SNE) or uniform manifold approximation and projection (UMAP) that collectively reduces the thousands of potential dimensions into two graphically accessible t-SNE/UMAP dimensions. PCA overcomes technical noise to identify "principal components" (PCs) which represent a linear set of experimental variables that are uncorrelated within the dataset, with most of the information contained within the first components. t-SNE and UMAP then take these PCs and reduce them to two dimensions for ease of visualization, gene expression overlays, cell clustering, and more. UMAP has certain advantages over the older t-SNE, including faster run times, greater preservation of the global transcriptional structure, and more consistency in cell clustering patterns between different runs; however, t-SNE remains popular due to different aesthetics, integration in older platforms, and familiarity vis-à-vis UMAP (165).

Following PCA, t-SNE, and/or UMAP-based dimensional reduction, cells are clustered using algorithms like *SC3*, *Seurat*, and *FlowSOM*. Clustering is intended to capture biologically

relevant cell subpopulations with similar gene expression profiles. In general, cells with more similar transcriptomes will cluster together, while cells with disparate transcriptomes will be more distant from one another in UMAP/t-SNE space (165).

Additional steps may be performed depending on experiment-specific analysis goals. Common steps following clustering include expert gating of cell populations to identify what cell types are contained within each cluster. Expert gating may involve graphically overlaying cell type surrogate marker gene expression on t-SNE/UMAP space and differential gene expression analysis to identify most upregulated or downregulated genes vs. other clusters. Expert gating can also be assisted by algorithms capable of autonomous clustering and assigning cell types to cells in t-SNE/UMAP space. These include algorithms *Seurat, scmap, SingleR, CHETAH, SingleCellNet, scID, Garnett, SCINA, CP,* and *RPC,* which were profiled in a 2020 paper by Huang *et al* (169). Of these, *Seurat* performed the best at identifying major cell types but performed worse at identifying rarer cell populations as well as telling the difference between relatively similar cell types (169).

The wealth of data supplied by scRNA-seq has allowed for the development and utilization of algorithms that can assess overall transcriptional programs through TF motif identification, cell development trajectories in pseudotime space, infer intercellular communication networks, and much more. *SCENIC* is an algorithm implemented in *R* and *python* script which identifies TF motifs on recovered RNA molecules. While computationally expensive, *SCENIC* can infer the activity of TFs that may have low mRNA expression at any point in time (170). Additionally, exploratory algorithms can compare the differentiation state between all cells in a scRNA-seq experiment to identify consensus trajectories that originate in more naïve clusters and terminate in more differentiated cell clusters. Cell processes such as

hematopoiesis and thymopoiesis can be examined using these algorithms, including *p-Creode* and *Monocle* with the potential of finding rare progenitor and/or transitory cell populations (171, 172). A final example of exploratory algorithms in scRNA-seq is cell-cell communication analysis algorithms like *CellChat*, *CellPhone DB*, and *SingleCellSignalR*. These algorithms have individual strengths and weaknesses that integrate information on the relative expression of receptors and cognate ligands, receptor/ligand structural composition, and regulation by stimulatory or inhibitory cofactors to infer intercellular communication networks at single-cell resolution (165).

Single-cell technology has also evolved to characterize cellular features beyond RNA, such as chromatin accessibility, methylation, and cell surface protein expression on a single-cell basis. Single-cell assay for transposase-accessible chromatin (scATAC-seq) can reveal consequential changes to chromatin accessibility resulting from epigenetic modifications (173). Complementing that assay, single-cell methylome and transcription sequencing (scMT-seq) can be used to assess DNA methylation and RNA transcription from single-cells (174). CITE-seq may be used to complement traditional scRNA-seq by quantifying individual cells' cell membrane protein expression. Differences between single-cell RNA and protein may reveal underlying post-transcriptional or post-translational processes that are biologically relevant (175). A final example of novel single-cell technologies is single-cell V(D)J-seq (scV(D)J-seq), which can sequence T-cell receptor-encoding genes from individual cells. High-resolution sequencing of T-cell responses using scV(D)J-seq can be used to understand T-cell responses in detail. This technology may be used to identify public T-cell clones, tumor-associated T-cell clonal sequences, clonality and diversity of T-cell clonal responses, and public antigens if there

is a small enough pool of potentially immunogenic peptides (176). Individual B cell receptor sequences in B cells can similarly be profiled using technology like LIBRA-seq (177).

While single-cell technology offers many benefits, the *in-silico* findings from these experiments must be reinforced and confirmed by *in vitro* and/or *in vivo* examination of the identified cell phenotype. Like any other experimental modality, single-cell technology is also subject to potential technical pitfalls that limit interpretations of data beyond the quality control measures mentioned earlier. Inefficient capture of RNA molecules post-lysis may miss a significant portion of cellular RNA pools, leading to biases in downstream amplification (178). Low-to-moderately expressed genes may also be detected sparsely in cells of the same type in a phenomenon known as "dropout". While genes may be stochastically expressed between cells of the same type, inefficiencies in mRNA capture confound whether dropout is biologically relevant or a technical artifact. Analysis programs attempt to address dropouts using implicit methods like dimension reduction or explicit methods like imputation, a process that attempts to assign appropriate expression values of dropout genes based on the expression patterns of highly variable genes in a dataset (179). While single-cell methods have the potential to identify rare populations that contribute to disease pathogenesis, much work remains before single-cell methods may be used as a standalone tool in biological research.

Outstanding Questions and Rationale for Dissertation Research

The intersection between hematopoietic metabolism, differentiation, and cell function remains incompletely understood. While it is known that HSCs and T-cells both regulate metabolic pathways to influence their differentiation potential and functional programs, targeting hematopoietic cell metabolism is largely untested and has the potential to improve their immune

function and/or therapeutic efficacy. Furthermore, deciphering the relationship between metabolic flux and epigenetic regulation of gene expression could reveal tools to direct HSC self-renewal and fate decisions and preserve T-cell effector function despite immunosuppressive metabolic headwinds experienced in the TME.

Metabolic regulation of HSCs is necessary for hematopoietic lineage commitment and the maintenance of self-renewal capabilities. Metabolic interventions in the hematopoietic compartment offer the potential for enhancing a desired fate decision or enhancing or prolonging HSC capacity for self-renewal. In the case of autologous and allogeneic stem cell transplant (ASCT) recipients, myelopoiesis post-transplant is already enhanced through treatment with G-CSF and/or chemotherapy to quickly replenish the innate immune compartment. However, for 5-40% of ASCT recipients, these conventional mobilization agents generate insufficient peripheral immune cells (180). In Chapter 2, we demonstrate the myeloproliferative effects of *in vitro* Acly inhibition on murine hematopoietic stem cells and progenitors that could serve as a model for future metabolism-based ASCT mobilization regimens.

The mechanisms that connect epigenetic regulatory and metabolic systems are also poorly understood. While metabolic enzymes like ACLY and ACSS2 both supply acetyl-CoA as a substrate to epigenetic modifiers, deficiencies in those enzymes may result in site-specific changes to histone acetylation marks at certain genes which potentially influences cell development (76, 181, 182). Acly expression can be increased in response to high concentrations of carbohydrates and is downregulated in response to high-fat feeding in rats and mice, respectively (183, 184). The metabolic microenvironment in the hematopoietic niche may impede epigenetic enzymes' activities and/or expression, contributing to hematopoietic maintenance and fate decisions.

In Chapter 3, we present our preliminary findings regarding T-cell clonal responses to ccRCC and factors which correlate to positive patient outcomes. Robust biomarkers that allow for the prediction of ccRCC patient response to ICB have not been identified, and the discovery of response prognostic factors would offer great utility to ccRCC patients. While previous studies have examined ccRCC patients' tumors and periphery using single-cell methods, we employ a novel multi-omic approach that integrates several single-cell methods to answer outstanding questions about how mitochondrial membrane potential ($\Delta\Psi m$) influences T-cell responses in ccRCC. While some studies have shown that $\Delta\Psi m$ low CD8+ T-cells have increased antitumor immunity and longer survival *in vivo*, others have demonstrated that co-culture of tumor cells with CD8+ T-cells resulted in a lowering of $\Delta\Psi m$ and the development of dysfunctional mitochondria. Furthermore, low and high extremes of $\Delta\Psi m$ are associated with cytochrome c-mediated apoptosis and increased ROS, respectively, with both being negative indicators for CD8+ T-cell function (185-187). Our examination of $\Delta\Psi m$ in T-cell responses to ICB in ccRCC patients will help determine the role of $\Delta\Psi m$ in this context.

Our findings may apply to metabolic influences on T-cell immunity in cancers beyond ccRCC and could inform questions on how to potentiate the CAR-T-cell therapies being developed for ccRCC treatment for improved antitumor immune responses. Furthermore, combined multi-omic profiling of ccRCC patient T-cells may reveal common TCRs shared between patients, the metabolic characteristics and gene signatures of tumor-associated peripheral T-cells, and patient differences in clonality of T-cell responses to ICB. Collectively, these studies offer insight into the role of mitochondrial metabolism on hematopoietic cell differentiation and function.

CHAPTER 2: ACLY DEFICIENCY ENHANCES MYELOPOIESIS THROUGH ACETYL-COA AND METABOLIC-EPIGENETIC CROSSTALK

This chapter is adapted from "Acly Deficiency Enhances Myelopoiesis through Acetyl Coenzyme A and Metabolic-Epigenetic Cross-Talk" published in Immunohorizons *and has been reproduced with the permission of the publisher and my co-authors.*

Originally published in *Immunohorizons*. *Dalton L. Greenwood, Haley E. Ramsey, Phuong T. T. Nguyen, Andrew R. Patterson, Kelsey Voss, Jackie E. Bader, Ayaka Sugiura, Zachary A. Bacigalupa, Samuel Schaefer, Xiang Ye, Debolanle O. Dahunsi, Matthew Z. Madden, Kathryn E. Wellen, Michael R. Savona, P. Brent Ferrell, and Jeffrey C. Rathmell.* 2022. Acly Deficiency Enhances Myelopoiesis through Acetyl Coenzyme A and Metabolic-Epigenetic Cross-Talk. *Immunohorizons* 6: 837-850.

Introduction

Cell differentiation allows long-term maintenance of populous short-lived cell types derived from more durable and rare stem cells. Stem cells respond to a combination of cytokine innervation, metabolic activation, and epigenetic changes to generate various cell types as needed (189-191). Hematopoietic stem cells (HSCs) reside within hypoxic, perivascular bone marrow (BM) niches surrounded by mesenchymal stromal cells, non-myelinating Schwann cells, megakaryocytes, macrophages, CXCL12-abundant reticulocytes, and other cells (192). These cells and local nutrients provide the mixture of microenvironmental metabolites and cytokines that promote hematopoiesis. Step-by-step relationships between hematopoietic progenitors demarcated by surrogate markers have been painstakingly established over time. However, hematopoiesis is a fluid landscape with a gradient of differentiation regulated by intersecting systems of cellular metabolism and epigenetic homeostasis that remain incompletely understood. Metabolic hubs including the tricarboxylic acid cycle (TCA-cycle) are closely connected to epigenetic regulation of gene expression and supply essential substrates such as S-adenosyl methionine, acetyl-CoA, and α-ketoglutarate which facilitate methylation, acetylation, and demethylation respectively (91). Understanding how metabolic and epigenetic stimuli influence

hematopoiesis will help build a more comprehensive paradigm of cellular development and stimulate new therapeutic approaches against disease.

While cytokines are the primary drivers of hematopoiesis, metabolic activation, and epigenetic intervention also influence these pathways to guide hematopoietic cell fate decisions (193, 194). It has been recognized that metabolic activation itself can also decrease stem cell potential and induce differentiation. Acetyl-CoA provides the substrate for lipid synthesis and protein acetylation reactions and derives from numerous bioenergetic pathways including glycolysis, fatty acid oxidation, amino acid deamination, TCA cycle flux, and acetate. Histone acetyltransferases (HATs) catalyze the addition of acetyl groups to histone tails and are sensitive to changes in the concentration of their primary substrate, acetyl-CoA. When the intracellular concentration of acetyl-CoA is at its nadir, the enzyme velocities of HATs decrease to alter the steady-state maintenance of histone acetylation and chromatin accessibility (91). Aberrant acetylation in hematopoiesis by HATs such as GCN5, CBP/p300, and MOZ has been implicated in transforming healthy hematopoietic stem cells and precursors into hematologic malignancies (195-197).

ATP Citrate-Lyase (Acly) catalyzes the reaction of ATP, citrate, and coenzyme A (CoA) into ADP, inorganic phosphate, acetyl-CoA, and oxaloacetate. Acly reactions are key contributors to the cytosolic nuclear pools of acetyl-CoA and are the primary path for acetyl-CoA derived from mitochondrial citrate. Acly represents one of several sources of cellular acetyl-CoA that contribute to histone acetylation (198, 199). The relative roles of these pathways, however, are poorly understood. Acly expression may play an important role in myeloid differentiation and myeloid cell function, as increased PU.1 was associated with reduced Acly expression and regulation of the cell cycle in a myeloid cell line (77). The impact of Acly is

not limited to myeloid cells as Acly has been noted as a regulator of CD8+ T-cell function, early CD8+ T-cell differentiation, and osteoclast differentiation (181, 200, 201).

Here we sought to test the role of Acly in the differentiation of primary hematopoietic stem and progenitor cells. Inhibiting Acly with the small-molecule inhibitor SB-204990 (SB2) or genetically deleting Acly in lineage-depleted and c-Kit enriched HSPCs led to increased myeloid differentiation in cytokine-replete methylcellulose media. Single-cell RNA and Assay for Transposase-Accessible Chromatin (ATAC) sequencing of HSPCs treated with SB2 showed altered gene expression and chromatin accessibility with increased myeloid cell abundance consistent with a role for Acly in the epigenetic regulation of HSPCs. Mechanistically, multiple members of the C/EBP TF family were affected and may contribute to increased myelopoiesis. Acly inhibition resulted in increased *Cebpe* and reduced *Cebpa* and *Cebpb* gene expression by qRT-PCR and increased chromatin accessibility at C/EBP TF binding sites by scATAC-seq. Mitochondrial metabolism was also altered and acetate restored normal myeloid differentiation to suggest that Acly inhibition resulted in limiting levels of acetyl-CoA. Acly thus contributes as one pathway to acetylation in hematopoiesis and can regulate myeloid differentiation through metabolic regulation of epigenetic marks and myeloid gene expression.

Results

Inhibition of ATP Citrate Lyase promotes myelopoiesis

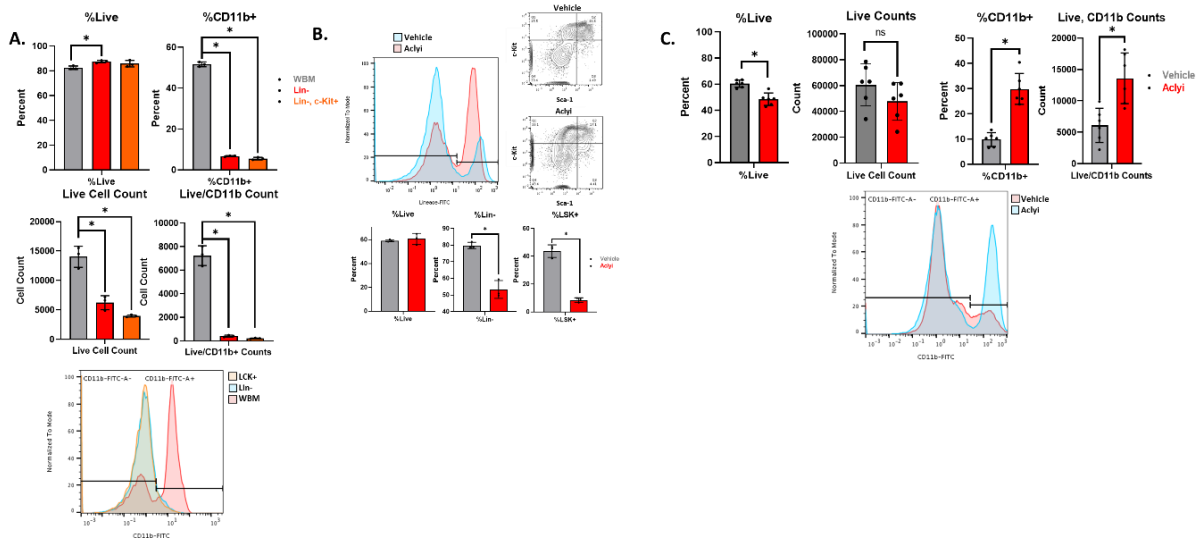

Figure 2.1. Acly inhibition drives CD11b expression in Methylcellulose-cultured Lin- HSPCs. (A) Whole BM cells were compared to lineage-depleted and lineage-negative, c-Kit enriched HSPCs by flow cytometry and evaluated for viability and CD11b expression with representative histograms (n = 3 mice). **(B, C)** MC-cultured HSPCs cultured with vehicle or Aclyi (SB204990) were analyzed by flow cytometry for viability and (**B**) stem cell markers (n = 3 mice) and (**C**) myeloid integrin CD11b (n = 6 mice) with representative histograms. Significance was judged using Student's two-tailed parametric t-test. Error bars represent standard deviation.

To test the role of Acly in hematopoiesis, hematopoietic stem and progenitor cells (HSPCs) were fist isolated by lineage depletion and c-Kit enrichment. We depleted cells expressing a surrogate marker for myeloid differentiation CD11b from BM (**Figure 2.1A**) (202-204). HSPCs were then cultured in cytokine-replete methylcellulose media (MC-cultured) for two weeks in the presence of vehicle or Acly inhibitor (Aclyi) SB204990 at 30 μM, a concentration previously used to provide a near-complete inhibition of glucose-derived lipid synthesis (205, 206). Cells were stained for lineage markers αCD3, αGr-1, αCD11b, αCD45R, and αTer-119 as well as Sca-1 and c-Kit that indicate the canonical LSK compartment that is enriched in stem cells (206, 207). Aclyi resulted in a significant decrease in lineage-negative,

Sca-1+, c-Kit+ (LSK+) cells (**Figure 2.1B**). We then asked which lineages Aclyi increased by assessing CD11b expression in MC-cultured HSPCs. Despite a modestly decreased viability, live cell numbers were unchanged and Aclyi significantly increased the frequency and number of myeloid CD11b+ cells to indicate a shift toward myelopoiesis in culture (**Figure 2.1C**). This effect was observed as early as day 4 of cell culture with high doses of SB204990 (**Figure 2.2**).

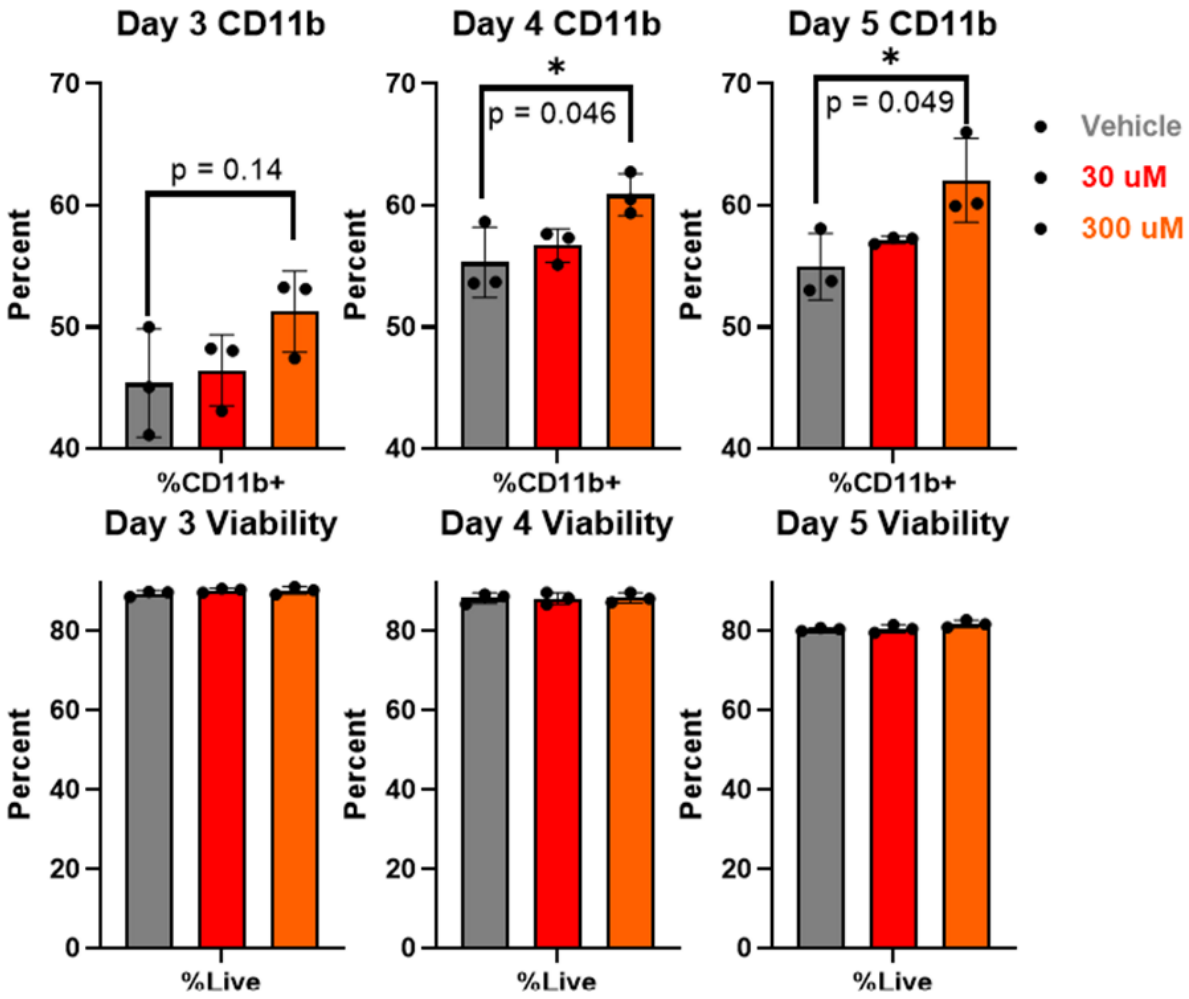

Figure 2.2- Aclyi increases HSPC CD11b expression at Days 3-5 in culture 1E4 Lin- depleted, c-Kit+ HSPCs were cultured in methylcellulose for 3, 4, and 5 days with Vehicle, 30 μM Aclyi, and 300 μM Aclyi. n=3 mice per treatment group, monitored over 3, 4, and 5 days. Significance was judged using Student's two-tailed parametric t-test. Error bars represent standard deviation.

Genetic deletion of ATP Citrate Lyase promotes CD11b+ myelopoiesis while suppressing Mast-like cells

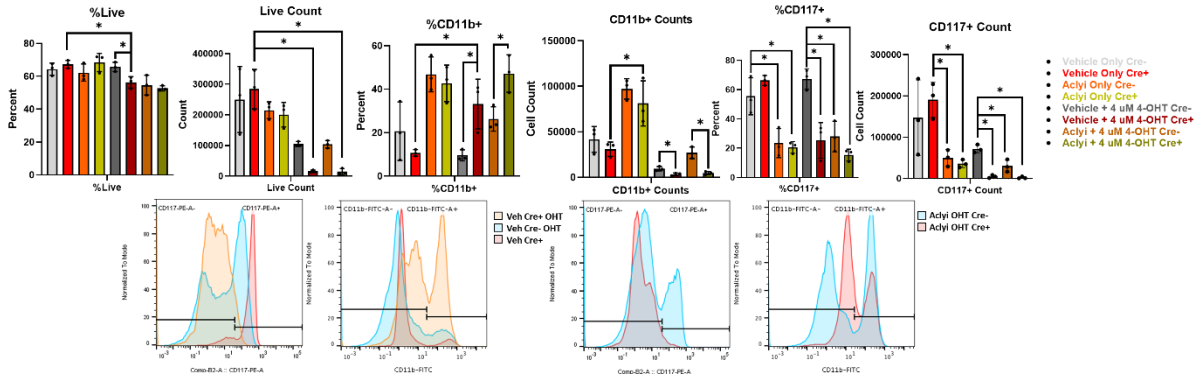

Figure 2.3. Acly deficiency drives CD11b while suppressing CD117 expression in Methylcellulose-cultured Lin- HSPCs. *UBC-Cre ERT2; Acly f/f* and *Acly f/f* HSPCs were treated with combinations of 4-hydroxytamoxifen (4-OHT), Aclyi, and DMSO and cultured for two weeks (n = 3 mice). Cells were assessed for CD11b, CD117, and viability by Fixable Viability Dye e780 by flow cytometry. Significance was judged using Student's two-tailed parametric t-test. Error bars represent standard deviation.

To corroborate that small-molecule inhibition of MC-cultured HSPCs resulted in increased myeloid differentiation, we tested if acute genetic deletion of Acly led to similar shifts toward myelopoiesis (**Figure 2.3**). *Acly* was genetically deleted using a UBC-Cre-ERT2 +/- *Acly f/f* model with tamoxifen-inducible *Acly* deletion by treating isolated HSPCs with 4-hydroxytamoxifen (4-OHT). Deleting *Acly* resulted in a significant increase in the percentage of CD11b+ cells that mirrored the percentage of CD11b+ myeloid cell increases induced by Acly small-molecule inhibition. Small-molecule inhibition of Acly in combination with Acly-deletion further increased the proportion of myeloid CD11b+ cells in MC-cultured HSPCs. This additive effect may be due to incomplete deletion of *Acly* or non-Acly effects of SB204990. Interestingly, while inhibition of Acly did not result in decreased overall cell numbers, treatment with 4-OHT and genetic deletion of Acly reduced total live cell numbers although with an increased frequency of CD11b+ cells. Both Aclyi and genetic deletion of *Acly* resulted in a significant reduction in the numbers and percentage of c-Kit (CD117) expressing cells (**Figure 2.3**). These

CD117+ cells most likely represent stem and progenitor or Mast cells, which often comprise HSPC-descended cells in methylcellulose cultures (208, 209).

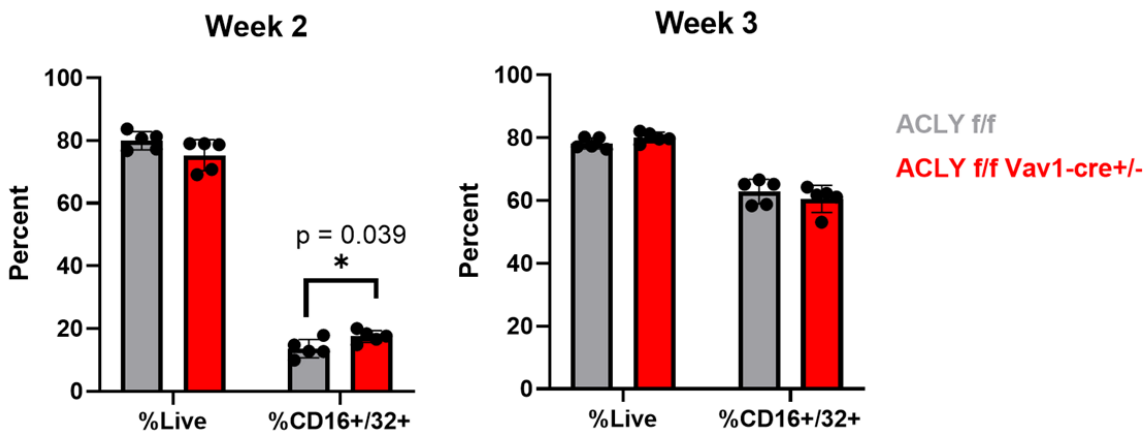

Figure 2.4 - Acly deficiency increases CD16/32 expression at Week 2 in a BM transplant. Whole BM from either *Acly* f/f or *Acly* f/f Vav1-cre+/- animals were transplanted into CD45.1 recipients. Recipients were taken down every week post-transplant to determine the viability and percent of cells expressing CD16/32 (FcγRIII). n=5 mice per treatment group per week. Significance was judged using Student's two-tailed parametric t-test. Error bars represent standard deviation.

To determine the role of Acly *in vivo*, we assessed demand-induced myelopoiesis in Acly-deficient BM chimeras using hematopoietic-specific, *Acly f/f Vav1-cre+/-*, Acly deficient BM chimeras. *Acly f/f Vav1-cre+/-* or *Acly f/f* BM was transplanted into lethally irradiated BL/6 CD45.1 hosts, and recipient BM was characterized by flow cytometry at 14 and 21 days post-transplant. Acly deficiency in *Acly f/f Vav1-cre+/-* BM recipients resulted in a modest initial increased CD16/32 (FcγRIII) expression consistent with Acly suppression of myelopoiesis, although B and NK cells may have also contributed to increased CD16/32 expression (**Figure 2.4**). One week later, myelopoiesis had increased in both control and Acly-deficient cultures and this difference was no longer apparent. The effect of genetic Acly-deficiency was modest and transient, demonstrating that Acly-independent pathways can compensate for Acly loss to generate cytosolic acetyl-CoA *in vivo*. Acly may thus act in concert with other pathways, such as

Acyl-CoA synthetase short-chain family member 2 (Acss2)-mediated conversion of acetate to acetyl-CoA, to influence hematopoietic differentiation under stressful or non-steady-state conditions following stem cell transplant with the effect of Acly compensated over time.

Acly inhibition promotes macrophage and neutrophil differentiation.

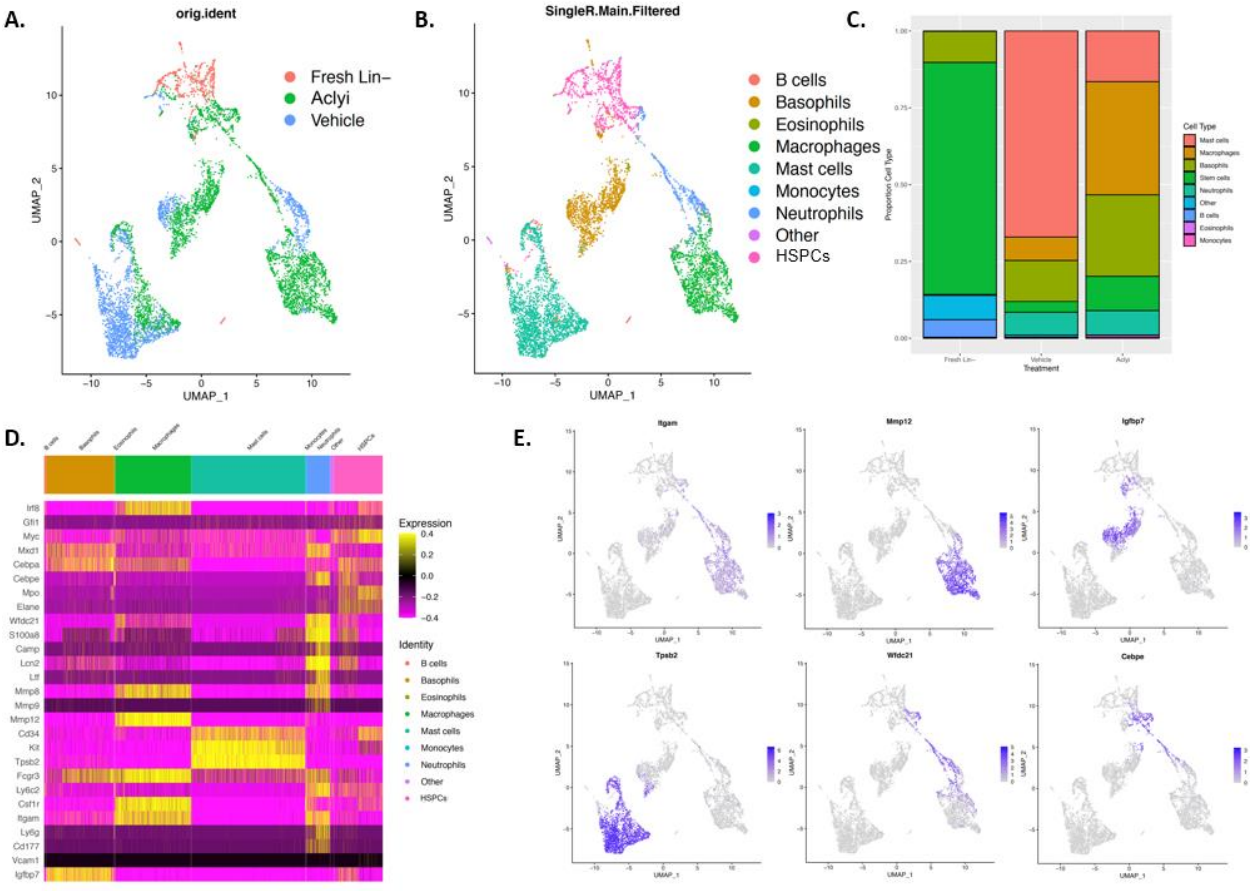

Figure 2.5. Acly inhibition drives Macrophage differentiation in Methylcellulose-cultured Lin- HSPCs. Lineage-negative HSPCs were cultured for two weeks with vehicle or Aclyi and assessed using single-cell RNA-seq. Cells from scRNA-seq are plotted in UMAP dimensional reduction depicting **(A)** original treatment sample IDs and **(B)** cell types defined by SingleR. **(C)** SingleR-defined cell types were quantified and graphed as a proportion of total cells per treatment. **(D)** Canonical cell type-associated gene expression from SingleR-identified cell types was plotted in a heatmap. **(E)** Canonical cell type-associated gene expression was overlaid over UMAPs.

To better understand how Aclyi affected HSPC cell populations and gene expression, single-cell RNA and ATAC sequencing (scRNA-seq and scATAC-seq) were performed. Freshly isolated and lineage-depleted C57BL/6 BM and MC-cultured lineage-depleted BM cells were treated with either Aclyi or vehicle before scRNA-seq (**Figure 2.5A-C**). Cell cluster identities were assigned using the software package SingleR, which compares scRNA-seq transcriptomes to bulk RNA-seq transcriptomes of expert-gated, sorted immune populations from the ImmGen database (210, 211). While the use of SingleR assigns clusters of differentiating cells from our cultures to defined and often mature cell populations that may not be fully equivalent, it nevertheless provides an unbiased approach to infer cell lineage and identity. These clusters consisted of B cells, basophils, eosinophils, macrophages, Mast cells, monocytes, neutrophils, HSPCs, and "other," with "other" comprising a minority of cells that had no viable comparisons to the ImmGen database using SingleR (**Figure 2.5B, C**). Most cells in the vehicle-treated HSPCs were categorized as Mast cells, and treatment with Aclyi increased the proportion of macrophages while suppressing Mast cell differentiation (**Figure 2.5C**). These MC-cultured HSPCs share gene expression similarities with canonical myeloid gene expression profiles and expert gating of scRNA-seq data revealed that expression of cell type-associated genes correlated with SingleR-identified cell type clusters (**Figure 2.5D, 3E**) (212).

	Cell Type									
	Mast Cells		Macrophages		Basophils		Neutrophils		HSPCs	
Rank-ordered Average Regulon AUC	TF	Mean AUC	TF	Mean AUC	TF	Mean AUC	TF	Mean AUC	TF	Mean AUC
1	Creb3l1	1.202	Mafb	1.786	Klf5	1.678	Ets2	2.238	Hdac2	1.87
2	Hes1	1.196	Bhlhe41	1.747	Nfil3	1.532	Relb	2.203	E2f4	1.834
3	Ahr	1.177	Atf3	1.74	Ets1	1.458	Irf7	2.08	Tfdp1	1.808
4	Pgr	1.125	Maf	1.729	Xbp1	1.303	Ltf	2.075	Myc	1.774
5	Patz1	1.119	Usf2	1.678	Creb3l2	1.295	Nfkb2	2.073	Trp53	1.729
6	Egr1	1.107	Mef2a	1.677	Arnt2	1.234	Cebpd	2.037	Klf1	1.726
7	Fosb	1.089	Nfe2l2	1.673	Foxq1	1.139	Pparg	1.958	Cebpz	1.715
8	Tal1	1.078	Etv1	1.516	Cebpa	0.981	Cebpe	1.875	Gtf2f1	1.551
9	Fos	1.077	Irf5	1.505	Zfp467	0.962	Fosl1	1.854	Ezh2	1.548
10	Gata1	1.074	Tcf7l2	1.42	Creb3	0.943	Stat2	1.806	Myb	1.367

	Cell Type							
	Eosinophils		Other		Monocytes		B Cells	
Rank-ordered Average Regulon AUC	TF	Mean AUC	TF	Mean AUC	TF	Mean AUC	TF	Mean AUC
1	Gm5294	3.361	Lef1	5.318	Klf8	1.529	Bhlha15	12.286
2	Tcf7l1	1.824	Tbx21	5.211	Klf4	1.453	Prdm1	10.989
3	Arid3a	1.667	Runx2	2.549	Bcl3	1.343	Pou2af1	10.841
4	Srebf1	1.636	Nfkb1	2.183	Irf5	1.254	Foxp2	9.204
5	Nfat5	1.587	Tcf7	2.153	Irf4	1.191	Ppard	4.353
6	Foxn2	1.576	Bmyc	2.126	Cebpd	1.161	Atf6	4.215
7	E2f2	1.548	Irf8	2.051	Irf8	1.022	Irf4	4.063
8	Cebpe	1.538	Sox4	1.68	Runx2	1.011	Hivep2	3.804
9	Nfe2	1.375	Irf9	1.671	Sap30	0.953	Foxo1	3.301
10	Sp4	1.297	Foxp4	1.647	Tfec	0.952	Xbp1	3.111

	Treatment					
	Fresh Lin-Depleted		Vehicle		ACLYi	
Rank-ordered Average Regulon AUC	TF	Mean AUC	TF	Mean AUC	TF	Mean AUC
1	Hdac2	2.2	Ahr	0.821	Spi1	0.581
2	Myc	2.132	Creb3l1	0.819	Cebpb	0.573
3	Cebpz	2.04	Fosb	0.818	Atf3	0.555
4	Gtf2f1	1.943	Atf4	0.816	Nfe2l2	0.519
5	Tcf3	1.917	Bhlhe40	0.814	Maf	0.503
6	E2f4	1.913	Junb	0.807	Bhlhe41	0.498
7	Sox4	1.832	Egr1	0.803	Cebpd	0.469
8	Ezh2	1.819	Fos	0.801	Creb3	0.458
9	Trp53	1.754	Batf	0.786	Usf2	0.454
10	Klf1	1.752	Crem	0.721	Mafb	0.45

Table 2.1 - SCENIC-identified Transcription Factor binding motifs reveal enrichment of *Cebp*-family, *Nfe2l2* enrichment in Macrophages and Aclyi. scRNA-seq data was assessed for TF binding motif enrichment in SingleR-defined cell types and original treatments using SCENIC. TF activity was defined using the mean area under the curve (AUC).

Although the HSPC-descended cell types did not fully match canonical immune cell transcriptomes, we refer to each based on SingleR categorization. TF binding-motif analysis of differentially expressed genes using SCENIC identified a variety of transcriptional drivers of myeloid differentiation in the presence of Aclyi that corroborated the SingleR-assigned cell clusters. These included the macrophage-associated TF-coding genes *Spi1*, as well as *Nfe2l2 (NRF2)* and binding partners *Maf*, and *Mafb* (213-215) (**Table 2.1**).

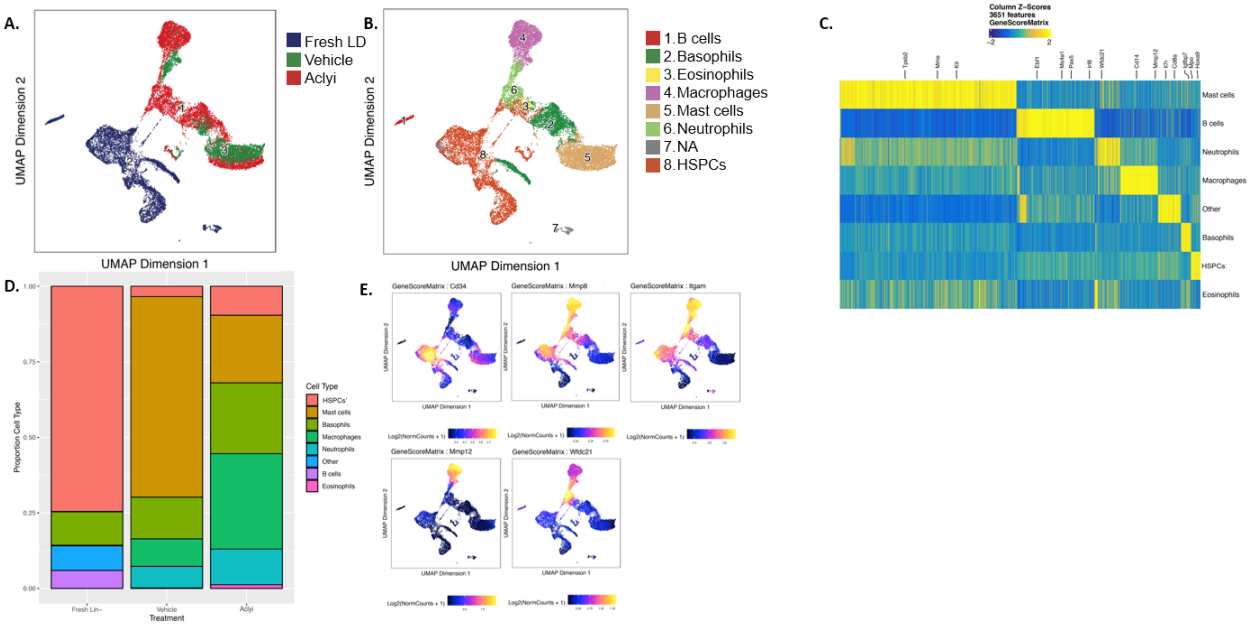

Figure 2.6. Acly inhibition provokes chromatin accessibility changes to drive Macrophage differentiation. Lineage-negative HSPCs were cultured for two weeks with vehicle or Aclyi and assessed using single-cell ATAC-seq. Cells from scATAC-seq are plotted in UMAP dimensional reduction depicting **(A)** original treatment sample IDs and **(B)** cell types identified with SingleR and ArchR **(C)** Gene scores were calculated for each identified cell type and plotted via heatmap **(D)** SingleR/ArchR-defined cell types were quantified and graphed as a proportion of total cells per treatment. **(E)** Gene scores of cell type-associated genes were calculated and overlaid on scATAC-seq UMAP plot.

Chromatin accessibility was measured by scATAC-seq and closely matched the scRNA-seq results. Cells from the same sample subjected to scRNA-seq were split and assessed by scATAC-seq with the freshly isolated and lineage-depleted murine BM clustering separately from the MC-cultured, lineage-depleted BM (**Figure 2.6A**). The software package ArchR was

used to map the gene expression signatures of the SingleR-identified populations from the scRNA-seq onto the scATAC-seq data (216). SingleR identified populations that correlated with expected populations based on scRNA-seq. HSPCs were enriched in the fresh lineage-depleted, undifferentiated sample, while mature myeloid populations like basophils, eosinophils, Mast cells, neutrophils, and macrophages were concentrated in the MC-cultured, lineage-depleted conditions (**Figure 2.6B**).

Gene scores, as defined by ArchR to measure chromatin accessibility within 100,000 base pairs of genes of interest, were used to uncover populations with distinct regions of chromatin accessibility (**Figure 2.6C**) (216). When overlaid onto the UMAP plot, expression of cell type-associated genes including *Cd34*, *Mmp8*, and *Itgam* (CD11b) revealed a close association with canonical cell-type gene expression patterns (**Figure 2.6D, E**). As in the scRNA-seq dataset, the proportion of Mast cells in the vehicle was significantly reduced while macrophages increased in the presence of Aclyi. Furthermore, one of the most differentially expressed genes between vehicle and Aclyi and between fresh lineage-depleted and Aclyi was *Gpnmb*, with an average 4.65-fold increase in expression with Aclyi compared to fresh lineage-depleted and a 3.34-fold increase in expression with Aclyi compared to vehicle, respectively. *Gpnmb*, or glycoprotein nonmetastatic B, is a soluble glycosylated transmembrane protein highly expressed in macrophages that negatively regulates inflammation (217, 218). There was also evidence that Aclyi promoted neutrophil differentiation, as the top differentially expressed gene between fresh lineage-depleted and Aclyi was *Ngp*, a gene coding for neutrophilic granule protein that accumulates in the cytoplasmic granules of neutrophilic precursors. Furthermore, *Ngp* is known to be regulated by C/EBPε and PU.1, which have TF motifs enriched in the Aclyi scATAC-seq condition (219). Our single-cell data demonstrate a pro-myelopoietic effect of

Aclyi that promotes macrophage and neutrophil differentiation by altering chromatin accessibility and gene expression in MC-cultured HSPCs.

Acly inhibition drives Cebpe and suppresses Cebpa and Cebpb expression

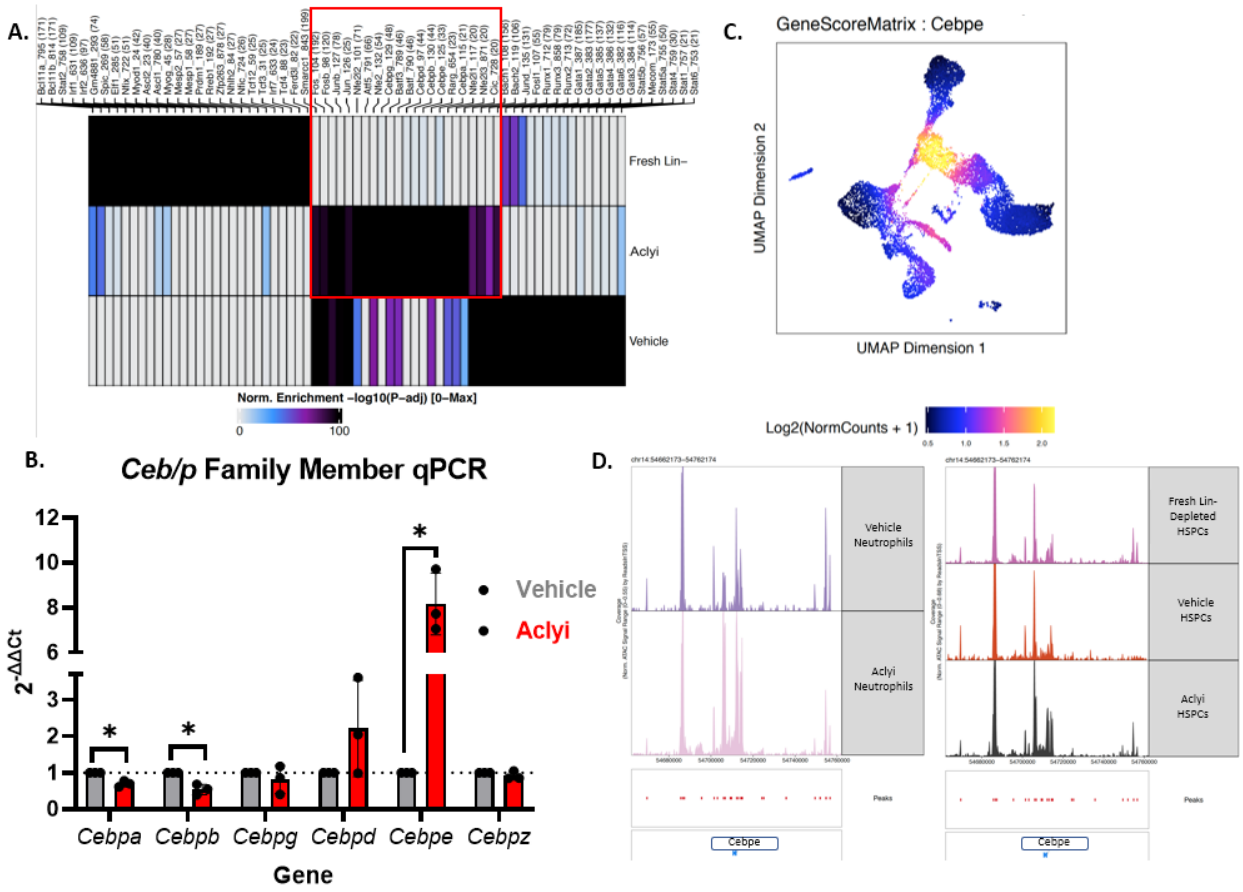

Figure 2.7. Aclyi drives expression of Cebpe while depressing Cebpa and Cebpb. (A) Transcription factor motif chromatin accessibility heatmap was derived from scATAC-seq showing TF motif chromatin accessibility enrichment in fresh lineage-depleted, Aclyi, and vehicle. **(B)** HSPCs were cultured for two weeks in methylcellulose with vehicle or Aclyi and assayed for *Ceb/p* family member mRNA expression by qPCR (n=3). (**C)** Gene score for *Cebpe* was overlaid on scATAC-seq UMAP **(D)** scATAC-seq chromatin accessibility tracks of *Cebpe* from Neutrophils and HSPCs were plotted from each treatment group. Values are normalized to β-actin. Significance was judged using Student's two-tailed parametric t-test. Error bars represent standard deviation.

After Aclyi was found to promote macrophage differentiation at the expense of Mast cell development, scATAC-seq of Aclyi-induced myeloid differentiation was analyzed to identify

potential sequence motifs and transcriptional regulatory families that may respond to Aclyi. Through ArchR-based analysis of scATAC-seq data, TF motifs were identified that were enriched in fresh lineage-depleted, Aclyi-treated, and vehicle-treated MC-cultured lineage-depleted murine BM. ArchR searched for TF binding motifs enriched in the open chromatin of analyzed samples. ArchR identified several TFs, including *Nfe2l2* and the *Cebpa, Cebpb, Cebpg, Cebpd, Cebpe,* and *Cebpz* members of the *C/EBP* family of TFs as enriched in the Aclyi condition (**Figure 2.7A**). These TFs are considered master regulators of hematopoiesis and cellular differentiation (220). C/EBP family TFs are also known regulators of the top differentially expressed gene between fresh lineage-depleted and Aclyi by scRNA-seq, *Ngp* (221). (**Table 2.2**). While all family members share a high binding affinity for the promoter CCAAT box sequence, each member has unique structural elements which render its function unique, and all play a role to balance hematopoiesis (222).

	avg_log2FC	pct.1	pct.2	p_val_adj
Chil3	4.24453518	0.22	0.097	4.14E-42
Hbb-bs	3.5309971	0.107	0.025	2.85E-37
Tph1	2.44016678	0.698	0.146	0
Tpsb2	2.41439743	0.695	0.241	0
Ly6a	2.24196157	0.725	0.383	1.37E-273
Cma1	2.22524205	0.723	0.19	0
Ctla2a	2.13666877	0.819	0.356	0
Fcer1a	2.10031164	0.794	0.368	0
Junb	2.02584097	0.947	0.829	0
Ier2	1.98170566	0.941	0.838	0
Gzmb	1.97214833	0.402	0.075	1.28E-204
Mcpt2	1.97209339	0.263	0.047	2.25E-126
Prtn3	-2.1626459	0.034	0.275	1.51E-126
Elane	-2.1966255	0.01	0.169	4.59E-85
Anxa1	-2.3199197	0.464	0.898	0
Prg2	-2.350247	0.014	0.4	4.56E-248
Mmp12	-2.3724861	0.089	0.392	3.60E-153
Ctss	-2.4609955	0.184	0.446	4.93E-124
Ctsb	-2.6754073	0.778	0.926	2.95E-229
Lyz2	-3.023029	0.174	0.757	0
Fabp5	-3.0867374	0.21	0.63	7.30E-260
Ngp	-3.2872571	0.084	0.718	0
Gpnmb	-3.339636	0.065	0.418	8.96E-209
Wfdc17	-3.5555623	0.073	0.464	2.07E-239

Table 2.2 - Aclyi increases expression of *Wfdc17, Gpnmb,* and *Ngp* and others vs. vehicle treatment. Most differentially expressed genes between Vehicle and Aclyi from scRNA-seq. avg_log2FC indicates the log fold change of the average expression between Vehicle and Aclyi. Positive values indicate higher expression in Vehicle while negative values indicate higher expression in Aclyi. Pct.1 indicates the percentage of cells where the gene is detected in Vehicle, while Pct.2 indicates the percentage of cells where the gene is detected in Aclyi. P_val_adj indicates the adjusted p-value calculated using Bonferroni correction using all genes in the dataset.

To identify which C/EBP family member was most changed in expression in response to Aclyi, we performed RT-qPCR for *Cebpa, Cebpb, Cebpg, Cebpd, Cebpe,* and *Cebpz* on RNA

isolated from MC-cultured HSPCs treated with Aclyi or vehicle. Aclyi resulted in significant reductions in *Cebpa* and *Cebpb* with a simultaneous significant increase in *Cebpe* (**Figure 2.7B**). Furthermore, *Cebpe*'s chromatin region is most open in neutrophils and HSPCs retained in methylcellulose culture when the gene score is overlaid on the UMAP plot (**Figure 2.7C**). Though the proportion of neutrophils is consistent between Vehicle and Aclyi, the substantial increase in *Ngp* expression and enrichment of *Cebpe* binding motif accessibility with Aclyi suggest that Aclyi could promote neutrophil differentiation (**Figure 2.7A**, **Table 2.2**). Additionally, neutrophils and HSPCs from Aclyi had greater chromatin accessibility at its *Cebpe* locus compared to vehicle and fresh lineage-depleted BM cells, suggesting Aclyi may open chromatin at *Cebpe* and poise HSPCs for neutrophilic differentiation (**Figure 2.7D**). These data support a potential role for C/EBP TFs to drive macrophage differentiation in response to Acly, but *Cebpe* is not essential for this process upon Acly inhibition.

Acly inhibition impacts mitochondrial health and superoxide production.

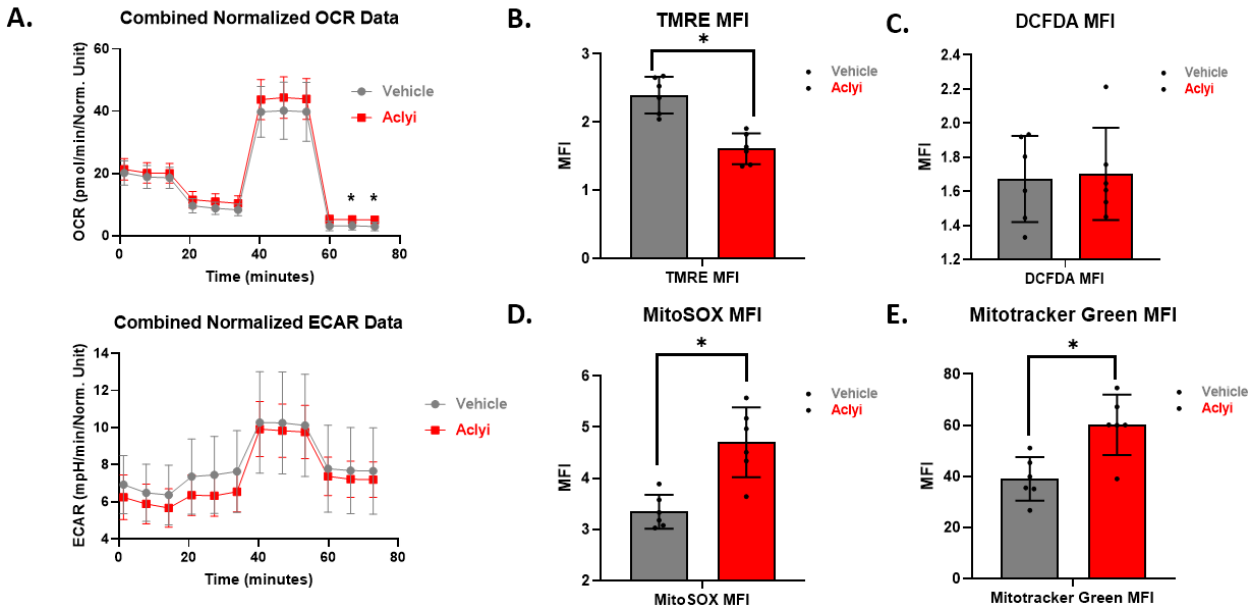

Figure 2.8. – Acly deficiency alters the metabolic behavior of MC-cultured HSPCs. (A) MC-cultured HSPCs cultured with either Aclyi or vehicle were assessed for OCR and ECAR using an extracellular flux mitostress test (n = 6 mice). **(B)** MC-cultured HSPCs cultured with either Aclyi or vehicle were assessed for mitochondrial membrane potential using tetramethyl rhodamine ester (TMRE) by flow cytometry (n = 6 mice). **(C)** HSPCs were assessed for general oxidative stress using 2',7'-dichlorodihydrofluorescein diacetate (DCFDA) by flow cytometry (n = 6 mice). **(D)** HSPCs were assessed for superoxide concentration using MitoSOX staining by flow cytometry (n = 6 mice). **(E)** HSPCs were assessed for mitochondrial mass using mitotracker green staining by flow cytometry (n = 6 mice). Significance was judged using Student's two-tailed parametric t-test. Error bars represent standard deviation.

Acly catalyzes the conversion of mitochondrially-derived citrate to acetyl-CoA and inhibition of this pathway may affect mitochondrial metabolism. C/EBP-family TFs are also known regulators of cellular metabolism, differentiation, and immune function (223, 224). We thus tested if Aclyi altered metabolic and mitochondrial characteristics of MC-cultured HSPCs by measuring extracellular flux. The oxygen consumption rate (OCR) and extracellular acidification rate (ECAR) of MC-cultured HSPCs were not significantly altered with Aclyi (**Figure 2.8A**). While the respective rates of oxidative phosphorylation and glycolysis did not change, the mitochondrial potential sensitive dye tetramethylrhodamine ester (TMRE) MFI significantly decreased with Aclyi, showing that mitochondrial membrane potential and electron transport chain efficiency was decreased (**Figure 2.8B**). General oxidative stress as measured by DCFDA MFI was not also significantly changed with Aclyi (**Figure 2.8C**), but mitochondrial superoxide and mass increased with Aclyi, suggesting a worsening of mitochondrial quality and health (225) (**Figure 2.8D, E**).

Acss2 inhibition, ROS, and α-ketoglutarate do not affect myelopoiesis.

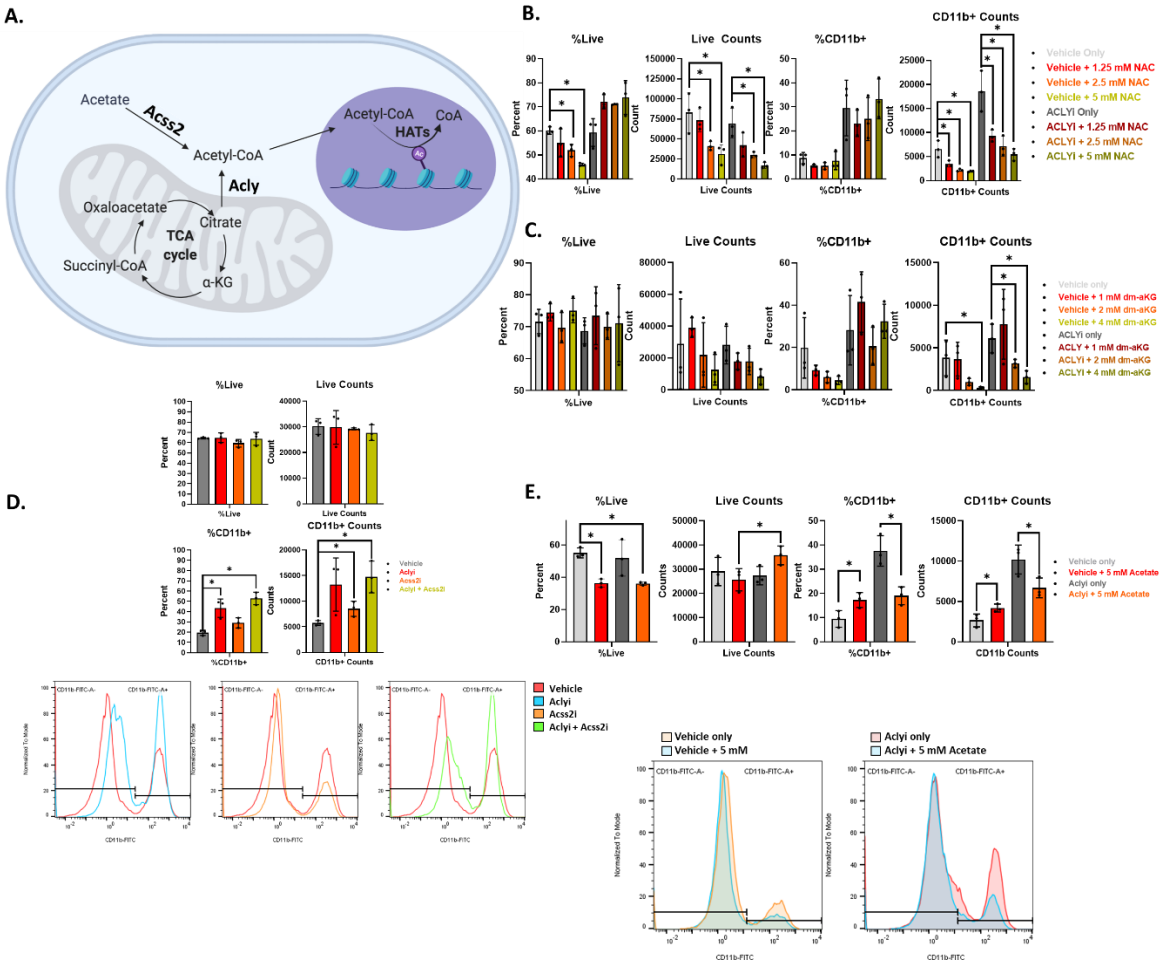

Figure 2.9. Acetate supplementation reverses Aclyi-driven myeloid differentiation. (A) Primary enzymes supplying acetyl-CoA are Acly using citrate as a substrate and Acss2 using acetate (n = 3 mice). **(B)** MC-cultured HSPCs cultured with either Aclyi or vehicle were supplemented with 1.25, 2.5, or 5 mM N-acetylcysteine and assessed for viability and CD11b expression by flow cytometry supplementation (n = 3 mice). **(C)** MC-cultured HSPCs cultured with either Aclyi or vehicle were supplemented with 1, 2, or 4 mM dimethyl 2-oxoglutarate and assessed for viability and CD11b expression by flow cytometry (n = 3 mice). **(D)** MC-cultured HSPCs cultured with either Aclyi, Acss2i, vehicle, or a combination of Aclyi and Acss2i and assessed for viability and CD11b expression by flow cytometry (n = 3 mice). **(E)** MC-cultured HSPCs cultured with either Aclyi or vehicle were supplemented with 5 mM acetate and assessed for viability and CD11b expression by flow cytometry (n = 3 mice). Significance was judged using Student's two-tailed parametric t-test. Error bars represent standard deviation.

Acly catalyzes the reaction between cytosolic citrate derived primarily from the TCA cycle into acetyl-CoA in an ATP-dependent manner. Acss2 can also generate cytosolic acetyl-

CoA from cytosolic acetate and may complement Acly to replenish cellular acetyl-CoA from acetate in an ATP-dependent reaction (226) (**Figure 2.9A**). When MC-cultured HSPCs were treated with Acss2i, the proportion of CD11b+ cells did not increase as with Aclyi. Two metabolic signaling mechanisms that may be influenced by Aclyi and failure to convert citrate to acetyl-CoA are reactive oxygen species (ROS) or accumulation of citrate and conversion to α-ketoglutarate, which regulates histone and DNA demethylation reactions and has been shown to impact hematopoietic differentiation. MC-cultured HSPCs were supplemented with N-acetylcysteine (NAC), a precursor to the ROS/RNS scavenger molecule glutathione. No significant effect of NAC was observed on myeloid differentiation as measured by the frequency of cells expressing CD11b (**Figure 2.9B**). Similarly, cultures supplemented with dimethyl α-ketoglutarate to directly increase α-ketoglutarate had no significant difference in the frequency of cells expressing CD11b+ cells in MC-cultured HSPCs vs. vehicle (**Figure 2.9C**).

In addition, combining Acss2i and Aclyi resulted in a trend towards increased frequency and number of myeloid CD11b+ cells relative to Aclyi alone (**Figure 2.9D**). While Acss2i alone did not impact myelopoiesis in our MC-cultured HSPCs, we next tested if Acss2 could rescue the Aclyi-induced myelopoiesis in the presence of exogenous acetate. MC-cultured HSPCs were then treated with Aclyi with or without exogenous acetate. Culture media supplemented with 5 mM exogenous acetate reversed the increase in the frequency and number of myeloid CD11b+ cells even in the presence of Aclyi to levels comparable to vehicle. These data suggest that although Acss2 is not essential, it can replenish lost acetyl-CoA and compensate for Acly-deficiency if cells are provided excess acetate (**Figure 2.9E**).

Discussion

Hematopoiesis balances extracellular stimuli including cytokines and microenvironmental nutrients to affect intracellular changes to metabolism and gene expression that regulate stemness and differentiation of blood cells. In this study, we investigated the role of citrate metabolism and Acly in the hematopoietic differentiation of HSPCs cultured in cytokine-replete methylcellulose. Small-molecule inhibition and LoxP-cre mediated genetic deletion of Acly similarly demonstrated that Acly deficiency promotes increased myeloid differentiation. We characterized the methylcellulose-based differentiation system of HSPCs by flow cytometry for specific cell markers and by single-cell RNA-seq and single-cell ATAC-seq for transcriptional and chromatin markers. Acly-deficiency was found in each approach to promote the differentiation of cells that transcriptionally resemble macrophages when assessed using SingleR. In contrast, LSK+ cells were decreased in number and frequency by Aclyi when cell surface markers were directly measured by flow cytometry yet increased by Aclyi when assessed transcriptionally by scRNA-seq or scATAC-seq and SingleR. Together, these data show that Acly-deficiency can promote myeloid differentiation although effects on HSPCs remain uncertain.

Cytosolic acetyl-CoA can be produced through several mechanisms. Most notably, Acly and Acss2 produce acetyl-CoA from citrate or acetate, respectively. While Aclyi led increased myelopoiesis *in vitro*, the effect of Acly-deficiency was modest and transient *in vivo* following bone marrow transplant. These data suggest that Acss2 may have compensated for Acly-deficiency *in vivo*. Consistent with Acss2-mediated compensation for Acly-deficiency, supplementation with the Acss2 substrate acetate could reverse the effects of Aclyi *in vitro*. Because Aclyi is under study as a potential therapeutic in cancer and inflammatory diseases, it

may be important to consider potential compensation, although this may also reduce the on-target toxicity of such drugs.

Acly regulated several genes that may promote or influence myelopoiesis. Inhibition of Acly in MC-cultured HSPCs resulted in increased expression of *Cebpe* and decreased expression of *Cebpa* and *Cebpb* with concomitant increases in chromatin accessibility for C/EBP-family TF binding sites. Aclyi also increased the activity of the TF *Nfe2l2*, enriched in the SingleR-identified macrophage population in the scRNA-seq data and the Aclyi condition in the scATAC-seq data. The increased *Nfe2l2* activity suggests a role for redox regulation in Aclyi-promoted myelopoiesis (227-229). It will be important in future studies to further examine genes affected by Aclyi to determine which change directly in response to decreased cytosolic acetyl-CoA and which changes as a secondary consequence of cell differentiation.

Endogenous citrate derived from mitochondrial TCA cycle enzyme citrate synthase can catalyze the reaction of oxaloacetate and acetyl-CoA into citrate. Transported into the cytosol by citrate transporter protein (CTP) and converted back into oxaloacetate and acetyl-CoA in the cytosol by Acly, citrate serves as a convenient acetyl-CoA shuttle from its mitochondrial origin to the cytosol and adjacent compartments (205, 230). After acetyl-CoA is derived from citrate in the cytosol, acetyl-CoA can then go on to serve as substrates in reactions including *de novo* lipid synthesis, and histone acetylation (90). Intracellular acetyl-CoA when present in low concentrations limits the reaction rate of histone acetyltransferases (HATs), with the potential to alter histone acetylome homeostasis, chromatin accessibility, and TF binding patterns (91, 231). Altered acetylation and chromatin accessibility have also been shown to change stem cell behavior and fate (232). Acly itself has been recognized as a key regulator of hematopoiesis, disease outcome in hematologic malignancies, and mature myeloid cell effector ability to clear

atherosclerotic plaques (95, 233, 234). Acetyl-CoA derived from citrate and other sources has wide-ranging intracellular activity, and the above results demonstrate an impact of Acly on chromatin accessibility patterns which result in altered gene expression and stem cell differentiation.

Cytokine-replete methylcellulose has been extensively used to assess *in vitro* hematopoietic stem cell differentiation and self-renewal (209, 235-238). The current classification of differentiation outcomes relies on light microscope-based colony morphology assessment, more recently aided by advances in imaging interpretation software (239). Potential lineages include but are not limited to: granulocytic (CFU-G), erythrocytic (CFU-E), macrophage (CFU-M), and multipotent progenitor (CFU-GEMM) (240). While flow cytometry has instead been used in the past to assess *in vitro* hematopoietic differentiation outcomes, this study to our knowledge represents the first application of single-cell RNA-seq and single-cell ATAC-seq to characterize populations derived from cytokine-replete methylcellulose culture (241). Several populations were identified in steady-state (vehicle) and perturbed (Aclyi) conditions using these methods, comprising cell types that transcriptionally resemble neutrophils, eosinophils, basophils, macrophages, monocytes, HSPCs, and Mast cells. Our characterization represents a quantitative evaluation of the methylcellulose method that can be used to support traditional and computer-aided imaging techniques.

These data highlight a role for Acly and cytosolic acetyl-CoA in the epigenetic regulation of HSPC and myeloid differentiation. When Acly is inhibited and acetyl-CoA production CoA decreases, macrophage differentiation is favored whereas Mast cell differentiation occurs when Acly is active and cytosolic acetyl-CoA is not limiting. Two limitations to the study are that acetyl-CoA can be generated through multiple means that may compensate in context-specific

manners and that Acly inhibitors may have off-target effects. The use of *Acly* genetic deletion, however, supports a direct and at least partially non-redundant role for Acly-derived acetyl-CoA in myelopoiesis. These data are like those of Rhee et al. 2019, who showed that Acly played a role to regulate the proliferation of myeloid cells in part through the TF PU.1 (77). It will be important in future studies of metabolic regulation of epigenetic marks, gene expression, and cell differentiation to further establish these associations and how these pathways may be modulated to promote myelopoiesis or differentiation of myeloid precursor cells.

Future Directions

In this study, we established that Acly deficiency results in increased CD11b+ myelopoiesis in MC-cultured HSPCs through altered transcriptional programs, mitochondrial metabolism, and chromatin accessibility. However, many questions remain regarding the role that Acly plays in murine hematopoiesis and the role that ACLY plays in human hematopoiesis. Future experiments should address the impact of Acly/ACLY inhibition and deficiency on the self-renewal capacity of Lin-, c-Kit+ HSPCs and more granular stem populations, the specific mature hematopoietic populations that result from Acly/ACLY-deficient hematopoiesis, and the site-specific histone acetylation and non-histone protein acetylation patterns that change across hematopoietic lineages with Acly/ACLY deficiency.

While we demonstrate in **Figure 2.1B** that Acly deficiency significantly reduces the proportion of canonical stem Lin-, Sca-1+, c-Kit+ (LSK) cells, serial replating and serial transplantation experiments are required to determine the functional self-renewal consequences of Acly/ACLY deficiency. Knocking down the transcription factors identified through SCENIC analysis that are most active in HSPCs such as Hdac2, E2f4, and Tfdp1 (and human homologs as appropriate) in **Table 2.1** in conjunction with Acly/ACLY deficiency could further inform the

nature of Acly/ACLY influence on HSC functional self-renewal capacity. Similarly, further investigation into SCENIC-identified TFs in SingleR-annotated other more mature hematopoietic populations could reveal methods to limit or promote specific cell type differentiation.

We identify cell types present in our single-cell datasets in **Figure 2.5** and **Figure 2.6** that most closely resemble mature bulk hematopoietic cell transcriptomes contained in the ImmGen database. Future work should examine *in vivo* hematopoietic populations in the blood and bone marrow of Acly deficient animals to ascertain, again, more functional results of Acly deficiency. Furthermore, transplantation of ACLY-deficient human HSCs into humanized mice could further inform the field about the role of ACLY in human hematopoiesis.

Furthermore, while we depict site-specific changes to chromatin accessibility in single-cells in **Figure 2.6** and **Figure 2.7**, we lack data regarding the exact histone and other protein residues that change acetylation state with Acly/ACLY deficiency. There is an understanding that general metabolic flux through glycolysis results in site-specific changes to histone acetylation (242). Performing mass spectrometry on histones and other proteins using a method like Sidoli *et al.* would reveal which specific epigenomic and general protein acetylation patterns change following Acly/ACLY deficiency (243). Assessing the relative contribution of Acss2/ACSS2 using the same method may reveal disparate roles between the two enzymes in promoting site-specific histone and general protein acetylation in hematopoiesis.

CHAPTER 3: MITOCHONDRIAL MEMBRANE POTENTIAL REGULATES TUMOR-ASSOCIATED T-CELL RESPONSES TO CLEAR CELL RENAL CELL CARCINOMA

Introduction

Clear cell renal cell carcinoma (ccRCC) is one of the most common urological cancers, with 400,000 new global cases diagnosed each year. ccRCC oncogenesis can most often be traced to loss-of-function mutations in the tumor suppressor Von Hippel-Lindau (*VHL*) which leads to stabilization of HIF-2α and resulting in constitutive hypoxic signaling (144). Activation of HIF-2α signaling induces angiogenesis, increased tumor vascularity, and growth via *VEGF, CCND1, ANGPTL4, EGLN3, ENO2, GLUT1, GFBP3,* and other HIF-responsive genes (244). ccRCC standard of care (SOC) that deviates from traditional chemotherapy approaches centers around tyrosine kinase inhibitors (TKIs) against VEGF-pathway enzymes and increasingly leverages T-cell antitumor immunity through immune checkpoint blockade (ICB)-based therapies. Historically, while 70-90% of localized RCC patients survive to five years, only 15.3% of metastatic RCC patients survive out to five years (160). Identification of patient features that predict response to ICB could increase the efficacy of ICB therapy in ccRCC.

ccRCC tumors are immunogenic solid tumors with high numbers of tumor-infiltrating lymphocytes (TILs); ccRCC tumors possess the highest TIL score across tumor types in The Cancer Genome Atlas (TCGA) (245, 246). Harnessing the T-cell population for increased antitumor immunity offers great promise for improving patient treatment outcomes. Indeed, monotherapies and combination therapies that utilize monoclonal antibodies antagonizing the T-cell coinhibitory surface markers PD-1, PD-L1, and CTLA4 have been approved for therapy against ccRCC, with the first drug, nivolumab (α-PD-1), approved in 2015 (247). ICB was first tested for use in ccRCC therapy in the US in 2007 with the assessment of the α-CTLA4 mAb monotherapy ipilimumab, in which treatment with ipilimumab showed an overall response rate

(ORR) of 12.5% and nearly 50% survival at 5 years in 40 patients (248). The current SOC for first-line treatment of intermediate/poor risk ccRCC is nivolumab (α-PD-1) combined with ipilimumab (Ipi/Nivo), approved for ccRCC therapy in 2018 (249). However, SOC has room for improvement in patient outcomes compared to VEGF inhibitors. In the currently ongoing CheckMate 214 clinical trial examining 1096 patients treated either with Ipi/Nivo or the VEGF pathway inhibitor sunitinib, interim data revealed that Ipi/Nivo-treated patients showed a 42% ORR and a median progression-free survival (PFS) of 11.6 months while sunitinib-treated patients showed a 27% ORR and 8.4 months median PFS in the intermediate/poor risk category (154). While ICB-treated patients demonstrated greater ORR and PFS than sunitinib-treated patients, more work is needed to further increase the efficacy of ICB.

While ccRCC immune infiltrate has a significant macrophage component, CD4+ and CD8+ T-cells have been shown as the primary immune populations in ccRCC tumors (250, 251). Both CD4+ and CD8+ T-cells clonally expand in response to T-cell receptor (TCR) engagement with tumor-associated antigen (TAA) peptides presented on MHC-II and MHC-I molecules, respectively, in conjunction with costimulatory signaling through molecules like CD28 to mediate antitumor immunity. ccRCC patient tumors exhibit greater TIL clonality than non-ccRCC renal tumors. In a study examining tumors resected from 14 treatment-naïve ccRCC patients, 9 out of 14 patients exhibited TIL repertoires with a single T-cell clone that made up 4.6% to 24% of the total identified sequences. T-cell “clones” are T-cells with a unique combination of T-cell receptor α (TRA) and β (TRB) complementarity determining region 3 (CDR3) sequences that confer sequence-dependent specificity for a unique cognate antigen (252).

Clonality of T-cell responses has been shown to correlate with positive outcomes and affect the balance of intratumoral CD4+ and CD8+ TIL populations. For example, less abundance and clonality of T-cell responses in ccRCC tumors are associated with increased recurrent disease (126). Analysis of ccRCC TIL repertoires indicates that expanded T-cell clones are most typically CD8+ while "singletons", clones only found once, are often CD4+, suggesting that CD8+ T-cells play an important role in ccRCC antitumor immunity with tumor-associated antigens (TAAs) potentially promoting TAA-specific CD8+ T-cell expansion (252).

To facilitate clonal expansion, T-cells increase metabolic flux through glycolysis and glutaminolysis pathways and increase mitochondrial membrane potential ($\Delta\Psi m$). T-cell metabolic activation supplies biosynthetic intermediates to sustain prolonged immune activity, including the production of inflammatory cytokines and direct T-cell killing (128, 129). Dysregulation of T-cell metabolism caused by nutrient scarcity in the tumor microenvironment (TME) can result in the suppression of antitumor immunity through the accumulation of mitochondria with low $\Delta\Psi m$ that coincides with T-cell exhaustion (253).

$\Delta\Psi m$ further impacts T-cell responses to immune checkpoint blockade and antitumor immunity. Adoptively transferred T-cells with low $\Delta\Psi m$ persist longer *in vivo* and eradicate tumors more effectively compared to high $\Delta\Psi m$ T-cells in the murine B16 melanoma model. B16 melanoma tumor-bearing mice receiving T-cells with high $\Delta\Psi m$ saw tumors grow nearly three times as large at 35 days post-transfer compared to their $\Delta\Psi m$ low T-cell recipient counterparts (254). In melanoma patients, the presence of $\Delta\Psi m$ high CD8+ T-cells with elevated OXPHOS correlates with resistance to ICB. These $\Delta\Psi m$ high T-cells upregulate CD8, PD-1, CD38, and CD39 and are enriched in the periphery of nonresponders compared to treatment-naïve patients (255).

In ccRCC, CD4+ and CD8+ T-cells utilize metabolic flux in different ways, with consequences for patient outcomes. *Ex vivo* activated ccRCC patient CD8+ TILs, unlike ccRCC patient CD4+ T-cells, fail to increase glucose uptake even with intact Glut1 and HK2 expression, suggesting subset-specific metabolic reprogramming in the TME (256). Metabolic activity in T-cell populations has been shown to stratify patients by disease outcome. Single-cell resolution RNA sequencing (scRNA-seq) and mass cytometry profiling of 68 ccRCC patient tumors have revealed a subset of proliferative CD8+ T-cells with higher metabolic activity indicated by greater expression of glycolysis and TCA cycle pathway genes and elevated CTLA4, ICOS, 4-1BB, TIM3, HLA-DR, and CD38 surface protein expression. Assigning patients based on that gene signature to a 267 primary tumor testing dataset categorized patients into groups with different disease outcomes. Patients that had less enrichment in this gene signature, representing ~25% of the 267-patient cohort, saw ~25% overall survival at 10 years. Compared to ~60% overall survival at 10 years for patients with greater enrichment of that gene signature, the presence of metabolically active CD8+ T-cells correlates with positive outcome in ccRCC patients (246). The identification of robust T-cell biomarkers based on ΔΨm, T-cell subsets, gene expression, and T-cell clonal expansion that can predict patient response to ICB, however, remains an unmet need in ccRCC.

To ascertain the role of ΔΨm on CD4+ and CD8+ T-cell clonal expansion and gene expression as a potential biomarker for patients with ccRCC on α-PD-1/α-CTLA-4 ICB, we performed scRNA-seq and single-cell V(D)J-sequencing (scV(D)J-seq) on ΔΨm Low and ΔΨm High peripheral blood T-cells, and TIL. In addition, peripheral blood samples from patients with ccRCC on PD1/CTLA4 treatment were analyzed for cell surface protein expression by cytometry time of flight (CyTOF). Clinical responses to ICB included partial response, mixed/partial

response, stable disease, and progressive disease. Across all patient peripheral T-cells, we identify an association between low ΔΨm and greater clonal expansion in CD4+ and CD8+ T-cells. Furthermore, ΔΨm Low and ΔΨm High populations had divergent CD8+ and CD4+ gene expression profiles and patient response-dependent relationships between peripheral and tumor T-cell repertoires. In short, ΔΨm Low T-cells express greater *CD8A, CD8B, PRF1, CTSW, CCL4, KLRB1, KLRD1,* and *KLRK1* and ΔΨm High express greater *CD4, LMNA, S100A11*, and *ITGB1*. We identified populations of T-cells with shared TRA and TRB CDR3 sequences between peripheral blood and TILs that associated with a distinct T-cell activated gene signature found in the patient with partial responder to ICB. Finally, we identified a small number of T-cell clones shared *between* patients that preferentially expand into the ΔΨm Low T-cell population. Collectively, through the assessment of ccRCC patient T-cell gene expression, cell surface protein, and T-cell clonality in single-cell resolution, our preliminary results constitute a conceptual framework for assessing the relationship between ΔΨm in T-cells and patient response to ICB.

Results

scRNA-seq, scV(D)J-seq, and ArcherDx VDJ-seq applied to ccRCC patient tumor TILs and PBMCs identify predominantly ΔΨm High T-cells.

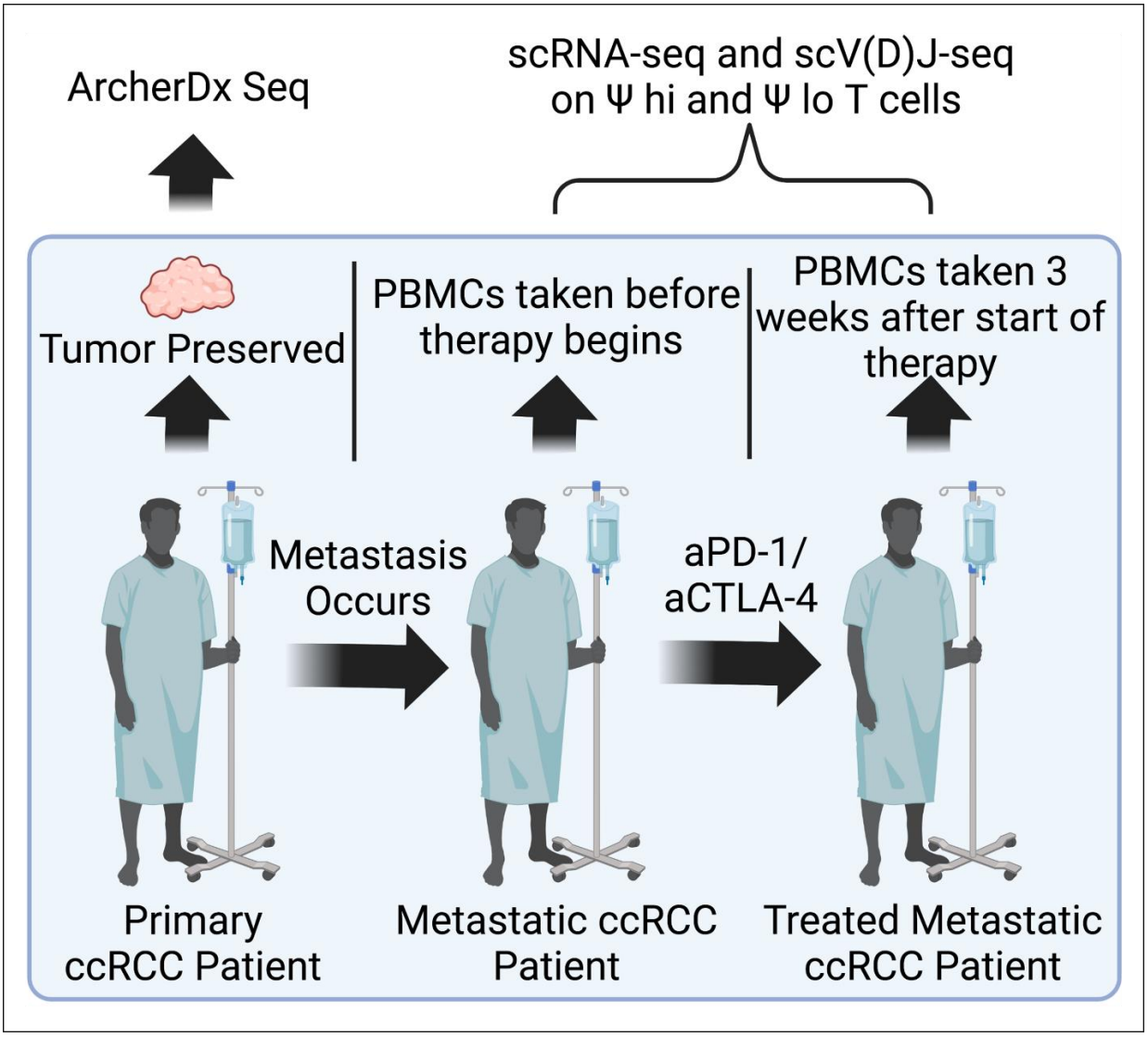

Figure 3.1. Single-cell Resolution Assessment of ccRCC Patient Tumor and Peripheral T-cells Before and After Immune Checkpoint Blockade. Primary ccRCC patient tumors were resected and preserved. Following the development of metastatic disease, PBMCs were extracted from patient blood before ICB with α-PD-1/α-CTLA4 and three weeks after ICB. PBMCs were preserved. Live, CD45+ cells were isolated from tumors via FACS and were subjected to CyTOF using 44 different metal-conjugated antibodies. Live, CD3+ cells were also isolated from the tumors and were subjected to single-cell resolution V(D)J sequencing using ArcherDx Immunoverse. Live, CD3+, TMRE low and Live, CD3+, TMRE hi cells were isolated from patient PBMCs via FACS. These cells were examined for gene expression and TCRα and TCRβ sequences with scRNA-seq and scV(D)J-seq.

To assess the impact of mitochondrial membrane potential on T-cell responses to ccRCC, we performed ArcherDx V(D)J-seq on CD3+ cells from formalin-fixed paraffin-embedded (FFPE) tumors resected from four ccRCC patients. We performed scRNA-seq and scV(D)J-seq on Live, CD3+, ΔΨm hi and Live, CD3+, ΔΨm Low PBMCs isolated from patient blood taken before and three weeks after administration of ICB. Live, CD45+ PBMCs from the blood of patients before and after ICB as well as a healthy control were subjected to CyTOF stained with a 44-member metal-antibody panel. Eight patients with progressive disease, four patients with stable disease, one patient with a mixed/partial response to ICB, seven patients with a partial response to ICB, and one healthy control were included in the CyTOF experiment. One patient each with progressive disease, stable disease, mixed/partial response to ICB, and partial response to ICB from the CyTOF cohort were then examined using scRNA-seq and scV(D)J-seq. The assessment of patient T-cells with single-cell transcriptomic and cell surface protein modalities allows for corroboration between techniques, reinforcing the findings of both.

These patients each presented with different outcomes in response to the treatment. Patient “2020-01” demonstrated a progressive response, indicating that their disease progressed after ICB. Patient “2020-103” presented with stable disease, with ccRCC neither expanding nor contracting in response to ICB. “2021-03” responded to ICB with a mixed/partial response, demonstrating that some disease sites regressed while other sites either were stable or expanded. “2020-139” was the only patient to experience a partial response to ICB, as their disease regressed in response to treatment. (**Figure 3.1**).

CyTOF characterization of ccRCC Patient Live, CD45+ PBMCs Reveals Distinct Immune Populations that Change Between Patients Before and After ICB.

To determine differences in cell surface protein expression between non-lymphoid immune populations, we isolated Live, CD45+ cells from patient blood and subjected those cells to CyTOF using a 44 metal-conjugated antibody panel. This panel consisted of hematopoietic lineage markers such as CD3, CD11b, CD4, and CD8, chemokine receptors like CCR4, CCR6, and CXCR3, coactivation and coinhibitory receptors like CD28, PD-1, and CTLA4, the proteins associated with cell proliferation Ki67, and three proteins implicated in cellular metabolism, CPT1A, GRIM-19, and GLUT1. We applied the machine learning workflow algorithm Tracking Responders Expanding (T-REX) combined with Marker Enrichment Modeling (MEM) to our data and characterized populations that expanded or contracted by ≥95% across six different comparisons (257, 258). MEM labels identify surface proteins that change in expression the most in that population, with labels reported between 0 (no expression or enrichment) to +10 (greatest enrichment). CD8+, CD4+, and γδ T-cells are assessed in the T-cell plots in **Figure 3.2A, B, E, and F**, while B cells, NK cells, and pan-myeloid cells are contained in the Non-T-cell plots **Figure 3.2C and D**.

Comparing T-cells from patients with progressive disease before and after ICB, we identified two populations which are at least 95% enriched in pre-ICB T-cells patients with progressive disease, with total marker lists depicted in the figure. Based on the surface protein expression of CD3, TIGIT, TCRγδ, CPT1A, CD4, Ki67, and/or CD44 in both populations, these cells are most likely **1)** exhausted γδ T-cells and **2)** exhausted CD4+ T-cells with elevated fatty acid metabolism and low-level proliferation. Upon chronic antigen stimulation, T-cells will up-regulate TIGIT which correlates with T-cell exhaustion (259). (**Figure 3.2A**). In short, these data

suggest patients with progressive disease possess exhausted, yet proliferative peripheral γδ and CD4+ T cell populations that significantly contract after ICB.

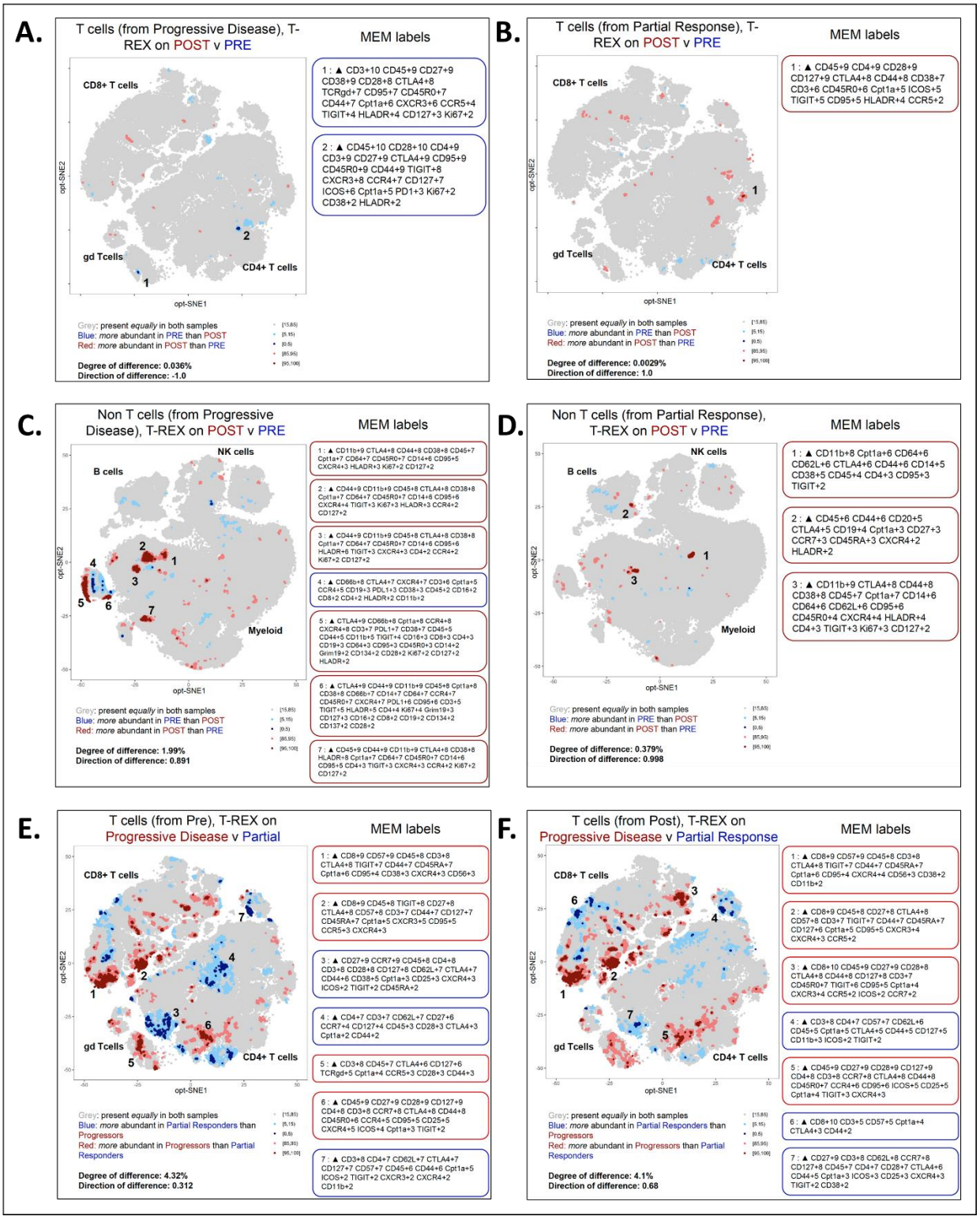

Figure 3.2. CyTOF Examination of ccRCC Patient PBMCs Reveals Distinct Cell Subset Changes with ICB and Patient Response. t-SNE plots of ccRCC patient Live, CD45+ PBMCs assessed using the T-REX platform along several axes of comparison**. (A)** T-cell surface protein expression differences between Pre and Post ICB in the patient with progressive disease. **(B)** T-

cell surface protein expression differences between Pre and Post ICB in the partial responder. **(C)** Non-T-cell surface protein expression differences between Pre and Post ICB in the patient with progressive disease. **(D)** Non-T-cell surface protein expression differences between Pre and Post ICB in the partial responder. **(E)** pre-ICB T-cell surface protein expression differences between progressive and partial responders. **(F)** post-ICB T-cell surface protein expression differences between progressive and partial responders.

Examining that same comparison between pre- and post-ICB T-cells from partial responders this time, we instead see an enrichment of a single population in post-ICB T-cells. This population is enriched in CD45, CD4, CD28, CD127, CTLA4, CD44, CD3, CD45R0, CPT1A, ICOS, TIGIT, CD95, HLADR, and CCR5 and is at least 95% enriched in post-ICB partial responder T-cells. Based on these markers, these cells also appear to be exhausted CD4+ T-cells with elevated lipid metabolism. However, this population is more enriched in CD38 and CCR5 and less enriched in CD95, CCR4, CXCR3, and Ki67 than the CD4+ T-cell population identified from patients with progressive disease (**Figure 3.2B**).

Next, we examined the non-T-cell populations in patients with progressive disease that change between pre- and post-ICB. We identified six populations that were enriched in post-ICB cells and one population that was enriched in pre-ICB cells. Based on their surface protein expression enrichment patterns, populations 1, 2, 3, and 7 are different types of monocytes/macrophages, while 4, 5, and 6 are different types of granulocytes (**Figure 3.2C**). The only population enriched in pre-ICB non-T-cells in patients with progressive disease is a granulocyte cluster enriched in CD66b, CTLA4, CPT1a, CXCR4, and other lower-enriched markers.

Conversely, non-T-cells from partial responders only possessed three populations enriched in post-ICB cells and none enriched in pre-ICB. Of these, populations 1 and 3 are immunosuppressive myeloid cells enriched in CD11b, CD14, CD64, CTLA4, and TIGIT. population 3 is notable for Ki67 enrichment, indicating recent cellular proliferation. Population 2

consists of B cells enriched for CD20, CD44, CTLA4, CD19, CXCR4, CCR7, and other markers (**Figure 3.2D**).

We then sought to determine key differences in immune populations between the patients with progressive disease and the partial responders to ICB. In pre-ICB T-cells, we identified four populations that were enriched in patients with progressive disease (1, 2, 5, and 6) and three enriched in the partial responder (3, 4, and 7). In this comparison, the patients with progressive disease showed enrichment in exhausted CD8+, TIGIT+ T-cells in populations 1 and 2, effector TCRγδ+, CD28+, CD44+, CTLA4+ γδ-T-cells in population 5, and CD4+, CD28+, CD27+, CD127+, CCR7+, CTLA4+ T-cells with low-level TIGIT enrichment in population 6. Populations 3, 4, and 7 were enriched in pre-ICB partial responder T-cells and consisted of different types of CD4+ T-cells, with population 3 with greater enrichment of CCR7 and low-level TIGIT, population 4 without TIGIT, relatively reduced CTLA4, and relatively reduced CD44, and population 7 enriched in CXCR3, CXCR4, TIGIT, and CD57 (**Figure 3.2E**). Overall, pre-ICB T cells from patients with progressive disease are enriched with $TIGIT^{hi}$ $CD57^{hi}$ CD8+ T cells, γδ T cells, and $CD28^{hi}$ $CD44^{hi}$ $TIGIT^{lo}$ CD4+ T cells, while the partial responders' pre-ICB T cells are enriched with CD4+ T cells only. These CD4+ T cells that are enriched in the partial responders pre-ICB are $CCR7^{hi}$ $TIGIT^{lo}$, $CD62L^{hi}$ $CCR7^{hi}$, and $CD62L^{hi}$ $CTLA4^{hi}$ $CD127^{hi}$ $TIGIT^{lo}$ T cell populations. This suggests that peripheral exhausted CD8+ T cells and γδ T cells pre-ICB may negatively influence ccRCC patient response to ICB.

In post-ICB T-cells, we also identified four populations that were enriched in patients with progressive disease and three enriched in the partial responders to ICB. These populations are 1, 2, 3, and 5. Post-ICB T-cells from patients with progressive disease were enriched with exhausted CD8+, $TIGIT^{Hi}$, $CTLA4^{High}$ T-cells in populations 1-3 and CD4+, CD28+, $CCR7^{Hi}$,

$TIGIT^{Lo}$ effector T-cells in population 5. Post-ICB T-cells from partial responders exhibited more modest enrichment in TIGIT expression across the three populations. Cluster/population 4 is CD4+, CD57+ $CTLA4^{Mid}$, $CD44^{Mid}$ T-cells, and population 7 is also a CD4+ T-cell cluster with much greater enrichment in CD27, CCR7, and CD127 in comparison to population 4. Population 6 consists of CD8+, CD57+, $CTLA4^{Lo}$ T-cells that lack TIGIT expression (**Figure 3.2F**). It is important to note that T-cell and non-T-cell populations before and after ICB had varying degrees of difference in *overall* gene expression profile in patients with progressive disease compared to the partial responders. While T-cells between pre- and post-ICB had a 0.036% degree of difference in progressive disease, the partial responders showed a lesser 0.0029% degree of difference. More strikingly, non-T-cells compared between pre- and post-ICB had a 1.99% degree of difference in patients with progressive disease while the partial responders exhibited a 0.379% degree of difference, suggesting that greater gene expression changes occur after ICB in patients with progressive disease.

CyTOF characterization of ccRCC Patient Live, CD45+ PBMCs Reveals Response-Specific Upregulation of Metabolic Protein Expression

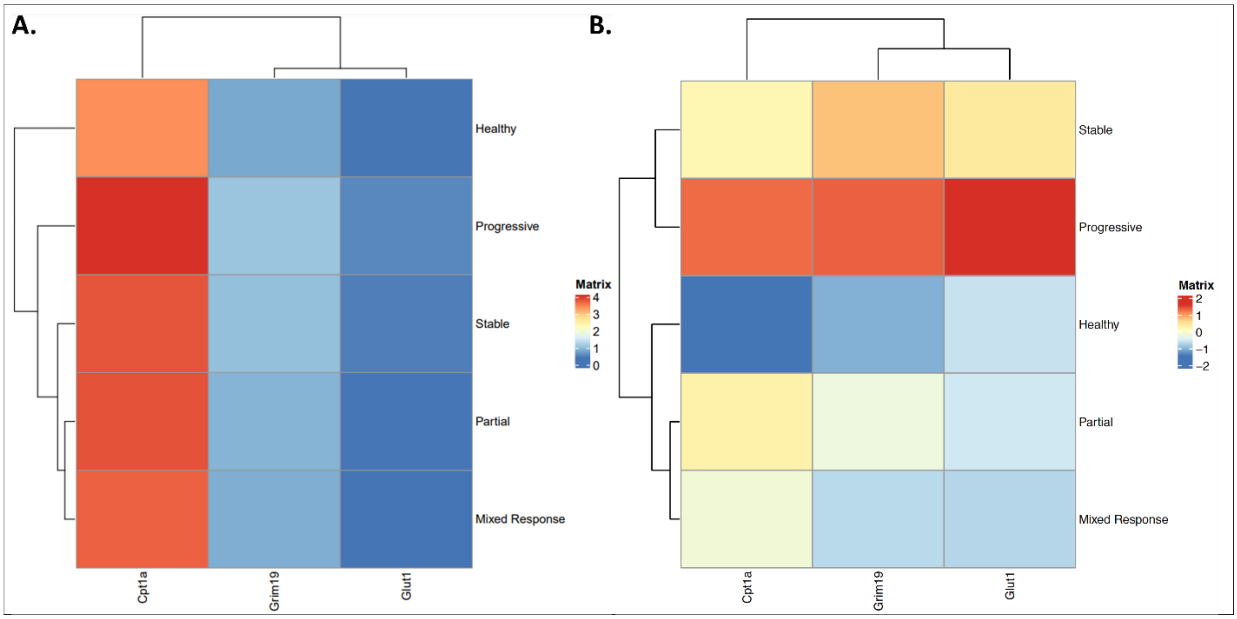

Figure 3.3. Progressive Response to ICB is Associated with Higher Cell Surface Expression of Metabolic Proteins CPT1a, GRIM-19, and GLUT1. (A) Asinh-normalized mean cell surface metabolic protein expression of combined pre- and post-ICB ccRCC Live, CD45+ PBMCs. **(B)** Relative mean cell surface metabolic protein expression of combined pre- and post-ICB ccRCC Live, CD45+ PBMCs.

After identifying immune populations that were most enriched in partial responders and patients with progressive disease and between pre- and post-ICB, we examined GLUT1, CPT1a, and GRIM-19 expressed on cell surface to determine the role of glycolysis, fatty acid oxidation (FAO), and oxidative phosphorylation (OXPHOS), respectively, in patient peripheral T-cells. GLUT1 transports glucose into the cell to fuel glycolysis and has been shown to enhance production of IFN-γ in effector subsets with different expression patterns between CD4+ and CD8+ T-cells (260). CPT1a is the rate-limiting enzyme for FAO, catalyzing the carnitine additive reaction to palmitoyl-CoA that permits entry into the mitochondrial matrix for additional steps of FAO; CPT1a has been shown to regulate T-cell function (261). GRIM-19 encodes for the NADH: ubiquinone oxidoreductase subunit A13 (NDUFA13) of Complex I of the ETC that

pumps four protons from the mitochondrial matrix into the intermembrane space through oxidation of NADH to NAD+ and H+. As the activity of other ETC members Complexes II through IV rely on Complex I activity to establish a proton gradient across the mitochondrial inner membrane, GRIM-19 is crucial to the maintenance of $\Delta\Psi m$ and OXPHOS. Deficiency in GRIM-19 results in disrupted $\Delta\Psi m$ and greater sensitivity to apoptotic stimuli (262).

We noticed that many of our identified populations had some level of enrichment in CPT1A while GRIM19 and GLUT1 were more sparsely represented, suggesting that CPT1A was higher expressed than GRIM19 and GLUT1. Comparing asinh-normalized mean gene expression between ccRCC patients and healthy control, CPT1A is indeed expressed at a higher level than GRIM19 or GLUT1 (**Figure 3.3A**). While some differences are evident between patients using the asinh-normalized protein expression data, scaling each protein using its own mean and standard deviation across the dataset provides a clearer graphical depiction of how each protein is expressed between each patient. Using scaled protein expression, patients with progressive disease exhibited a greater relative expression of all three genes, followed by the stable responders. The healthy control had the lowest relative expression of all profiled metabolic genes (**Figure 3.3B**).

scV(D)J-seq on Live, CD3+ PBMCs Pre- and Post-ICB reveals effects of ΔΨm on T-cell Clonal Responses to ICB.

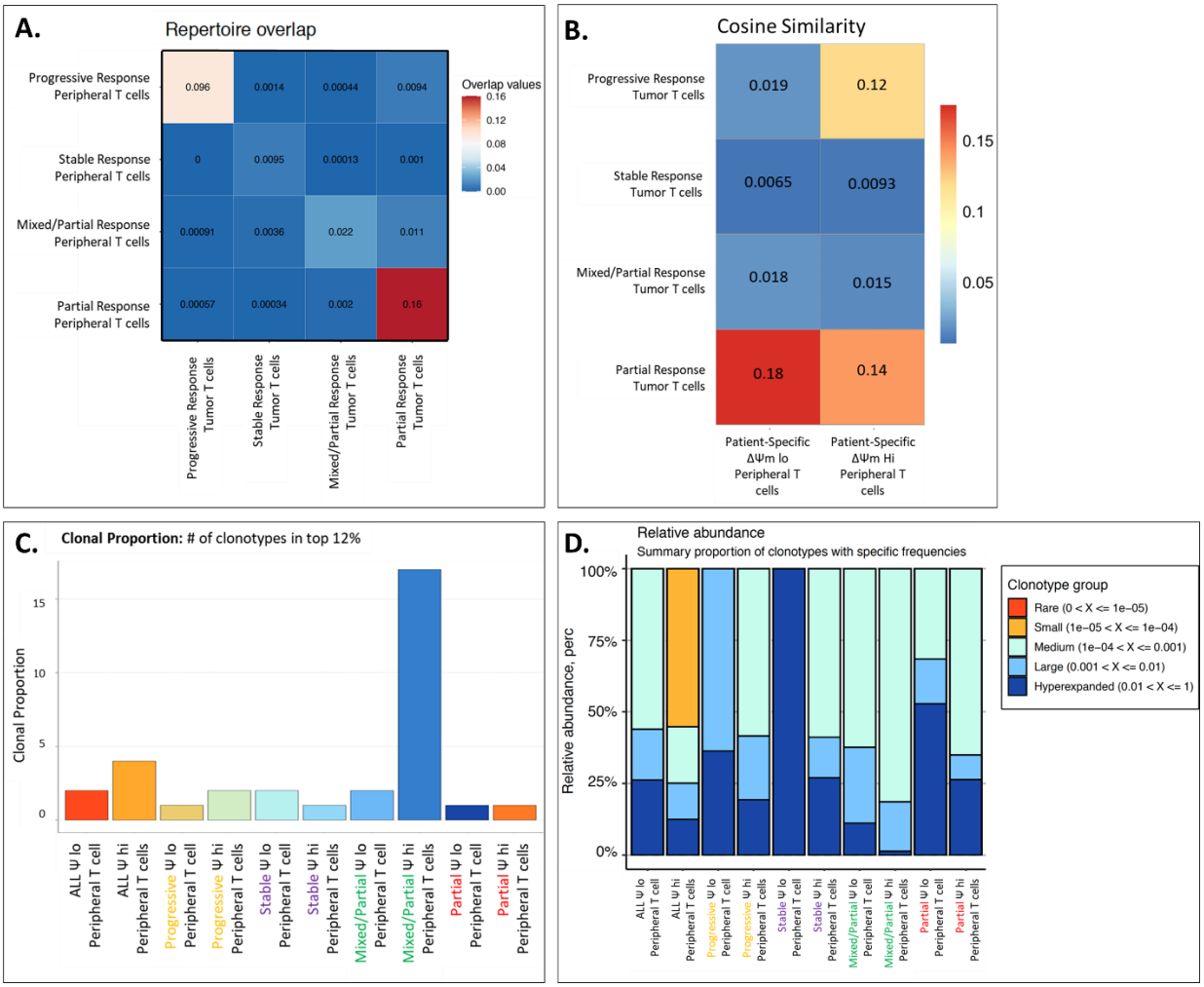

Figure 3.4. ΔΨm Exerts Response-Specific Influence on Tumor-Peripheral T-cell Repertoire Overlap, Cosine Similarity, and Clonality. Assessment of **(A)** normalized repertoire overlap, **(B)** cosine similarity, **(C)** the number of T-cell unique clones in the repertoire's top 12%, and **(D)** relative abundance of rare, small, medium, large, and hyperexpanded binned clones between ccRCC patient peripheral and tumor T-cells.

After examining the cell surface protein expression differences in pre- and post-ICB patient Live, CD45+ PBMCs, we next turned to assess the TCR clonal composition of the Live, CD3+ T-cell response to ccRCC and ICB in single-cell resolution. We performed scV(D)J-seq of pre- and post-ICB ccRCC patient ΔΨm Hi, Live, CD3+ T-cells and ΔΨm Lo, Live, CD3+ T-cells from peripheral blood and ArcherDx V(D)J-seq on Live, CD3+ T-cells isolated from

patient tumors resected before PBMCs were taken for the pre-ICB timepoint. Using this approach, we were able to characterize the similarities between peripheral and tumor T-cell TCRα clonal repertoires and determine the effects of ΔΨm on the clonality of peripheral T-cell responses to ccRCC. While all the results presented here reflect T-cell clonality determined using TCRα CDR3 sequences, the TCRβ sequences mirror the results of the presented TCRα data.

Using the overlap coefficient metric, defined as the number of shared TCRα nucleotide sequences divided by the smaller of the two repertoires, we determined that the partial responder's combined pre- and post-ICB peripheral T-cell repertoire had the greatest normalized overlap to the tumor T-cell repertoire at 0.16. Baseline overlap coefficient measurements comparing T-cell peripheral repertoires in 36 healthy patients was reported in 2021 by Hou *et al.* to range between 0.001 and 0.085 (263). While this is promising and reflects results in the field that show that increased peripheral-tumor T-cell repertoire overlap is associated with positive responses to ICB, the second-highest normalized overlap was between the periphery and tumor repertoire of the progressive disease patient (**Figure 3.4A**). Next, we examined cosine similarity between ΔΨm Low T-cells and ΔΨm High T-cells in the periphery and the TIL repertoire for each patient. Cosine similarity is another normalized metric of repertoire overlap that measures the vector angle between two repertoires. Cosine similarity is a continuous score between 0, representing no similarity at all, and 1, indicating completely equivalent repertoires. A baseline cosine similarity score is difficult to determine experimentally in ccRCC patients, as a "control" repertoire would represent a set of peripheral and tumor T-cell repertoires that share little antigen-specific clonal expansion. However, computational approaches incorporating parameters of V(D)J recombination and thymic selection have produced synthetic T-cell clonal repertoires with mean cosine similarity scores less than 0.01 when compared with real naïve, central

memory, effector, and regulatory T-cell subsets (264). Cosine similarity is best used here as a relative comparison between patients and not as an absolute difference metric.

We determined that the ΔΨm Low peripheral T-cell repertoire was more like the tumor T-cell repertoire than ΔΨm High peripheral T-cells were in the partial responder, with cosine similarity scores of 0.18 and 0.14, respectively. Conversely, ΔΨm High peripheral T-cells were more like the tumor T-cell repertoire than ΔΨm Low peripheral T-cells by a much wider margin, with scores of 0.12 and 0.019 (**Figure 3.4B**).

We then determined that ΔΨm influences the clonality of T-cell responses in the periphery. Examining the number of unique clonotypes in the top 12% of all T-cells, we found that ΔΨm Low peripheral T-cells had fewer unique clones, at 2, represented in the top 12% (more clonal) while ΔΨm High T-cells had more unique clones, at 4, represented in the top 12% of pre- and post-ICB peripheral T-cell repertoires across all patients (**Figure 3.4C**). The threshold of 12% was chosen arbitrarily, yet it captures the dynamic differences in clonal proportion between the extremes of 1 and 18. While there was variability in that metric on a patient-by-patient basis, when we looked at the proportion of hyperexpanded clones that make up 1-100% of the entire T-cell repertoire, ΔΨm Low peripheral T-cells had a greater proportion of hyperexpanded clones than ΔΨm High peripheral T-cells across all patients (**Figure 3.4D**).

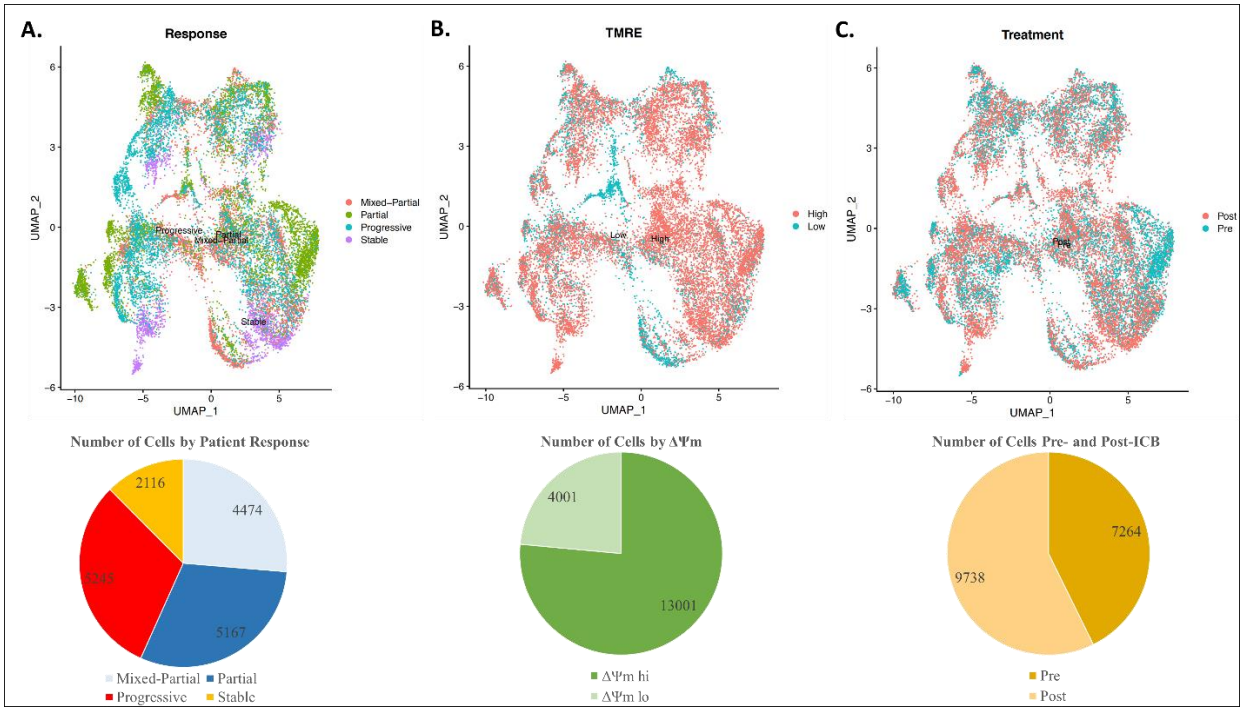

Figure 3.5. ccRCC Patient Peripheral T-cells are Predominantly ΔΨm hi. UMAP plots and cell category pie charts of ccRCC peripheral T-cells by **(A)** patient response, **(B)** ΔΨm hi vs. low, and **(C)** Pre vs. Post ICB**.**

In the scRNA-seq data assessing Live, CD3+, ΔΨm High and Live, CD3+, ΔΨm Low cells from pre- and post-ICB patient blood, we recovered 2116 to 5245 cells from each patient post quality control (**Figure 3.5A**). These cells were predominantly ΔΨm Hi, representing 76.5% of all cells identified, while ΔΨm Low cells made up 23.5% of cells from all patients and conditions (**Figure 3.5B**). Although the gating strategy succeeded in capturing the top (ΔΨm Hi) and bottom (ΔΨm Lo) 50% of Live, CD3+ patient PBMCs by TMRE fluorescence, greater numbers of ΔΨm Low cells than ΔΨm High cells were removed from the scRNA-seq data following quality control. Since ΔΨm is closely tied to mitochondrial DNA (mtDNA) which encodes for components of the electron transport chain (ETC), mtDNA may play different functional roles in ΔΨm High and ΔΨm Low cells, although less mtDNA transcription has been

associated with a failure to maintain ΔΨm (265). The use of mtDNA cutoffs for QC may need to be further assessed for biological relevance beyond as an indicator for poor cell health. Slightly more cells were recovered from post-ICB patient T-cells, with post-ICB cells making up 57.3% of all patient T-cells (**Figure 3.5C**).

	avg_log2FC	pct.1	pct.2	p_val_adj
HLA-DRB1	1.01932738	0.398	0.22	2.97E-103
SMDT1	0.98296662	0.61	0.301	1.29E-294
XIST	0.96208255	0.312	0.046	1.34E-266
TNFAIP3	0.77522674	0.614	0.455	2.82E-84
SOCS3	0.72778529	0.471	0.244	3.57E-141
RPS4X	0.7117718	0.977	0.968	0
TRBV7-6	0.69867294	0.141	0.037	9.53E-72
HLA-DRA	0.68274276	0.163	0.062	8.87E-59
CXCR4	0.63180956	0.701	0.513	1.92E-110
BHLHE40	0.62638788	0.317	0.207	5.56E-41
TRAV29DV5	0.60815824	0.171	0.091	2.48E-31
FGFBP2	0.5492536	0.314	0.296	0.00205681
CST7	-0.5759672	0.473	0.567	1.00E-39
PRKY	-0.5765092	0.008	0.177	3.47E-188
TIGIT	-0.6777843	0.111	0.284	2.63E-111
TNF	-0.6989611	0.298	0.414	2.98E-36
USP9Y	-0.7016254	0.014	0.227	1.95E-237
UTY	-0.7133159	0.009	0.223	4.32E-248
RPS26	-0.7377342	0.957	0.971	1.19E-271
GZMK	-0.8338997	0.153	0.279	1.54E-54
CMC1	-0.8876655	0.205	0.381	2.67E-108
EGR1	-1.0888042	0.183	0.347	2.69E-90
DDX3Y	-1.2033755	0.021	0.398	0
RPS4Y1	-2.4230884	0.063	0.812	0

Table 3.1. T-cells from the Patient with Progressive Disease Expresses Significantly More TIGIT and TNF and Less HLA-DRB1 and HLA-DRA Compared to Partial Responder. Top differentially expressed genes between all partial response and patient with progressive disease T-cells, with genes enriched in the patient with progressive disease in gray. Avg_log2FC indicates the average log 2-fold change in gene expression between conditions, pct.1 indicates the number of cells expressing a gene in the partial responder, and pct.2 indicates the number of cells expressing a gene in the patient with progressive disease. p_val_adj indicates the adjusted p-value via the Bonferroni method of multiple-testing correction.

To assess gene expression differences on the mRNA level that could shed light on the differences in T-cell responses between the partial responder and the patient with progressive disease, we performed differential gene expression analysis on our scRNA-seq data. Examining the top differentially expressed genes, we found that pre- and post-ICB combined peripheral T-cells from the patient with progressive disease expressed significantly more *TIGIT, TNF CST7*, and *GZMK* while partial responder peripheral T-cells expressed greater *HLA-DRB1, HLA-DRA*, *TNFAIP3, SOCS3, TRBV7-6, TRAV29DV5, BHLHE40*, and *CXCR4*, among other genes (**Table 3.1**).

	avg_log2FC	pct.1	pct.2	p_val_adj
LINC02446	0.91142735	0.287	0.09	1.29E-223
TYROBP	0.7727689	0.11	0.027	6.36E-104
CD8B	0.74636607	0.536	0.288	3.34E-182
KLRB1	0.69699288	0.274	0.178	1.71E-44
CD8A	0.6376742	0.618	0.339	1.86E-185
KLRD1	0.59778823	0.386	0.201	7.10E-116
KLRK1	0.58737804	0.543	0.3	1.63E-152
TRAV1-2	0.58041928	0.104	0.019	2.36E-126
CCL5	0.51817211	0.684	0.56	2.24E-67
PRF1	0.4930864	0.494	0.349	2.19E-62
CTSW	0.48568609	0.757	0.575	2.54E-112
CCL4	0.47730608	0.357	0.276	4.98E-18
SESN3	-0.3256865	0.122	0.185	4.38E-17
CD82	-0.3274776	0.114	0.204	2.07E-34
GSTK1	-0.3359684	0.801	0.826	2.01E-54
LINC00861	-0.344403	0.542	0.59	2.85E-11
CD4	-0.36472	0.136	0.248	1.17E-46
GPR183	-0.3665174	0.196	0.297	1.35E-32
FXYD5	-0.3822887	0.869	0.879	1.82E-76
ARID5B	-0.3938314	0.215	0.334	3.65E-44
LMNA	-0.398181	0.092	0.138	9.47E-12
S100A11	-0.399802	0.497	0.584	3.46E-37
RPS26	-0.5150154	0.907	0.945	6.65E-99
ITGB1	-0.7821007	0.4	0.583	3.30E-112

Table 3.2. ΔΨm Correlates with CD4 and CD8A/CD8B Differential Gene Expression. Top differentially expressed genes between all ccRCC patient ΔΨm hi and ΔΨm low T-cells, with

genes enriched in ΔΨm hi T-cells in gray. Avg_log2FC indicates the average log 2-fold change in gene expression between conditions, pct.1 indicates the number of cells expressing a gene in ΔΨm lo, and pct.2 indicates the number of cells expressing a gene in ΔΨm hi. p_val_adj indicates the adjusted p-value via the Bonferroni method of multiple-testing correction.

T-cell responses to ccRCC also possess divergent transcriptional programs depending on ΔΨm status. While ΔΨm hi T-cells in combined pre- and post-ICB T-cell populations possessed greater *ITGB1, S100A11, LMNA, ARID5B, GSTK1*, and *CD4* expression, ΔΨm Low T-cells comparatively up-regulate genes associated with cytotoxicity including *CTSW, PRF1, KLRB1, KLRD1, KLRK1, CD8A,* and *CD8B,* among others (**Table 3.2**).

	avg_log2FC	pct.1	pct.2	p_val_adj
CCR7	0.48375145	0.453	0.329	1.50E-68
PIM1	0.32126266	0.524	0.418	1.34E-47
MYC	0.30899161	0.286	0.188	1.84E-48
CISH	0.30880648	0.32	0.223	4.36E-44
LEF1	0.25588994	0.474	0.373	7.82E-35
HLA-C	-0.2510332	0.973	0.973	6.21E-43
CD99	-0.2538246	0.729	0.777	6.96E-36
PLAAT4	-0.2547179	0.644	0.68	4.96E-26
TUBB4B	-0.2549999	0.381	0.428	2.22E-14
GZMA	-0.2558082	0.424	0.507	5.77E-23
SRGN	-0.2566034	0.717	0.743	1.68E-29
CMC1	-0.2567081	0.241	0.279	1.19E-07
EGR1	-0.3035207	0.21	0.253	2.11E-07
RPS4Y1	-0.3097993	0.508	0.652	3.03E-61
HLA-DPA1	-0.316627	0.323	0.408	3.65E-32
SH3BGRL3	-0.3223686	0.898	0.913	1.03E-61
UBE2S	-0.32299	0.441	0.489	8.10E-23
CD74	-0.3894272	0.782	0.808	1.69E-41
GZMH	-0.4240105	0.309	0.394	7.31E-31
GNLY	-0.4426422	0.32	0.393	5.66E-23
JUN	-0.4453586	0.657	0.674	3.15E-25
CCL5	-0.4549479	0.545	0.622	2.62E-43
CST7	-0.4812344	0.419	0.511	2.60E-44
NKG7	-0.5589945	0.471	0.56	2.79E-47

Table 3.3. ICB in Four ccRCC Patients Significantly Reduces CCR7, PIM1, MYC, CISH, and LEF1 while Increasing Gene Expression Associated with Cytotoxicity and Antigen Presentation. Top differentially expressed genes between all ccRCC patients pre- and post-ICB

T-cells, with genes enriched in post-ICB T-cells in gray. Avg_log2FC indicates the average log 2-fold change in gene expression between conditions, pct.1 indicates the number of cells expressing a gene in pre-ICB T-cells, and pct.2 indicates the number of cells expressing a gene in post-ICB T-cells. p_val_adj indicates the adjusted p-value via the Bonferroni method of multiple-testing correction.

We then examined DE genes between pre- and post-ICB peripheral T-cells in all patients combined. Only five genes were identified that were significantly upregulated in pre-ICB peripheral T-cells in aggregated patient data: *CCR7, PIM1, MYC, CISH,* and *LEF1*. On the other hand, several genes are upregulated post-ICB. The top significantly upregulated genes post-ICB by average $\log_2$ fold change were genes associated with cytotoxicity, chemotaxis, and inflammation: *NKG7, CST7, CCL5, JUN,* and *GNLY* (**Table 3.3**).

Periphery-TIL Shared T-cell Clones are Found Primarily in the Partial Responder, Have Lower ΔΨm than Average, and Have a Distinct Gene Expression Program

Integrating our scRNA-seq, scV(D)J-seq, and ArcherDx VDJ-seq data, we discovered a subset of cells in the periphery that shared both a TRA and TRB CDR3 amino acid sequence with those found in the tumor. These cells often clustered together, indicating they are guided by transcriptional programs distinct from other T-cell populations in the experiment (**Figure 3.6A+B**). Out of 17002 total cells that passed QC for scRNA-seq and scV(D)J-seq, 1996 cells representing 11.7% of the total T-cells profiled shared TRA and TRB CDR3 sequences with tumor T-cells. Of these, 69% were derived from the partial responder, 14.7% from the stable responder, 9.9% from the patient with progressive disease, and 6.3% from the mixed/partial responder (**Figure 3.6C**). Furthermore, these cells had lower ΔΨm than the average T-cell in this experiment. While 642/1996 (32.2%) of shared peripheral-tumor T-cells had low ΔΨm, the aggregate of all sequenced peripheral T-cells had 4001/17002 (23.5%) of cells with low ΔΨm (**Figure 3.6D**). This enrichment of low ΔΨm in shared peripheral-tumor T cells suggests that low

ΔΨm is important for tumor-specific T cells that expand into the periphery and could predict positive response to ICB in ccRCC patients.

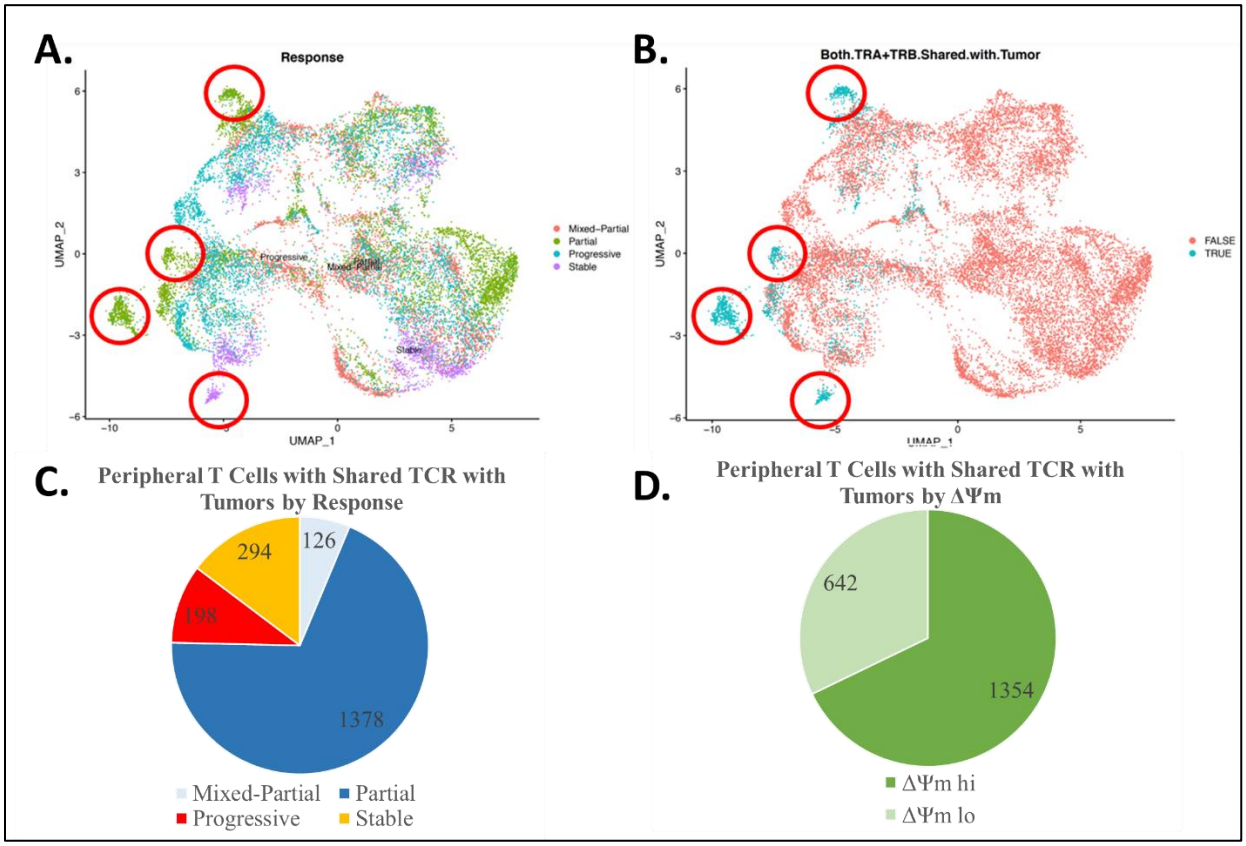

Figure 3.6. Shared Peripheral-Tumor T-cell Clones are ΔΨm hi and found in the Partial Responder to ICB. UMAP and cell proportion plots of ccRCC patient peripheral T-cells, highlighting the distribution of T-cell clones found in both the tumor and peripheral repertoires. **A)** UMAP stratified by patient response, with T-cells that share both TRA and TRB CDR3 amino acid sequences with ccRCC tumor-associated T-cells circled in red. **(B)** UMAP labeling shared peripheral-tumor T-cells as TRUE and other cells as FALSE. **(C)** ccRCC patient T-cell proportional abundance by patient response. **(D)** ccRCC patient T-cell proportional abundance by ΔΨm status.

We examined the DE genes between shared peripheral-tumor T-cells and periphery-exclusive T-cells, and we determined that shared peripheral-tumor T-cells upregulated genes associated with cytotoxicity and antigen presentation while downregulating genes associated with naïve T-cells and T-cell stemness. These DE genes also possessed a wide difference in mean expression and percent expression in each population. Notable genes associated with

cytotoxicity upregulated in shared peripheral-tumor T-cells are *GNLY, FGFBP2, GXMH, NKG7, PRF1, GZMB, KLRD1,* and *KLRC1.* Shared peripheral-tumor T-cells also upregulated the chemokine ligand *CCL4* and the specific TRA and TRB genes *TRAV29DV5* and *TRBV7-6.* Conversely, periphery-exclusive T-cells significantly upregulate *CCR7, TCF7, LEF1, SELL,* and *IL7R.* These cells also upregulate the TNF family gene *LTB* (**Table 3.4**).

	avg_log2FC	pct.1	pct.2	p_val_adj
GNLY	1.97323205	0.818	0.301	0
FGFBP2	1.80124977	0.699	0.181	0
TRAV29DV5	1.78757488	0.39	0.063	0
CCL4	1.62811549	0.62	0.252	2.31E-273
TRBV7-6	1.56526023	0.328	0.034	0
GZMH	1.55988186	0.876	0.289	0
NKG7	1.55237159	0.979	0.461	0
PRF1	1.51897421	0.841	0.322	0
HLA-DRB1	1.49415941	0.646	0.21	0
GZMB	1.43791091	0.657	0.198	0
KLRD1	1.43471959	0.659	0.189	0
KLRC1	1.39674225	0.3	0.016	0
TRAT1	-0.8333682	0.137	0.389	3.61E-104
LDHB	-0.8992466	0.624	0.796	1.74E-177
NOSIP	-0.9506618	0.352	0.587	1.38E-120
IL7R	-0.9951737	0.6	0.802	3.15E-137
RCAN3	-1.0049444	0.074	0.37	8.04E-143
MAL	-1.0071728	0.036	0.321	2.74E-145
SELL	-1.1001808	0.306	0.567	1.57E-126
RPS4Y1	-1.1490139	0.249	0.636	2.03E-201
LEF1	-1.33235	0.11	0.457	1.05E-188
TCF7	-1.4045782	0.25	0.647	1.46E-265
CCR7	-1.6455971	0.045	0.427	7.35E-225
LTB	-1.8998645	0.419	0.777	0

Table 3.4. Peripheral T-cells that share TCRs with Tumor T-cells Significantly Upregulate Cytotoxicity, Antigen-Presenting Genes and Downregulate Naïve T-cell Genes. Top differentially expressed genes between all ccRCC patient peripheral T-cells that share TCRs with tumor T-cells and peripheral T-cells that do not share TCRs with tumor T-cells, with genes enriched in periphery-exclusive T-cells in gray. Avg_log2FC indicates average log 2-fold change in gene expression between conditions, pct.1 indicates the number of cells expressing a gene in peripheral-tumor shared T-cells, pct.2 indicates the number of cells expressing a gene in

periphery-exclusive T-cells. p_val_adj indicates the adjusted p-value via the Bonferroni method of multiple-testing correction.

Periphery Shared Peripheral-Tumor T-cells Expand or Contract from the Tumor to the Periphery Depending on Patient Response

We next examined the pattern of expansion of shared peripheral-tumor T-cell clones from the tumor into the periphery. To do this, we first determined the percent representation of each clone within the tumor T-cell repertoire and combined all the clones' percent representation in the tumor repertoire to represent the total shared clone representation in the tumor. Next, we followed that same process for shared clone proportion in peripheral pre-ICB and post-ICB T-cells in **Figure 3.7** and peripheral ΔΨm Low and ΔΨm High T-cells in **Figure 3.8**. If the representation of all shared clones increased in the periphery, those clones *expanded*. If the representation of all shared clones *decreased* in the periphery, those shared clones *contracted*. T-cells that were not contained in all three groups were excluded from this analysis.

We determined that each patient response exhibited a different pattern of expansion and contraction into pre-ICB and post-ICB peripheral T-cell populations. The partial responder's shared peripheral-tumor T-cells expanded in repertoire proportion from the tumor into pre-ICB T-cells while maintaining overall representation in the post-ICB periphery. However, certain clones including the clone with the TRA CDR3 amino acid sequence CVTDQTGANNLFF expanded significantly in both pre-ICB and post-ICB peripheral T-cell repertoires. The partial responder also exhibited the most shared peripheral-tumor unique T-cell clones, 57, compared with the other patients who did not have tumor shrinkage. The partial responder also had the greatest percent representation of shared clones in the tumor and periphery (**Figure 3.7A**). Conversely, the mixed/partial responder had fewer shared clones, less representation of those

shared clones in the tumor repertoire, and a contraction of those clones into both pre-ICB and post-ICB peripheral T-cell repertoires. The mixed/partial responder also had the second least number of unique shared peripheral-tumor T-cell clones at 14 clones (**Figure 3.7B**). The stable responder had the least overall percent representation of shared peripheral-tumor T-cell clones in the tumor. While the overall representation of shared clones contracted in pre-ICB peripheral T-cells, overall shared clonal representation nearly tripled from tumor to post-ICB periphery. The stable tumor also had the second most unique shared peripheral-tumor T-cell clones out of the four patients at 21 clones (**Figure 3.7C**). The patient with progressive disease had only three shared peripheral-tumor T-cell clones, with the overall representation of those clones decreasing roughly 7-fold in both pre-ICB and post-ICB periphery (**Figure 3.7D**).

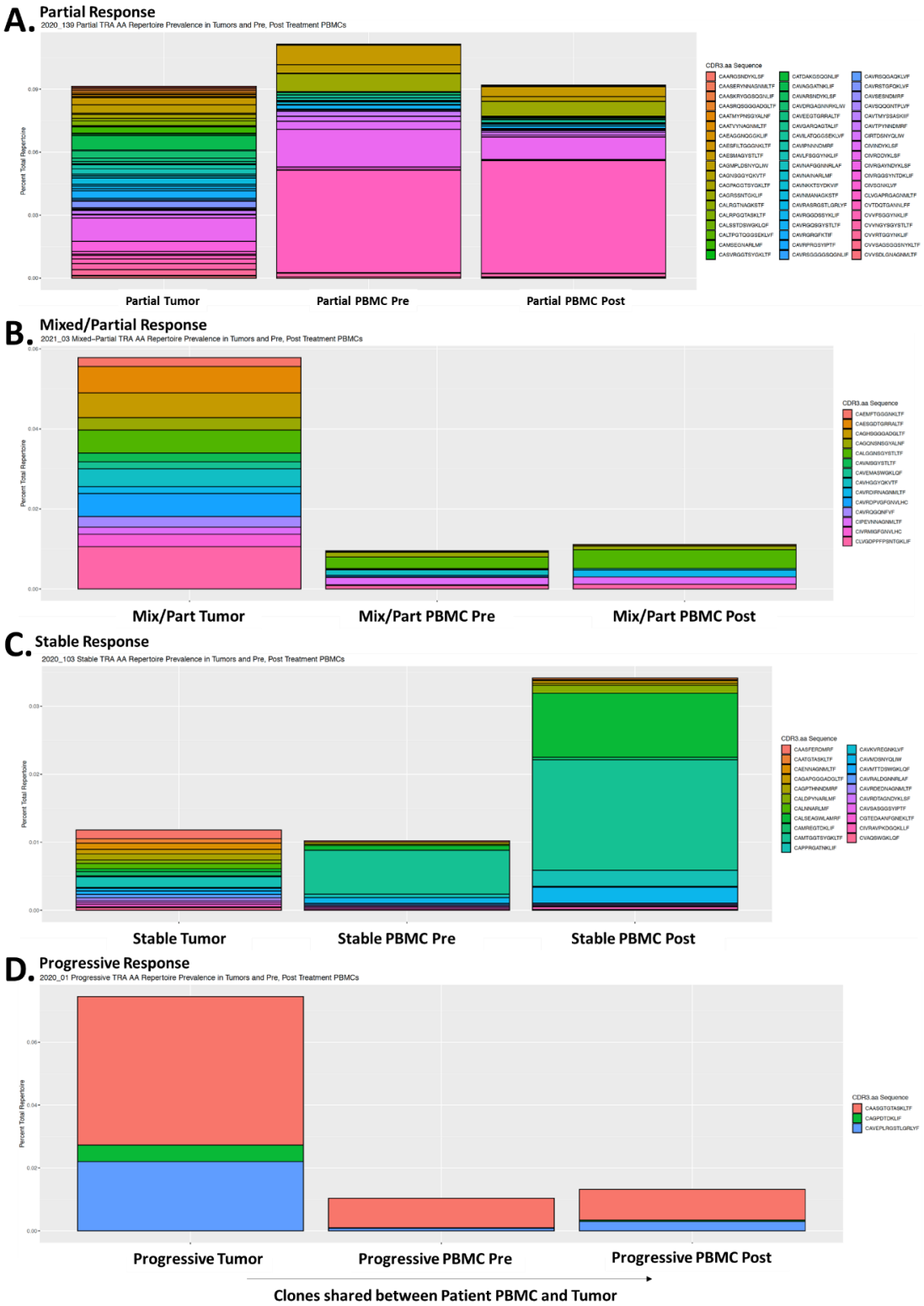

Figure 3.7. Peripheral-Tumor Shared T-cell Clones Expand in Partial Responder and Recede in the Patient with Progressive Disease Before ICB. Percent representation of peripheral-tumor shared T-cell clones pre- and post-ICB in patients with **(A)** partial, **(B)** mixed/partial **(C)** stable, and **(D)** progressive responses to ICB.

Next, we examined the role of ΔΨm on clonal expansion in the periphery by binning both the pre-ICB and post-ICB peripheral T-cell repertoires together and dividing all cells based on ΔΨm Low and ΔΨm Hi. We compared the representation of the same shared peripheral-tumor T-cell clones in the tumor, ΔΨm Lo, and ΔΨm High in **Figure 3.8** in a similar fashion to the tumor, pre-ICB, and post-ICB in **Figure 3.7**. Generally, a greater overall representation of shared peripheral-tumor T-cell clones in the ΔΨm Low than in ΔΨm High is seen in the partial and mixed/partial responders, whereas greater representation in ΔΨm High than in ΔΨm Low characterizes the more negative outcomes: progressive and stable response patients. The partial responder has greater clonal representation in peripheral ΔΨm Low cells than both tumor T-cells and peripheral ΔΨm High cells (**Figure 3.8A**). While the mixed/partial responder had roughly the same clonal representation in pre-ICB and post-ICB T-cells with overall representation shrinking in the periphery, peripheral ΔΨm Low cells have greater overall shared clonal representation than ΔΨm High peripheral cells (**Figure 3.8B**). The stable responder, conversely, had a greater overall shared clonal representation

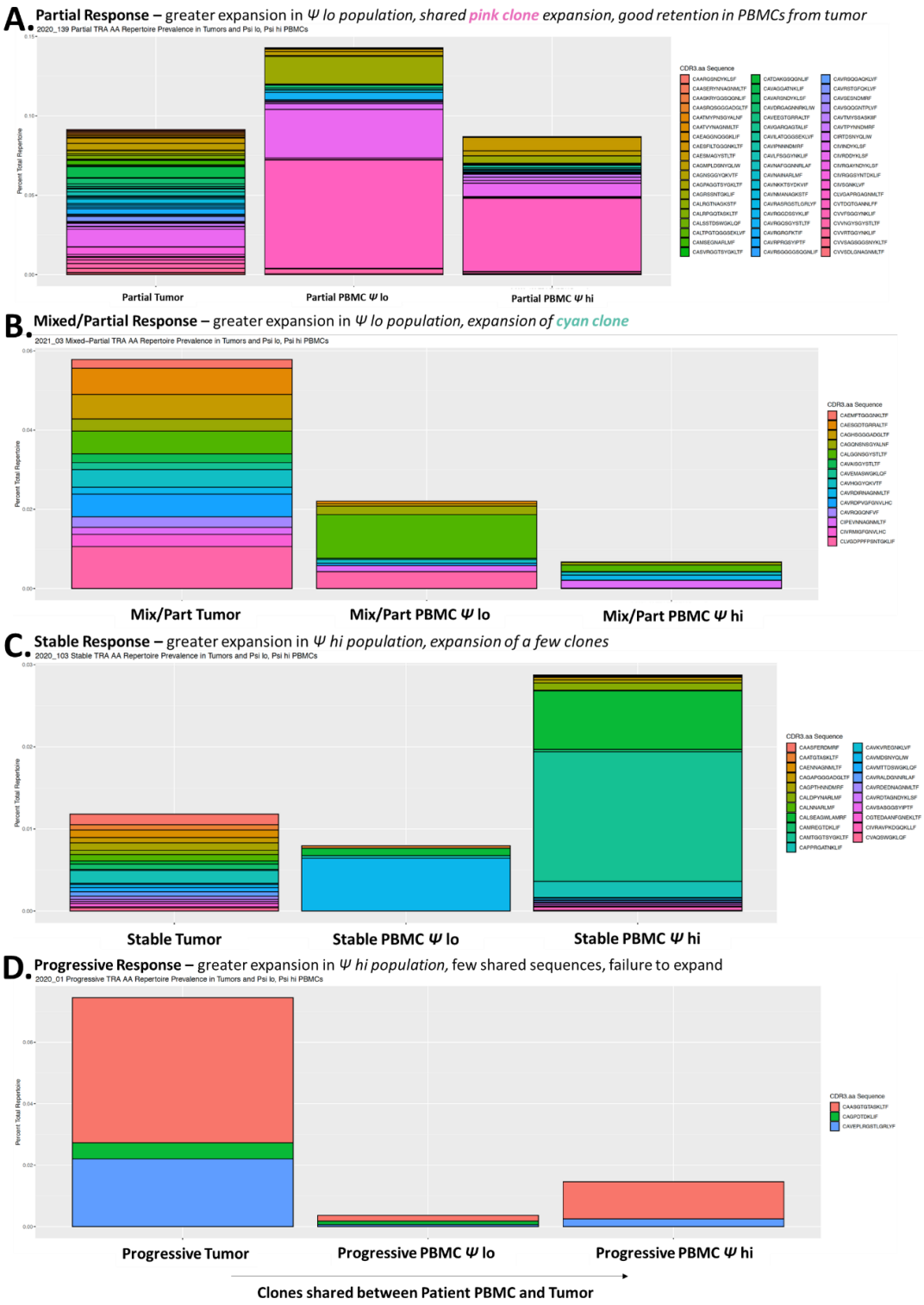

Figure 3.8. Peripheral-Tumor Shared T-cell Clone Enrichment in ΔΨm Low Population is Associated with Positive Responses to ICB. Percent representation of peripheral-tumor shared T-cell clones in the tumor, ΔΨm lo, and ΔΨm hi in patients with **(A)** partial, **(B)** mixed/partial **(C)** stable, and **(D)** progressive responses to ICB.

in peripheral ΔΨm High cells than ΔΨm Low cells, with the clones with TRA CDR3 amino acid sequence CAMTGGTSYGKLTF, CALSEAGWLAMRF, and CAPPRGATNKLIF much more represented in ΔΨm High than ΔΨm Low cells (**Figure 3.8C**). Next, peripheral T-cells from the patient with progressive disease showed roughly three times more overall representation from shared peripheral-tumor clones in the ΔΨm High fraction than the ΔΨm Low fraction. Compared to the more even representation of the three shared clones in the pre-ICB vs. post-ICB axis, this difference is much more pronounced (**Figure 3.8D**).

Finally, we identified a handful of public T-cell clones shared between the tumor repertoire of one patient and at least two other patients' peripheral repertoires. While the complexity of the overall peripheral T-cell repertoire could render these public clones a coincidence, two of these clones exhibit expansion between the tumor and the periphery which suggests a tumor-specific ontology for these public clones. The top two public clones that were identified were clones with the TRA CDR3 nucleotide sequence TGTGTCACCGATCAAACTGGGGCAAACAACCTCTTCTTT (denoted PC1), found in the partial responder tumor repertoire, and TGTGCAGGGAGATCTAGCAACACAGGCAAACTAATCTTT (denoted PC2), also found in the partial responder tumor repertoire. PC1 was shared between the partial responder's tumor repertoire, the progressive peripheral repertoire, and the mixed/partial peripheral repertoire and was identified in 27 total cells in the combined progressive and mixed/partial responder peripheries. PC2 was shared between the partial responder's tumor repertoire and the peripheral repertoire of the patient with progressive disease, and it was identified in 5 total cells in the patient with progressive disease's periphery.

All TCR Sequences Shared between Different Patient Periphery and Tumor T cells		Expansion of Clone from Tumor to Periphery			
TRA CDR3 NT Sequence	Frequency	%Repertoire ΔΨm Lo / %Repertoire Tumor	%Repertoire ΔΨm Hi / %Repertoire Tumor	%Repertoire Pre / %Repertoire Tumor	%Repertoire Post / %Repertoire Tumor
TGTGCCGTGAATGCATTTGGGGGGAACAACAGACTCGCTTTT	2	NA	0.32	NA	0.43
TGTGCTGTCAGATCCGGAGGGGGAGGAAGCCAAGGAAATCTCATCTTT	1	NA	0.16	NA	0.22
TGTGCAGGGAGATCTAGCAACACAGGCAAACTAATCTTT	5	115.9	29.78	56.46	46.06
TGTGTCACCGATCAAACTGGGGCAAACAACCTCTTCTTT*	27	41.22	27.84	29.36	32.39
TGTGCTGTGAGAGGACAATCAGGATACAGCACCCTCACCTTT	1	4.36	0.46	1.77	1.12
TGCATCGTCAGGGACGACTACAAGCTCAGCTTT	2	2.79	0.77	1.62	0.98
TGTGCTGTGATTCTTGCGACTCAGGGCGGATCTGAAAAGCTGGTCTTT	1	2.03	3.45	3.01	3.19
TGTGCCTTGGGGGGGAATTCAGGATACAGCACCCTCACCTTT	2	1.92	0.27	0.47	0.82
TGTGTGGTGAACGGGTATTCAGGATACAGCACCCTCACCTTT	2	1.07	0.37	0.59	0.5
TGCATCCCCGAGGTTAATAATGCAGGCAACATGCTCACCTTT**	2	0.87	1.1	1.06	1.04
TGTGCTGGGCAGAACTCAAATTCCGGGTATGCACTCAACTTC	2	0.69	0.22	0.39	0.3
TGTGCTGGGATGCCCTTGGATAGCAACTATCAGTTAATCTGG	1	0.6	0.77	0.96	0.55
TGCCTCGTGGGTGACCCTCCTTTCCCTAGCAACACAGGCAAACTAATCTTT	1	0.51	NA	0.1	0.14
TGTGCAGAGAGTATGGCCGGATACAGCACCCTCACCTTT	4	0.46	2.53	2.82	1.42
TGTGCCGTGACCCCGTATAACAATGACATGCGCTTT	1	0.34	0.97	1.32	0.43
TGTGCAGCAAGCGGAACCGGCACTGCCAGTAAACTCACCTTT	1	0.04	0.26	0.2	0.21

Shared between patients and **expands** from tumor to patient periphery
Shared between patients and **recedes** from tumor to patient periphery

Table 3.5. Peripheral-Tumor T-cell Clones from One Patient's Tumor May Be Found in Other Patients' Peripheral Repertoires. All T-cell clones shared between the periphery of one or more patients and the tumor repertoire of another patient. The clones highlighted in yellow are the most frequent clones with the greatest expansion from tumor to periphery. Frequency indicates the total number of cells with that TCRα CDR3 nucleotide sequence found in all patient peripheral repertoires except the original patient. Expansion of the clone is determined by dividing the clonal representation in the original patient's ΔΨm lo, ΔΨm hi, pre-ICB, or post-ICB peripheral T-cell repertoire by that clone's percent representation in the tumor T-cell repertoire. Positive numbers indicate expansion from the tumor, while negative numbers indicate shrinking. *Clone from progressive and mixed-partial responder periphery shared with partial tumor.

We then examined the expansion patterns of these shared clones from the tumor into ΔΨm Lo, ΔΨm Hi, pre-ICB, and post-ICB peripheral T-cell repertoires in the partial responder. By dividing the percent repertoire representation of the clone of interest in a peripheral fraction by its percent representation in the tumor, we determined that both clones expanded considerably from the tumor into the periphery. PC1 was 29.36 times more represented in the pre-ICB fraction and 32.39 times more represented in the post-ICB fraction compared to its representation in the tumor repertoire. Comparing along the ΔΨm axis, PC1 expanded to 41.22 times its tumor repertoire representation in the ΔΨm Low repertoire while expanding to a lesser 27.84 times its tumor representation in ΔΨm Hi. PC2 expanded to a greater degree in the periphery from the tumor. In the pre-ICB repertoire, PC2 expanded 56.46 times while it expanded 46.06 times in the post-ICB repertoire. We see a striking difference when compared to the expansion patterns bifurcated by ΔΨm status, however, as PC2 expanded 115.9 times into the ΔΨm low fraction and a lesser 29.78 times into the ΔΨm hi fraction (**Table 3.5**).

Discussion and Future Directions

ccRCC patient T-cells increase metabolic flux through glycolysis, oxidative phosphorylation, and other pathways and increase ΔΨm to facilitate antitumor responses. However, the field lacks consensus as to the role of ΔΨm in ccRCC antitumor T-cell immunity, T-cell clonality, and T-cell gene expression programs. In this study, we investigated the role of ΔΨm on T-cell responses in ccRCC patients treated with the ICB α-CTLA4/α-PD-1 (Ipi/Nivo) using scRNA-seq and scV(D)J-seq analysis of peripheral ΔΨm High and ΔΨm Low T-cells

before and after ICB, ArcherDx VDJ-seq analysis of ccRCC patient tumor TILs, and CyTOF analysis of ccRCC patient PBMCs.

We determined that ccRCC patient peripheral T-cells were ΔΨm High by a roughly 3:1 margin. We also identified significantly differing populations before and after ICB and between partial and progressive disease by CyTOF in peripheral immune populations through T-REX and MEM analysis. The patient with progressive disease had a greater proportion of exhausted TIGIT+ γδ T-cells and exhausted TIGIT+ CD4+ T-cells with low Ki67 enrichment post-resection and before ICB. The partial responder gained a population of similarly exhausted TIGIT+ CD4+ T-cells with comparatively greater expression of CD38 and CCR5 with reduced CD95, CCR4, CXCR3, and Ki67. The greater enrichment of CD95 (Fas) and Ki67 in the patient with progressive disease suggests this T-cell population may be more proliferative and prone to FasL-mediated signaling than its partial responder corresponding populations. Fas-FasL signaling in this population could lead to inhibition or activation of CD3-TCR signaling given the dose of FasL. Alternatively, greater Fas in the patient with progressive disease population could indicate a greater sensitivity to Fas-FasL mediated apoptosis (266). Given the high expression of CTLA4 and the presence of TIGIT-inducible proteins like CXCR3, CCR4, and CCR5, these CD4+ populations could be distinct types of Tregs that serve different functions in different patients. In the patient with progressive disease, their enrichment pre-ICB suggests they could limit the antitumor T-cell response to ICB, while their enrichment in post-ICB in the partial responder could indicate that these cells emerge to limit the effective immune response potentiated by ICB (267).

We also observed the emergence of four monocyte/macrophage populations and two granulocyte populations combined with the contraction of a single granulocyte population in the

patient with progressive disease post-ICB. In the partial responder, ICB induced two monocyte/macrophage populations and a single B cell population, suggesting that B cell responses may be a factor in determining response to ICB. The granulocyte populations present in the patient with progressive disease were each enriched with CD66b, CTLA4, and CD11b. Interestingly, the granulocyte population enriched in pre-ICB PBMCs lacked the adhesion molecule CD44, while the post-ICB granulocyte populations gained CD44 expression, suggesting different population capacities for extravasation (268). Comparing pre-ICB T-cells from the patient with progressive disease to the partial responder, the patient with progressive disease was enriched with exhausted TIGIT+ CD8+ T-cell populations and a γδ T-cell population while the partial responder was enriched in CD4+ cell populations with lower TIGIT enrichment. The pre-ICB patient with progressive disease was also enriched in one CD4+ T-cell population with elevated activation proteins and the chemokine receptors CCR4 and CXCR4.

Comparing post-ICB progressive vs. partial, the patient with progressive disease again is enriched in three populations of exhausted CD8+ T-cells with high TIGIT enrichment and a CD4+ T-cell population with higher CTLA4 enrichment than the partial responder. The partial responder gained two CD4+ T-cell populations and one CD8+ T-cell population with low TIGIT enrichment. One CD4+ population and the CD8+ T-cell population also had mid to high expression of CD57, a marker associated with heightened antitumor capacity in CD8+ T-cells responding to non-small cell lung cancer (NSCLC) (269). CD4+, CD57+ T-cells also exhibit transcriptional programs like CD8+ T-cells in the context of HIV infection (270). While there is great variation among identified populations, the noted trends associated with TIGIT and CTLA4 as well as CD4, CD8, and γδ T-cell populations may influence response to ICB in ccRCC patients. Furthermore, heightened PBMC metabolic activity through glycolysis and fatty acid

oxidation, inferred through greater surface expression of CPT1a and GLUT1, correlates with progressive disease in response to ICB. More characterization of these populations is needed to make firm conclusions on their etiologies.

We also characterized the role of ΔΨm on T-cell clonal responses in our four patients, indicating that expansion of tumor-associated T-cell clones into ΔΨm High fractions may be associated with progressive response. Furthermore, ΔΨm Low cells are associated with greater clonal responses across patients and increase the proportion of hyperexpanded clones in each patient. The greatest similarity between the peripheral T-cell repertoire and the tumor T-cell repertoire was found in the partial responder, a finding that is consistent with results published by the Matsushima group in 2021, which indicate that greater overlap between tumor and peripheral repertoires is associated with positive outcomes to ICB in GI cancer (119). The next largest similarity between peripheral and tumor T-cell repertoires was found in the patient with progressive disease. However, ΔΨm hi cells from the patient with progressive disease were most like tumor T-cells, suggesting a CD4+ T-cell dominated expansion, while the partial responder's ΔΨm Low T-cells were most like their tumor T-cell repertoire suggesting a preferential CD8+ T-cell response with a significant CD4+ T-cell component.

We next identified gene expression programs enriched across partial responder vs. patient with progressive disease, ΔΨm status, and pre-ICB vs. post-ICB T-cells. While the partial responder upregulated genes associated with antigen presentation and specific TCR genes, the patient with progressive disease had greater expression of *TIGIT*, *TNF*, and *GZMK*, all genes that are known to be associated with poorer clinical outcomes in cancer (271, 272). *GZMK* is enriched in a clonal population of exhausted-like, senescent CD8+ T-cells present in aged mice and humans that potentially contribute to systemic inflammation and dysregulated immune

responses in the elderly. The enrichment of *GZMK* expression in the patient with progressive disease suggests that this population of T cells may also contribute to negative responses to ICB (273). Furthermore, the partial responder exhibited significantly greater expression of the TF *BHLHE40* compared to the patient with progressive disease. *BHLHE40,* mentioned in the introduction of this dissertation, has been reported as necessary for reinvigorating TIL mitochondrial fitness and function following α-PD-L1 ICB (133).

Interestingly, ΔΨm appears to influence CD4+ vs. CD8+ T-cell responses, as ΔΨm Low cells expressed greater *CD8A/B* while ΔΨm High cells expressed greater *CD4,* which can be inferred by CD4+ T-cells' greater capacity to upregulate glycolysis compared to CD8+ T-cells upon activation. ΔΨm Low T-cells also upregulate genes associated with chemotaxis and cytotoxicity compared to ΔΨm High T-cells.

Most significant to the field, we identified a population of peripheral T-cells with shared TCR sequences with tumor T-cells preferentially found in the partial responder and greater ΔΨm Low T-cells than the experimental average. The DE gene expression profile of these shared peripheral-tumor T-cells indicates that they are more chemotactic through *CCL4* and upregulate cytotoxic genes like *NKG7, PRF1, GNLY,* and *GZMB.* They are also competent for antigen presentation through the upregulation of *HLA-DRB1* and significantly upregulate specific TCR genes *TRAV29DV5* and *TRBV7-6*. These TCR genes were previously reported as prognostic factors in melanoma, with hazard ratios of 0.79 and 0.76 and p-values of 0.018 and 0.016, respectively (274). However, these TCR genes have not been reported as prognostic in ccRCC. The gene signatures of shared peripheral-tumor T-cells and periphery-exclusive T-cells match closely with previously reported results establishing gene expression profiles of peripheral-tumor shared T-cell clones in the blood in the murine MC38 model and human melanoma patients.

Pauken *et al.* reported in 2021 that these "TM" cells exhibited reduced markers associated with T central memory cells like *LTB, CCR7, TCF7, SELL* and elevated effector markers *GZMB, NKG7,* and *PRF1*, just like the peripheral-tumor shared T-cells reported here (275). However, while they shared genes with the ones reported here, they did not report increased expression of *GNLY*, *FGFBP2*, and *GZMH* on their TM cells.

Examining these shared cells further, we determined patient-specific expansion patterns of shared peripheral-tumor T-cells that correlated with response. Shared T-cells expanded in the pre-ICB periphery of the partial responder, suggesting that the presence of these cells influenced patient response post-ICB, as many of these clones persisted three weeks later in the periphery at similar proportions to pre-ICB. Conversely, all other responses saw shared T-cell representation decrease pre-ICB. Only the stable responder saw an expansion of shared T-cells from tumor to post-ICB. Finally, we identified several public clones shared between two or more patients. These public clones could indicate common tumor-associated neoantigens in ccRCC, but further analysis is required to assess that possibility. The two top public clones identified expanded preferentially in the ΔΨm Low periphery from the tumor of the partial responder, suggesting that ΔΨm Low T-cells serve a unique function against ccRCC public neoantigens.

These results are preliminary, and more data collection and analysis are required to ensure that the effects documented here are robust and maintained in the larger patient population. While we document in this chapter the expansion patterns of shared T-cell clones, gene expression, and cell surface protein expression that changes based on patient response, we record only n = 1 for each patient response. Any differences documented between patients using this small sample size could just as likely be based on patient differences exogenous from ICB treatment outcomes. Immediate next steps include the scRNA-seq and scV(D)J-seq of ΔΨm

High and ΔΨm Low peripheral T-cells and ArcherDx VDJ-seq of tumor T-cells from lung adenocarcinoma patients treated with ICB. Comparisons between tumor types would provide our study with the potential to identify novel biomarkers that predict response to ICB across cancers. Combined with previously reported gene expression profiles of shared peripheral-tumor T-cells as in Pauken *et al.* 2021, we could develop a cell surface protein signature that could assist flow cytometry-based blood tests in predicting cancer patient response to ICB (275). Future analysis of our existing data includes comparing the gene expression profiles and clonality of pre-ICB ΔΨm High and pre-ICB ΔΨm Low T-cells and their post-ICB counterparts, identifying differences in gene expression between shared T-cell clones in pre-ICB vs. those in the post-ICB periphery, and predicting potential antigens that shared T-cell clone TCRs are specific for.

CHAPTER 4: OVERALL DISCUSSION AND FUTURE DIRECTIONS

Discussion

This dissertation investigates the role of mitochondrial metabolism on hematopoietic cell fate and function. These projects, while focusing on different species and cell types, are united by a focus on mitochondrial-derived metabolic influences on hematopoietic cell differentiation and function. Chapter 2 addresses the impact of Acly deficiency on hematopoietic cell fate, demonstrating how Acly deficiency results in altered chromatin accessibility, mitochondrial metabolism, transcriptional programs, and fate decisions in MC-cultured HSPCs. However, competing models in the field combined with the complexity of hematopoiesis and the fragility of the BM microenvironment in the context of *in vivo* ASCT transplant models remain an impediment to understanding the nature of Acly's role across all hematopoietic subtypes. Promising research has been published in the last year by Umemoto *et al.* examining the role of Acly in murine HSCs regenerative potential post-5-FU insult, demonstrating that greater Acly activity is associated with increased acetylation at H3K27 and increased differentiation potential of HSCs into CD48+ progenitor cells using methods similar to those presented here, coupled with functional *in vivo* transplant experiments (95) . However, much work remains to assess the role of Acly across the entire spectrum of hematopoiesis, a continuous spectrum of cell development from stem to mature that has traditionally been comprehended using surrogate markers and functional self-renewal and differentiation experiments. The use of single-cell methods to interrogate rare populations and visualize this spectrum is a necessity to gain a holistic, systems biology perspective of metabolic-epigenetic crosstalk in hematopoiesis.

In chapter 3, we discussed the impact of mitochondrial membrane potential ($\Delta\Psi m$) on T-cell clonal responses to α-CTLA4/α-PD-1 immune checkpoint blockade therapy in ccRCC

patients. While these results are preliminary, we presented our findings that low ΔΨm results in increased general clonal responses in the periphery, greater hyperexpanded clones in each patient, single-cell surface protein and transcriptomic changes with ICB and between patient peripheral immune populations, patient-specific clonal expansion patterns that appear to correlate with response, and a gene expression program associated with shared peripheral-tumor T-cell clones in the periphery. Should the results here be replicated in other patients and other tumors, as the gene expression pattern associated with shared T-cells already has been as outlined previously in the context of murine MC38 and human melanoma, ΔΨm could be leveraged with the specific protein and mRNA patterns outlined here to further inform how ccRCC patients will respond to ICB.

In HSPCs, Acly processes mitochondrially derived citrate into acetyl-CoA to fuel histone acetylation, affecting hematopoietic cell fate as has been seen in previously published research. The main advantage of our approach in chapter 2 is a detailed glimpse of the long-used methylcellulose *ex vivo* culturing method, revealing key similarities as well as differences with *in vivo* hematopoiesis. In ccRCC patient T-cells, ΔΨm is associated with altered T-cell differentiation into effector subsets and shared peripheral-tumor clonal expansion patterns that change between patients. ΔΨm extremes indicate CD4 vs. CD8 transcriptional programs and are lower than average in shared peripheral-tumor T-cells. While the differentiation from naïve T-cell into effector T-cell and eventually memory T-cell in antitumor immunity is more compartmentalized than broad hematopoiesis, mitochondria influence both systems to affect cell fate and function.

As more articles are published on the interconnection between metabolism and functional consequences that influence hematopoietic cell fate and function, including epigenetic regulation

of gene expression and others, it is becoming increasingly clear that metabolism is not merely a method of obtaining nutrients but a key arm of macroscopic homeostasis balancing cell development and function to meet the needs that situations demand. A better working understanding of the interplay between metabolic influences on hematopoietic cell fate and function is being developed. In the coming years, therapeutic CAR-T-cells could be metabolically conditioned to have longer-lasting and more potent effector functions against liquid tumors before becoming exhausted. HSCs could also be primed for more rapid reconstitution of the hematopoietic compartment and more robust emergency myelopoiesis. Finally, understanding the role of metabolism in HSCs will elucidate the mechanisms behind the loss of HSCs associated with aging; learning how HSC loss connects with increased bone marrow adiposity could present a therapeutic target to treat aging-associated anemia and leukopenia.

While the contents of this dissertation fall short of immediately enabling these therapeutically valuable innovations, future researchers can build on these data to weaponize metabolic-epigenetic interplay to eventually fine-tune hematopoietic cells for clinical benefit.

Future Directions

There are numerous directions that future researchers could take in elucidating the mechanisms and details surrounding both projects presented in this dissertation. For the sake of time, concision, budget, and other factors, potentially informative experiments and analyses were not performed. Here, I will outline a few immediate future directions to build on the findings presented in this dissertation.

For chapter 2, four future directions would provide more detail on the mechanistic and functional impacts of Acly deficiency on other hematopoietic precursors and mature cells *in vivo* and *in vitro* in both murine and human systems. First, researchers could perform genetic knockdown/deletion of Acly in murine and ACLY in human stem cell populations defined using the strategy used by Umemoto *et al.*'s ECPR-based definition and perform bone marrow chimera transplantation experiments with either cell into appropriate syngeneic or humanized murine hosts (95). While human and mouse HSCs may present with different results, assessing how hematopoietic progenitors and mature populations are changed by Acly/ACLY genetic deficiency would be informative as to the role of Acly.

Second, researchers could assess the functional "stemness" of Acly-deficient murine HSCs by serial replating assays and serial transplantation experiments. While we show that Acly inhibition decreases LSK cells while promoting CD11b expression, this functional aspect would better inform how HSCs use Acly in the fate decision process. Third, performing ChIP-seq for H3K27ac, H3K4ac, and H3K36ac on HSCs with genetically abrogated Acly would reveal site-specific changes to these epigenetic marks that could corroborate the scATAC-seq findings. Finally, assessing changes to organelle-specific acetyl-CoA pools in Acly-deficient hematopoietic populations via organelle fractionization could shed more light on the kinetic consequences of acetyl-CoA substrate availability on histone and other acetyltransferases velocities.

Future directions for the project in chapter 3, would help validate and expand upon the per-patient differences in surface protein expression, gene expression, and clonal expansion that depend on the response to ICB and ΔΨm status in our presented findings. An immediate and ongoing future direction is the assessment of ΔΨm Low and ΔΨm High T-cell clonal responses

to ICB in lung adenocarcinoma patients, performing the same experiments utilized in our approach to ccRCC. The identification of cross-tumor phenotypes would lend a second novel angle in addition to our novel approach examining ΔΨm Low and ΔΨm High T-cells. Next, expanding our analyses in ccRCC to NSCLC patients' T-cell responses to ICB would offer more valuable perspectives on any difference in the role of ΔΨm in pre-ICB vs. post-ICB peripheral T-cells. Expanding the T-REX/MEM analysis of PBMC CyTOF data to compare not only partial response and progressive disease to ICB but also healthy, mixed/partial, and stable disease would inform how common our changed populations are between responses and between patients.

Next, expanding the plots in **Figure 3.4** to assess repertoire overlap, cosine similarity, clonal proportion, and relative abundance of expanded clones between tumor T-cells and patient-specific pre-ICB, post-ICB, ΔΨm Hi, and ΔΨm Low fractions would be more informative. Further identifying repertoire similarities between tumor T-cells and patient-specific pre-ICB ΔΨm Hi, pre-ICB ΔΨm Lo, post-ICB ΔΨm Hi, and post-ICB ΔΨm Low would grant further insight into the respective contributions of ΔΨm and ICB in T-cell clonal responses to ICB in lung and renal cancer. Finally, validating our gene signature of shared peripheral-tumor T-cells in lung cancer patients and assessing that signature's presence in pre-ICB vs. post-ICB populations could serve as a robust biomarker for cancer patient response to ICB if it is present in sufficient quantities in pre-ICB correlating with positive patient response. The ultimate goal of a qRT-PCR or flow cytometry-based test of the presence of this gene program could be translatable into the clinic to grant utility to cancer patients considering treatment with ICB.

CHAPTER 5: MATERIALS AND METHODS

Mice

Wild-type C57BL/6 (The Jackson Laboratory Strain 000664) mice were obtained from Jackson Laboratories. Bones from UBC-Cre ERT2*; Acly f/f* mice were provided by K. Wellen. Animals were maintained under specific pathogen-free conditions and handled per the Association for Assessment and Accreditation of Laboratory Animals Care international guidelines. The Institutional Animal Care and Use Committee at Vanderbilt University approved the experiments. Six- to 16-week-old female mice were used in all experiments.

Bone Marrow Chimeras

Acly f/f Vav1-cre+/- and *Acly f/f* mouse BM were injected into lethally irradiated (2 x 5 Gy separated by 3 hours), BL/6 CD45.1 (The Jackson Laboratory Strain 002014) recipients and were monitored for four weeks post-transplant. Each mouse received 1E7 whole BM cells via a retroorbital injection after being placed on sulfamethoxazole/trimethoprim-treated water. Groups of five mice per condition (*Acly f/f Vav1-cre+/-* or *Acly f/f*) were taken down at 7, 14, 21, and 28 days post-transplant.

Methylcellulose Culturing of Lin-, c-Kit HSPCs

BM was taken from C57BL/6 mouse bones, strained through a MACS Smart Strainer 70 μm (Miltenyi 130-110-916), and lysed for red blood cells using ACK Lysis Buffer (Thermo Fisher Scientific A1049201). Cells were counted and depleted of cells expressing CD5, CD45R (B220), CD11b, Gr-1 (Ly-6G/C), 7-4, and Ter-119 using Miltenyi MACS Lineage Cell Depletion Kit (Miltenyi 130-090-858) according to the Miltenyi protocol. Cells were then counted again and enriched for cells expressing c-Kit/CD117 using Miltenyi MACS CD117

MicroBeads (Miltenyi 130-091-224). Unless otherwise stated, cells were counted and resuspended at a concentration of 1E4/mL in PBS. Cells were added to tubes of StemCell Technologies' Methocult™ GF M3434, cytokine-replete methylcellulose media to dilute the original cell concentration 1:10 for a final cell concentration of 1E3 cells/mL. 1 mL of this mixture was then added to a 35 mm culture dish (StemCell 27150) and cultured for two weeks in incubators with 5% CO_2 at 37 C. Cells were then harvested and resuspended in 2% Fetal Bovine Serum (VWR 97068-085) PBS for flow cytometry. When applicable, unless otherwise stated, 30 uM Aclyi ("Aclyi"), 4 uM (Z)-4-Hydroxytamoxifen, ≥98% Z isomer (Sigma-Aldrich Cat# H7904-5MG), 5 mM acetate (Sodium acetate trihydrate, BioXtra, ≥99.0% Sigma-Aldrich Cat# S7670-250G), 1.25 – 5 mM N-Acetyl-L-cysteine (≥99% (TLC), powder, Sigma-Aldrich Cat# A7250-10G), 1 – 4 mM Dimethyl 2-oxoglutarate (96%, Sigma-Aldrich Cat# 349631-5G), and/or 10 uM Acyl-CoA synthetase short-chain family member 2 (Acss2) inhibitor (Selleck S8588) were added and vortexed well into M3434 methylcellulose media before cells were added.

Staining of cells for Flow Cytometry

Cells were Fc-blocked in 1:50 FcX Plus TruStain FcX™ PLUS (BioLegend Cat# 156604) in 2% FBS PBS for 10 minutes, followed by a stain of at least 30 minutes of 1:200 CD11b-FITC (Thermo Fisher Scientific Cat# 11-0112-82), 1:400 CD117-PE (Thermo Fisher Scientific Cat# 12-1171-82), 1:200 Sca-1-PE/Cy7 (BioLegend Cat# 122514), 1:1000 Ghost Dye™ Red 780 Fixable Viability Dye (Cell Signaling Technology #18452), and/or 1:200 Lineage-FITC (BioLegend Cat# 133301). Cells were then washed twice with 2% FBS PBS and run on the flow cytometer. For compensation, UltraComp eBeads™ Compensation Beads

(Thermo Fisher Scientific Cat# 01-2222-42) were stained at the same concentration for the same amount of time as the cells to be analyzed, washed twice with 2% FBS PBS and run on the flow cytometer. For viability dye compensation, an aliquot of cells was stained only with 1:1000 Ghost Dye™ Red 780 Fixable Viability Dye (Cell Signaling Technology #18452) for the same duration as the cells to be analyzed, washed twice with 2% FBS PBS and run on the flow cytometer.

Mitochondrial Stains

Cells were incubated with CM-H2DCFDA (General Oxidative Stress Indicator) (Thermo Fisher Scientific, Cat# C6827), TMRE reagent (Mitochondrial membrane potential) (Thermo Fisher Scientific, Cat# T-669), Mitotracker Green (Mitochondrial mass) (Thermo Fisher Scientific Cat# M7514), or MitoSOX (Superoxides) (Thermo Fisher Scientific Cat# M36008). Cells were incubated for 30 minutes at 37C, covered from light, washed twice with 2% FBS PBS, and run on the flow cytometer.

Analysis of Flow Cytometry Data

Data were analyzed using FlowJo 10.5.3. %CD11b+ gate indicates live (gated on Ghost Dye™ Red 780 Fixable Viability Dye), singlet (gated on FSC-A, FSC-H) cells positive for CD11b.

Sample Preparation for scRNA-seq

C57BL/6 Lineage-depleted BM cells were seeded at 1E3 cells per 35 mm dish in StemCell Technologies' Methocult^{TM} GF M3434 methylcellulose media and cultured for two

weeks with either 30 uM SB204990 (Tocris Cat# 4962) or an equivalent volume of DMSO. Cells were harvested and resuspended in PBS alongside freshly isolated lineage-depleted BM cells from a C57BL/6 mouse. Cells were then stained for viability Ghost Dye™ Red 780 Fixable Viability Dye and flow-sorted for viable cells. Cells were then submitted to Vanderbilt University's VANTAGE Core, where they were prepared for single-cell 5' RNA sequencing using the 10x Genomics Chromium system. Libraries were prepared using P/N 1000014, 1000020, 1000080, and 120262 according to the manufacturer's protocol. The libraries were sequenced using the NovaSeq 6000 with 150 bp paired-end reads. RTA (version 2.4.11; Illumina) was used for base calling, and analysis was completed as follows.

Analysis of scRNA-seq Data

CellRanger software (v3.0.2, https://github.com/10XGenomics/cellranger) was used with default parameters for library demultiplexing, aligning reads, fastq file generation, and unique molecular identifier (UMI) quantification to create the gene expression matrix. Gene expression matrices containing total numbers of UMIs per cell per gene were filtered to optimize data quality. To enrich for live cells, cells were retained with at least 200 genes detected and less than 5% mitochondrially-derived reads out of total UMIs. All detected genes were retained for the following analysis. Principal component analysis (PCA) and Uniform Manifold Approximation and Projection (UMAP) and clustering were applied to the filtered matrix using Seurat version 4.0.3 with default parameters, except the top 20 dimensions of PCA were used for UMAP dimensional reduction (276, 277). Cell type assessment was performed using SingleR (v1.8.1) (210) inferring the most transcriptionally similar bulk transcriptome from sorted cell populations from the ImmGen database (211) executed in tandem with expert gating. Gating validation was

performed using Seurat to overlay gene expression onto cell-type clusters and create heatmaps of cell-type-associated genes. Data were visualized using Seurat-specific tools or Rathmell lab scripts using ggplot2. Datasets have been deposited in Gene Expression Omnibus (GEO) and are publicly available under the accession GSE217080 (https://www.ncbi.nlm.nih.gov/geo/query/acc.cgi?acc=GSE217080).

scRNA-seq data from chapter 3 were analyzed with Seurat using mostly the same procedure with several differences. Viable cells were retained with at least 500 and at most 10000 detected total mRNA molecules and less than 10% mitochondrially-derived reads out of total UMIs. These thresholds were determined using sample-specific nCount_RNA and percent.mito distributions. Additionally, 20 samples were hashed into 10 lanes on the 10X chromium controller using BioLegend TotalSeq™-C0251 (cat. 394661) and C0252 (cat. 394663) Hashtag antibody-oligo conjugates by Rama Gangula in the Immunogenomics, Microbial Genetics and Single-cell Technologies core. Hashing of PBMCs was performed for 30 minutes on ice using 1 µL of hashtag antibody per sample in 55 µL BioLegend Cell Staining Buffer (Cat. #420201) following Fc blocking with Human TruStain FcX™ (BioLegend Cat. #422301). Cells were washed 3X in PBS + 2% BSA, centrifuged, and aspirated until 50 µL of buffer remained. Cells were then counted, and viability was assessed using Trypan Blue. Viability post-hashing was 86-97%, with the median viability of the ten samples at 96.5%.

Hashed cells were deconvoluted by binning the data derived from the ten sequencing lanes into 20 samples based on the ratio of C0251 to C0252 reads. Differential gene expression was determined using Seurat's FindMarkers function.

SCENIC Analysis

Regulatory network analysis was performed using the docker image aertslab/pyscenic (v0.9.18) using the default parameters. The co-expression modules were based on cisTarget databases (mm10: mm10__refseq-r80__10kb_up_and_down_tss.mc9nr.feather). Then the scored regulon of cells was imported and integrated into Seurat object with other analyses and visualized under R (v3.6.1).

Sample Preparation for scATAC-seq

C57BL/6 Lineage-depleted BM cells were seeded at 1E3 cells per 35 mm dish in StemCell Technologies' Methocult^{TM} GF M3434 methylcellulose media and cultured for two weeks with either 30 uM SB204990 (Tocris 4962) or an equivalent volume of DMSO. Cells were harvested and resuspended in PBS alongside freshly isolated lineage-depleted BM cells from a C57BL/6 mouse. Nuclei were then isolated and submitted to Vanderbilt University's VANTAGE Core, where they were prepared for scATAC-seq following the manufacturer's protocol using P/N 1000111, 1000086, and 1000084.

Analysis of scATAC-seq Data

Files were imported into R using ArchR (filterTSS = 8, filterFrags = 2819), with filterFrags value set based on the distribution of transcription start site (TSS) vs. the log transform of unique fragments generated by ArchR (216). The ArchR project was created, doublets filtered, LSI dimensional reduction performed, clusters plotted, and UMAP dimensional reduction embedded using default settings. Gene scores were also calculated using ArchR, representing chromatin accessibility within 100 kb on either side of a gene, using default values.

Cell type labels were assigned to scATAC-seq using ArchR's addGeneIntegrationMatrix function. Cells from scATAC-seq were directly aligned with cells from scRNA-seq by comparing the scATAC-seq gene score matrix with the scRNA-seq gene expression matrix. Chromatin accessibility tracks were plotted using default settings.

Other R packages used for data analysis and visualization include Dplyr, Patchwork, Formattable, Ggplot2, Gridextra, Sctransform, GenomicRanges, Reticulate, loomR, Scater, Pheatmap, Celldex, scRNAseq, scuttle, Stringr, Plyr, scales, Devtools, Rcpp, Presto, Msigdbr, Fgsea, SummarizedExperiment, and chromVARmotifs (278-301).

Extracellular Flux Analysis

Cells were resuspended in Seahorse XF Media (Agilent Cat# 103576-100) supplemented with 2 mM glutamine (Agilent Cat# 103579-100), 1 mM Pyruvate (Agilent Cat# 103578-100), and 10 mM glucose (Agilent Cat# 103577-100) at 4E6/mL, seeding 2E5 cells per well in the Seahorse assay plate (Agilent Cat# 102416-100). The rest of the protocol was conducted according to the manufacturer's XF Cell Mito Stress Test Kit (Agilent Cat# 103015-100) user guide. Seahorse XF Calibrant Solution (Agilent Cat# 100840-000) was used to calibrate the extracellular flux analyzer. Values were normalized to bright-field cell counts taken per well by Cytek Cytation 5 Cell Imaging Multi-Mode Reader.

qRT-PCR

RNA was isolated using Qiagen's RNeasy Mini Kit (Qiagen Cat# 74104) according to the manufacturer's protocol. cDNA was then synthesized using the Biorad iScript cDNA Synthesis Kit (Biorad Cat# 1708890) according to the manufacturer's protocol. Finally, a

quantitative reverse-transcriptase polymerase chain reaction (qRT-PCR) was performed using the Biorad SsoAdvanced Universal SYBR Green Supermix (Biorad Cat# 1725271) according to the manufacturer's protocol. The amplification program consisted of 95C for 30 seconds followed by 40 cycles of the set of 95C for 15 seconds, and T_{anneal} for 30 seconds. Finally, 95C for 5 seconds. Each *Cebp* isoform's reaction was run alongside a control *β-Actin* reaction with different T_{anneal} values for each *Cebp* isoform, depending on the specific primer characteristics.

qRT-PCR primers used include *β-Actin* (F: AAGTGTGACGTTGACATCCGTAA, R: TGCCTGGGTACATGGTGGTA) (302), *Cebpa* (F: AATGGCAGTGTGCACGTCTA, R: CCCCAGCCGTTAGTGAAGAG) (303), *Cebpb* (F: TTGATGCAATCCGGATCAAACG, R: CAGTTACACGTGTGTTGCGTC) (304), *Cebpg* (F: TTCGTAACCGTCGCTCCTCC, R: TCAGAGCAATGTGATCCGAGG), *Cebpd* (F: GAACCCGCGGCCTTCTAC, R: GAAGAGTTCGTCGTGGCACA) (305), *Cebpe* (F: CCCTTCTAGGTCCCCAGAGT, R: TCATTTGGTCCCGACCTTCC), *Cebpz* (F: AGCCAGATCCCAGTGGATGA, R: GTGGGAAGCAGTTGTCGTCT).

Quantification and statistics.

Statistical analyses were performed with GraphPad Prism software version 8.1.0. For data involving 2 groups, analysis was performed using Student's t-test.

Processing of ccRCC Patient PBMCs

PBMCs were isolated from ccRCC patient blood using a Katy Beckermann lab protocol developed by Rachel Hongo and Madelyn Landis. Before processing, BC Vacutainer Glass Mononuclear Cell Preparation (CPT) Tubes (Fisher Scientific Cat. #02-685-125) containing

patient blood were inverted ~5 times and then centrifuged at 1500 x G for 20 minutes at RT. The top layer containing plasma was removed, and any remaining plasma and buffy coat were transferred into a new 15 mL conical tube, diluted up to the top with PBS, centrifuged at 1500 RPM for 4 minutes, and the supernatant aspirated. Cells were then resuspended in 1 mL ACK lysis buffer for 1 minute followed by the addition of 1 mL PBS. Cells were centrifuged again at 1500 RPM for 4 minutes followed by repeated ACK lysis until loss of red blood cell pellet content.

Cell viability and number were then determined using Trypan Blue staining assessed using the BioRad TC20 cell counter (Cat. # 1450102). 5-10E6 viable cells were then resuspended in 1 mL freeze media (88% FBS, 12% DMSO), transferred immediately to a Mr. Frosty Freezing Container (ThermoFisher Scientific Cat. #5100-001), and frozen down at -80C in each Corning cryovial for PBMCs (Fisher Scientific Cat. #13-700-500). Vials were capped using Corning cryovial cap inserts (Fisher Scientific, Cat. #07-202-620). After a minimum of 24 hours and a maximum of 1 week, the cryovials of PBMCs were then transferred into liquid nitrogen for long-term storage.

ccRCC Patient Peripheral T-cell Sort Strategies for scRNA-seq, scV(D)J-seq, and CyTOF

ΔΨm High and ΔΨm Low T-cells were isolated from ccRCC patients' PBMCs following the gating strategy: 1) Single-cells gated on FSC-A vs. FSC-H and SSC-A vs. SSC-H, 2) cell size scatter based on lymphocyte cell size, 3) viability, 4) CD3+, and 5) TMRE High vs. TMRE Lo. TMRE was used as a proxy for ΔΨm with the ΔΨm High vs. ΔΨm Low gate determined experimentally by Madelyn Landis. Reagents used for this purpose were αCD3-BV421 (BioLegend, Cat #317344), TMRE (Life Tech, Cat #T-669), Fixable Ghost Viability Dye e780

(Cell Signaling, Cat #18452S). After cell staining and washing, cells were resuspended in 2% FBS PBS (FACS buffer) at 1E6 cells/100 μL for flow sorting and flow-sorted using the 70 μm nozzle.

ccRCC patients' PBMCs were sorted and processed similarly. Instead of sorting on CD3, however, PBMCs were sorted on CD45. Additionally, cells were not sorted according to ΔΨm status using TMRE.

RNA Isolation from ccRCC Tumors for ArcherDx VDJ-seq

ccRCC patient tumors were taken before the development of metastatic disease and embedded into paraffin blocks. 5 μm scrolls were cut by the Translational Pathology Shared Resource (TPSR) at Vanderbilt University Medical Center (VUMC). These samples had RNA isolated by the VUMC Innovative Translational Research Shared Resource (ITR) core using the Maxwell RSC RNA FFPE Kit (Promega Cat #AS1440) and associated protocol.

Isolated RNA was then processed using the Immunoverse™-HS TCR alpha/delta/beta/gamma Kit, for Illumina® - 8 reactions (Integrated Sciences Cat. #DB0219) kit and associated protocol. Sequencing was performed on the Illumina NovaSeq6000 via the (S4) PE150 method.

Analysis of scV(D)J-seq and ArcherDx VDJ-seq data

TCR α and β nucleotide and amino acid sequences were integrated with the Seurat scRNA-seq dataframe based on cell UMI barcode identity between scRNA-seq and scV(D)J-seq. Only cells with both α and β genes sequenced were included for analysis.

The repOverlap and repClonality functions from Immunarch (0.8.0, https://github.com/immunomind/immunarch) were used to assess repertoire similarity and clonal expansion of peripheral T-cell responses (306). Repertoire overlap was determined using the repOverlap function's "public" method, cosine similarity was determined using the repOverlap function's "cosine" method, the clonal proportion was determined using the repClonality function's "clonal.prop" method, and relative abundance was determined using the repClonality function's "homeo" method. These methods were applied to a table of **1**: TRA clonal sequences with **2**: the abundance of each sequence in each group of interest (e.g., the "Stable Ψ High Peripheral T-cells" contained all TRA clonal sequences and the abundance of each sequence in ΔΨm High peripheral T-cells from the stable responder).

Cells that shared both their TRA and TRB CDR3 nucleotide sequences with those found in tumor TRA and TRB CDR3 nucleotide sequences were considered shared peripheral-tumor T-cell clones, labeled "TRUE" in **Figure 3.6B**. Expansion plots of shared peripheral-tumor T-cell clones were graphically presented using Ggplot2-based code developed in the Rathmell lab showing the stacked combined percent representation of each clone shared between the tumor and all peripheral fractions. Clones that were detected in the periphery of patients that were shared with the tumor of another patient were listed in **Table 3.5**. Expansion patterns were determined by dividing the representation in ΔΨm Low by tumor representation, in ΔΨm High by tumor representation, in pre-ICB, and in post-ICB by tumor representation.

MEM and T-REX Analysis of CyTOF data

CyTOF data were normalized and scaled using arcsinh transformation. Arcsinh cofactor was chosen for each channel based on the standard operating procedure for fluorescence and

mass cytometry data (307, 308). Following QC, UMAP analyses were performed on the samples using surface markers associated with T-cells and surface markers associated with non-T-cells. Metabolic markers, Ki67, rhodium, and iridium were excluded from UMAP embedding. The resulting embeddings were used to visualize and select T-cells and non-T-cells for downstream analyses. T-cells and non-T-cells from these UMAPs were extracted and analyzed using t-SNE to create the all-patient T-cell and non-T-cell common t-SNE embeddings. Patients were equally sampled. All patient samples were then aggregated and assessed for T-cell and non-T-cell population changes using T-REX between partial vs. progressive response and before vs. after ICB (258). Enriched features in each T-REX region of significant change were quantified using MEM (257). CyTOF MEM and T-REX analyses were primarily performed by Sierra Barone, Caroline Roe, Jonathan Irish, and other members of the Jonathan Irish group.

The pheatmap package was used for heatmap plotting of asinh-normalized (A) and scaled (B) metabolic average cell surface protein expression in **Figure 3.3**. Scaling was performed using the R base package scale, which calculated the mean and standard deviation of the gene of interest across all samples. Then, the mean expression was subtracted from each sample asinh-normalized mean. This value was then divided by the standard deviation of that gene across all samples (309).

Table 5.1: Metal-conjugated CyTOF antibodies used for patient Live, CD45+ PBMCs.

Channel	Marker	Clone	Vendor	Catalog No.	[Optimal] (µg/ml)	Species
89Y	CD45	HI30	Fluidigm	3089003B	Ex, 1:200	Human
106Pd	CD66b	80H3	Biolegend	305102	Ex, 1:100, CC	Human
110Cd	CD16	3G8	Biolegend	302051	Ex, 1:100, CC	Human

111Cd	CD8	RPAT8	Biolegend	301053	Ex, 1:100, CC	Human
112Cd	CD14	M5E2	Biolegend	301843	Ex, 1:100, CC	Human
113Cd	CD4	RPA-T4	Biolegend	300541	Ex, 1:100, CC	Human
114Cd	CD3	UCHT1	Biolegend	300443	Ex, 1:100, CC	Human
116Cd	CD19	HIB19	Biolegend	302247	Ex, 1:100, CC	Human
141Pr	CCR6	G034E3	Fluidigm	3141003A	Ex, 1:100	Human
142Ce	Cpt1a	8F6AE9	Abcam	ab128568	Me, 1:100, CC	Human
143Nd	CD117	104D2	Fluidigm	3143001B	Ex, 1:100	Human
144Nd	CCR5	NP-6G4	Fluidigm	3144007A	Ex, 1:100	Human
145Nd	Grim19	6E1BH7	Abcam	ab110240	Me, 1:100, CC	Human
146Nd	CD64	10.1	Fluidigm	3146006B	Ex, 1:100	Human
147Sm	CD20	2H7	Fluidigm	3147001B	Ex, 1:200	Human
148Sm	PDL1	29E.2A3	Fluidigm	3148017B	Ex, 1:100	Human
149Sm	CCR4	205410	Fluidigm	3149029A	Ex, 1:200	Human
150Sm	CD134	ACT35	Fluidigm	3150023C	Ex, 1:100	Human
151Eu	ICOS	C398.4A	Fluidigm	3151020B	Ex, 1:200	Human
152Sm	TCRgd	11F2	Fluidigm	3152008B	Ex, 1:200	Human
153Eu	CD62L	DREG-56	Fluidigm	3153004B	Ex, 1:100	Human
154Gd	TIGIT	MBSA43	Fluidigm	3154016B	Ex, 1:100	Human
155Gd	CD27	L128	Fluidigm	3155001B	Ex, 1:100	Human
156Gd	CXCR3	G025H7	Fluidigm	3156004B	Ex, 1:200	Human
158Gd	CD137	4B4-1	Fluidigm	3158013B	Ex, 1:200	Human
159Tb	CCR7	G043H7	Fluidigm	3159003A	Ex, 1:100	Human
160Dy	CD28	CD28.2	Fluidigm	3160003B	Ex, 1:100	Human
161Dy	CTLA4	14D3	Fluidigm	3161004B	Me, 1:100	Human
162Dy	Ki67	B56	Fluidigm	3162012B	Me, 1:200	Human
163Dy	Glut1	polyclonal	Novus Biologicals	NB110-39113	Me, 1:100, CC	Human
164Dy	CD95	DX2	Fluidigm	3164008B	Ex, 1:200	Human
165Ho	CD45R0	UCHL1	Fluidigm	3165011B	Ex, 1:100	Human
166Er	CD44	BJ18	Fluidigm	3166001C	Ex, 1:100	Human
167Er	CD38	HIT2	Fluidigm	3167001B	Ex, 1:100	Human

168Er	CD127	A019D5	Fluidigm	3168017B	Ex, 1:100	Human
169Tm	CD25	2A3	Fluidigm	3169003B	Ex, 1:200	Human
170Yb	CD45RA	HI100	Fluidigm	3170010B	Ex, 1:200	Human
171Yb	CXCR5	RF8B2	Fluidigm	3171014B	Ex, 1:200	Human
172Yb	CD57	HCD57	Fluidigm	3172009B	Ex, 1:100	Human
173Yb	CXCR4	12G5	Fluidigm	3173001B	Ex, 1:200	Human
174Yb	HLADR	II L243	Fluidigm	3174001B	Ex, 1:200	Human
175Lu	PD1	EH12.2H7	Fluidigm	3175008B	Ex, 1:200	Human
176Lu	CD56	CMSSB	Fluidigm	3176003B	Ex, 1:200	Human
209Bi	CD11b	ICRF44	Fluidigm	3209003B	Ex, 1:200	Human

Ex: Extracellular marker, live stain
Me: stained post-methanol permeabilization
CC: custom conjugated reagent

REFERENCES

1. Roh, J. S., and D. H. Sohn. 2018. Damage-Associated Molecular Patterns in Inflammatory Diseases. *Immune Netw* 18: e27.
2. Riera Romo, M., D. Pérez-Martínez, and C. Castillo Ferrer. 2016. Innate immunity in vertebrates: an overview. *Immunology* 148: 125-139.
3. Karesh, W. B., A. Dobson, J. O. Lloyd-Smith, J. Lubroth, M. A. Dixon, M. Bennett, S. Aldrich, T. Harrington, P. Formenty, E. H. Loh, C. C. Machalaba, M. J. Thomas, and D. L. Heymann. 2012. Ecology of zoonoses: natural and unnatural histories. *Lancet* 380: 1936-1945.
4. Benton, M. L., A. Abraham, A. L. LaBella, P. Abbot, A. Rokas, and J. A. Capra. 2021. The influence of evolutionary history on human health and disease. *Nat Rev Genet* 22: 269-283.
5. Domínguez-Andrés, J., and M. G. Netea. 2019. Impact of Historic Migrations and Evolutionary Processes on Human Immunity. *Trends Immunol* 40: 1105-1119.
6. Fernandez Vina, M. A., J. A. Hollenbach, K. E. Lyke, M. B. Sztein, M. Maiers, W. Klitz, P. Cano, S. Mack, R. Single, C. Brautbar, S. Israel, E. Raimondi, E. Khoriaty, A. Inati, M. Andreani, M. Testi, M. E. Moraes, G. Thomson, P. Stastny, and K. Cao. 2012. Tracking human migrations by the analysis of the distribution of HLA alleles, lineages and haplotypes in closed and open populations. *Philos Trans R Soc Lond B Biol Sci* 367: 820-829.
7. Liston, A., S. Humblet-Baron, D. Duffy, and A. Goris. 2021. Human immune diversity: from evolution to modernity. *Nat Immunol* 22: 1479-1489.
8. Robinson, G. A., J. Peng, H. Peckham, G. Butler, I. Pineda-Torra, C. Ciurtin, and E. C. Jury. 2022. Investigating sex differences in T regulatory cells from cisgender and transgender healthy individuals and patients with autoimmune inflammatory disease: a cross-sectional study. *Lancet Rheumatol* 4: e710-e724.
9. Zekavat, S. M., S. H. Lin, A. G. Bick, A. Liu, K. Paruchuri, C. Wang, M. M. Uddin, Y. Ye, Z. Yu, X. Liu, Y. Kamatani, R. Bhattacharya, J. P. Pirruccello, A. Pampana, P. R. Loh, P. Kohli, S. A. McCarroll, K. Kiryluk, B. Neale, I. Ionita-Laza, E. A. Engels, D. W. Brown, J. W. Smoller, R. Green, E. W. Karlson, M. Lebo, P. T. Ellinor, S. T. Weiss, M. J. Daly, C. Terao, H. Zhao, B. L. Ebert, M. P. Reilly, A. Ganna, M. J. Machiela, G. Genovese, and P. Natarajan. 2021. Hematopoietic mosaic chromosomal alterations increase the risk for diverse types of infection. *Nat Med* 27: 1012-1024.
10. Chen, M. H., L. M. Raffield, A. Mousas, S. Sakaue, J. E. Huffman, A. Moscati, B. Trivedi, T. Jiang, P. Akbari, D. Vuckovic, E. L. Bao, X. Zhong, R. Manansala, V. Laplante, M. Chen, K. S. Lo, H. Qian, C. A. Lareau, M. Beaudoin, K. A. Hunt, M. Akiyama, T. M. Bartz, Y. Ben-Shlomo, A. Beswick, J. Bork-Jensen, E. P. Bottinger, J. A. Brody, F. J. A. van Rooij, K. Chitrala, K. Cho, H. Choquet, A. Correa, J. Danesh, E. Di Angelantonio, N. Dimou, J. Ding, P. Elliott, T. Esko, M. K. Evans, J. S. Floyd, L. Broer, N. Grarup, M. H. Guo, A. Greinacher, J. Haessler, T. Hansen, J. M. M. Howson, Q. Q. Huang, W. Huang, E. Jorgenson, T. Kacprowski, M. Kähönen, Y. Kamatani, M. Kanai, S. Karthikeyan, F. Koskeridis, L. A. Lange, T. Lehtimäki, M. M. Lerch, A. Linneberg, Y. Liu, L. P. Lyytikäinen, A. Manichaikul, H. C. Martin, K. Matsuda, K. L. Mohlke, N. Mononen, Y. Murakami, G. N. Nadkarni, M. Nauck, K. Nikus, W. H. Ouwehand, N. Pankratz, O. Pedersen, M. Preuss, B. M. Psaty, O. T. Raitakari, D. J. Roberts, S. S. Rich, B. A. T. Rodriguez, J. D. Rosen, J. I. Rotter, P. Schubert, C. N. Spracklen, P. Surendran, H. Tang, J. C. Tardif, R. C. Trembath, M. Ghanbari, U. Völker, H. Völzke, N. A. Watkins, A. B. Zonderman, P. W. F. Wilson, Y. Li, A. S. Butterworth, J. F. Gauchat, C. W. K. Chiang, B. Li, R. J. F. Loos, W. J. Astle, E. Evangelou, D. A. van Heel, V. G. Sankaran, Y. Okada, N. Soranzo, A. D. Johnson, A. P. Reiner, P. L. Auer, and G. Lettre. 2020. Trans-

ethnic and Ancestry-Specific Blood-Cell Genetics in 746,667 Individuals from 5 Global Populations. *Cell* 182: 1198-1213.e1114.
11. King Thomas, J., H. Mir, N. Kapur, and S. Singh. 2019. Racial Differences in Immunological Landscape Modifiers Contributing to Disparity in Prostate Cancer. *Cancers (Basel)* 11.
12. Paludan, S. R., T. Pradeu, S. L. Masters, and T. H. Mogensen. 2021. Constitutive immune mechanisms: mediators of host defence and immune regulation. *Nature Reviews Immunology* 21: 137-150.
13. Brenna, E., and A. J. McMichael. 2022. The Importance of Cellular Immune Response to HIV: Implications for Antibody Production and Vaccine Design. *DNA Cell Biol* 41: 38-42.
14. Li, D., and M. Wu. 2021. Pattern recognition receptors in health and diseases. *Signal Transduct Target Ther* 6: 291.
15. Rosales, C., and E. Uribe-Querol. 2017. Phagocytosis: A Fundamental Process in Immunity. *Biomed Res Int* 2017: 9042851.
16. Roche, P. A., and K. Furuta. 2015. The ins and outs of MHC class II-mediated antigen processing and presentation. *Nat Rev Immunol* 15: 203-216.
17. Hewitt, E. W. 2003. The MHC class I antigen presentation pathway: strategies for viral immune evasion. *Immunology* 110: 163-169.
18. Raskov, H., A. Orhan, J. P. Christensen, and I. Gögenur. 2021. Cytotoxic CD8(+) T cells in cancer and cancer immunotherapy. *Br J Cancer* 124: 359-367.
19. Vorobjeva, N. V., and B. V. Chernyak. 2020. NETosis: Molecular Mechanisms, Role in Physiology and Pathology. *Biochemistry (Mosc)* 85: 1178-1190.
20. Huang, L., and J. A. Appleton. 2016. Eosinophils in Helminth Infection: Defenders and Dupes. *Trends Parasitol* 32: 798-807.
21. Obata-Ninomiya, K., P. P. Domeier, and S. F. Ziegler. 2020. Basophils and Eosinophils in Nematode Infections. *Front Immunol* 11: 583824.
22. Hepworth, M. R., E. Daniłowicz-Luebert, S. Rausch, M. Metz, C. Klotz, M. Maurer, and S. Hartmann. 2012. Mast cells orchestrate type 2 immunity to helminths through regulation of tissue-derived cytokines. *Proc Natl Acad Sci U S A* 109: 6644-6649.
23. Hellman, L., S. Akula, Z. Fu, and S. Wernersson. 2022. Mast Cell and Basophil Granule Proteases - In Vivo Targets and Function. *Front Immunol* 13: 918305.
24. Stone, K. D., C. Prussin, and D. D. Metcalfe. 2010. IgE, mast cells, basophils, and eosinophils. *J Allergy Clin Immunol* 125: S73-80.
25. Liu, C., D. Chu, K. Kalantar-Zadeh, J. George, H. A. Young, and G. Liu. 2021. Cytokines: From Clinical Significance to Quantification. *Adv Sci (Weinh)* 8: e2004433.
26. Jeyachandran, A., B. Mertens, E. A. McKissick, and C. S. Mitchell. 2015. Type I Vs. Type II Cytokine Levels as a Function of SOD1 G93A Mouse Amyotrophic Lateral Sclerosis Disease Progression. *Front Cell Neurosci* 9: 462.
27. Julier, Z., A. J. Park, P. S. Briquez, and M. M. Martino. 2017. Promoting tissue regeneration by modulating the immune system. *Acta Biomater* 53: 13-28.
28. Henry, E. K., J. M. Inclan-Rico, and M. C. Siracusa. 2017. Type 2 cytokine responses: regulating immunity to helminth parasites and allergic inflammation. *Curr Pharmacol Rep* 3: 346-359.
29. Wynn, T. A. 2015. Type 2 cytokines: mechanisms and therapeutic strategies. *Nat Rev Immunol* 15: 271-282.
30. Fabre, T., M. F. Molina, G. Soucy, J. P. Goulet, B. Willems, J. P. Villeneuve, M. Bilodeau, and N. H. Shoukry. 2018. Type 3 cytokines IL-17A and IL-22 drive TGF-β-dependent liver fibrosis. *Sci Immunol* 3.
31. Valle-Noguera, A., A. Ochoa-Ramos, M. J. Gomez-Sánchez, and A. Cruz-Adalia. 2021. Type 3 Innate Lymphoid Cells as Regulators of the Host-Pathogen Interaction. *Front Immunol* 12: 748851.

32. Lacy, P., and J. L. Stow. 2011. Cytokine release from innate immune cells: association with diverse membrane trafficking pathways. *Blood* 118: 9-18.
33. Mortha, A., and K. Burrows. 2018. Cytokine Networks between Innate Lymphoid Cells and Myeloid Cells. *Front Immunol* 9: 191.
34. Castro, F., A. P. Cardoso, R. M. Gonçalves, K. Serre, and M. J. Oliveira. 2018. Interferon-Gamma at the Crossroads of Tumor Immune Surveillance or Evasion. *Front Immunol* 9: 847.
35. Bao, K., and R. L. Reinhardt. 2015. The differential expression of IL-4 and IL-13 and its impact on type-2 immunity. *Cytokine* 75: 25-37.
36. Liu, R., H. M. Lauridsen, R. A. Amezquita, R. W. Pierce, D. Jane-Wit, C. Fang, A. S. Pellowe, N. C. Kirkiles-Smith, A. L. Gonzalez, and J. S. Pober. 2016. IL-17 Promotes Neutrophil-Mediated Immunity by Activating Microvascular Pericytes and Not Endothelium. *J Immunol* 197: 2400-2408.
37. Shimabukuro-Vornhagen, A., P. Gödel, M. Subklewe, H. J. Stemmler, H. A. Schlößer, M. Schlaak, M. Kochanek, B. Böll, and M. S. von Bergwelt-Baildon. 2018. Cytokine release syndrome. *J Immunother Cancer* 6: 56.
38. Crotty, S. 2019. T Follicular Helper Cell Biology: A Decade of Discovery and Diseases. *Immunity* 50: 1132-1148.
39. Pilzecker, B., and H. Jacobs. 2019. Mutating for Good: DNA Damage Responses During Somatic Hypermutation. *Front Immunol* 10: 438.
40. Stavnezer, J., and C. E. Schrader. 2014. IgH chain class switch recombination: mechanism and regulation. *J Immunol* 193: 5370-5378.
41. Akkaya, M., K. Kwak, and S. K. Pierce. 2020. B cell memory: building two walls of protection against pathogens. *Nat Rev Immunol* 20: 229-238.
42. Lau, E. H. Y., O. T. Y. Tsang, D. S. C. Hui, M. Y. W. Kwan, W. H. Chan, S. S. Chiu, R. L. W. Ko, K. H. Chan, S. M. S. Cheng, R. Perera, B. J. Cowling, L. L. M. Poon, and M. Peiris. 2021. Neutralizing antibody titres in SARS-CoV-2 infections. *Nat Commun* 12: 63.
43. Mélik-Parsadaniantz, S., and W. Rostène. 2008. Chemokines and neuromodulation. *J Neuroimmunol* 198: 62-68.
44. Mastrogiovanni, M., M. Juzans, A. Alcover, and V. Di Bartolo. 2020. Coordinating Cytoskeleton and Molecular Traffic in T Cell Migration, Activation, and Effector Functions. *Front Cell Dev Biol* 8: 591348.
45. Griffith, J. W., C. L. Sokol, and A. D. Luster. 2014. Chemokines and chemokine receptors: positioning cells for host defense and immunity. *Annu Rev Immunol* 32: 659-702.
46. Taneja, V. 2018. Sex Hormones Determine Immune Response. *Front Immunol* 9: 1931.
47. Martín-Fontecha, A., A. Lanzavecchia, and F. Sallusto. 2009. Dendritic cell migration to peripheral lymph nodes. *Handb Exp Pharmacol*: 31-49.
48. Kranich, J., and N. J. Krautler. 2016. How Follicular Dendritic Cells Shape the B-Cell Antigenome. *Front Immunol* 7: 225.
49. Azarov, I., K. Peskov, G. Helmlinger, and Y. Kosinsky. 2019. Role of T Cell-To-Dendritic Cell Chemoattraction in T Cell Priming Initiation in the Lymph Node: An Agent-Based Modeling Study. *Front Immunol* 10: 1289.
50. Marrack, P., J. Scott-Browne, and M. K. MacLeod. 2010. Terminating the immune response. *Immunol Rev* 236: 5-10.
51. Riddell, N. E. Immune Responses: Primary and Secondary. In *eLS*. 316-326.
52. Liggett, L. A., and V. G. Sankaran. 2020. Unraveling Hematopoiesis through the Lens of Genomics. *Cell* 182: 1384-1400.
53. Bar-Shavit, Z. 2007. The osteoclast: a multinucleated, hematopoietic-origin, bone-resorbing osteoimmune cell. *J Cell Biochem* 102: 1130-1139.

54. Mass, E., and R. Gentek. 2021. Fetal-Derived Immune Cells at the Roots of Lifelong Pathophysiology. *Front Cell Dev Biol* 9: 648313.
55. Kondo, M., I. L. Weissman, and K. Akashi. 1997. Identification of clonogenic common lymphoid progenitors in mouse bone marrow. *Cell* 91: 661-672.
56. Buenrostro, J. D., M. R. Corces, C. A. Lareau, B. Wu, A. N. Schep, M. J. Aryee, R. Majeti, H. Y. Chang, and W. J. Greenleaf. 2018. Integrated Single-Cell Analysis Maps the Continuous Regulatory Landscape of Human Hematopoietic Differentiation. *Cell* 173: 1535-1548.e1516.
57. Karamitros, D., B. Stoilova, Z. Aboukhalil, F. Hamey, A. Reinisch, M. Samitsch, L. Quek, G. Otto, E. Repapi, J. Doondeea, B. Usukhbayar, J. Calvo, S. Taylor, N. Goardon, E. Six, F. Pflumio, C. Porcher, R. Majeti, B. Göttgens, and P. Vyas. 2018. Single-cell analysis reveals the continuum of human lympho-myeloid progenitor cells. *Nat Immunol* 19: 85-97.
58. Scala, S., and A. Aiuti. 2019. In vivo dynamics of human hematopoietic stem cells: novel concepts and future directions. *Blood Adv* 3: 1916-1924.
59. Nombela-Arrieta, C., G. Pivarnik, B. Winkel, K. J. Canty, B. Harley, J. E. Mahoney, S. Y. Park, J. Lu, A. Protopopov, and L. E. Silberstein. 2013. Quantitative imaging of haematopoietic stem and progenitor cell localization and hypoxic status in the bone marrow microenvironment. *Nat Cell Biol* 15: 533-543.
60. Pinho, S., and P. S. Frenette. 2019. Haematopoietic stem cell activity and interactions with the niche. *Nature Reviews Molecular Cell Biology* 20: 303-320.
61. Fröbel, J., T. Landspersky, G. Percin, C. Schreck, S. Rahmig, A. Ori, D. Nowak, M. Essers, C. Waskow, and R. A. J. Oostendorp. 2021. The Hematopoietic Bone Marrow Niche Ecosystem. *Front Cell Dev Biol* 9: 705410.
62. Kokkaliaris, K. D., L. Kunz, N. Cabezas-Wallscheid, C. Christodoulou, S. Renders, F. Camargo, A. Trumpp, D. T. Scadden, and T. Schroeder. 2020. Adult blood stem cell localization reflects the abundance of reported bone marrow niche cell types and their combinations. *Blood* 136: 2296-2307.
63. Bispo, J. A. B., P. S. Pinheiro, and E. K. Kobetz. 2020. Epidemiology and Etiology of Leukemia and Lymphoma. *Cold Spring Harb Perspect Med* 10.
64. Hasserjian, R. P. 2019. Myelodysplastic Syndrome Updated. *Pathobiology* 86: 7-13.
65. DiNardo, C. D., and J. E. Cortes. 2016. Mutations in AML: prognostic and therapeutic implications. *Hematology Am Soc Hematol Educ Program* 2016: 348-355.
66. Baumgartner, C., S. Toifl, M. Farlik, F. Halbritter, R. Scheicher, I. Fischer, V. Sexl, C. Bock, and M. Baccarini. 2018. An ERK-Dependent Feedback Mechanism Prevents Hematopoietic Stem Cell Exhaustion. *Cell Stem Cell* 22: 879-892.e876.
67. Townsend, L., A. H. Dyer, A. Naughton, S. Imangaliyev, J. Dunne, R. Kiersey, D. Holden, A. Mooney, D. Leavy, K. Ridge, J. Sugrue, M. Aldoseri, J. H. Kelliher, M. Hennessy, D. Byrne, P. Browne, C. L. Bacon, C. Doyle, R. O'Riordan, A. M. McLaughlin, C. Bannan, I. Martin-Loeches, A. White, R. M. McLoughlin, C. Bergin, N. M. Bourke, C. O'Farrelly, N. Conlon, and C. N. Cheallaigh. 2022. Severe COVID-19 is characterised by inflammation and immature myeloid cells early in disease progression. *Heliyon* 8: e09230.
68. Mamun, A. A., H. Hayashi, A. Yamamura, M. J. Nayeem, and M. Sato. 2020. Hypoxia induces the translocation of glucose transporter 1 to the plasma membrane in vascular endothelial cells. *J Physiol Sci* 70: 44.
69. Gleadle, J. M., and P. J. Ratcliffe. 1997. Induction of hypoxia-inducible factor-1, erythropoietin, vascular endothelial growth factor, and glucose transporter-1 by hypoxia: evidence against a regulatory role for Src kinase. *Blood* 89: 503-509.

70. Shi, S., J. Xu, B. Zhang, S. Ji, W. Xu, J. Liu, K. Jin, D. Liang, C. Liang, L. Liu, C. Liu, Y. Qin, and X. Yu. 2016. VEGF Promotes Glycolysis in Pancreatic Cancer via HIF1α Up-Regulation. *Curr Mol Med* 16: 394-403.
71. Morganti, C., N. Cabezas-Wallscheid, and K. Ito. 2022. Metabolic Regulation of Hematopoietic Stem Cells. *Hemasphere* 6: e740.
72. Bonora, M., K. Ito, C. Morganti, P. Pinton, and K. Ito. 2018. Membrane-potential compensation reveals mitochondrial volume expansion during HSC commitment. *Exp Hematol* 68: 30-37.e31.
73. de Almeida, M. J., L. L. Luchsinger, D. J. Corrigan, L. J. Williams, and H. W. Snoeck. 2017. Dye-Independent Methods Reveal Elevated Mitochondrial Mass in Hematopoietic Stem Cells. *Cell Stem Cell* 21: 725-729.e724.
74. Youle, R. J., and A. M. van der Bliek. 2012. Mitochondrial fission, fusion, and stress. *Science* 337: 1062-1065.
75. Plaitakis, A., E. Kalef-Ezra, D. Kotzamani, I. Zaganas, and C. Spanaki. 2017. The Glutamate Dehydrogenase Pathway and Its Roles in Cell and Tissue Biology in Health and Disease. *Biology (Basel)* 6.
76. Mews, P., G. Donahue, A. M. Drake, V. Luczak, T. Abel, and S. L. Berger. 2017. Acetyl-CoA synthetase regulates histone acetylation and hippocampal memory. *Nature* 546: 381-386.
77. Rhee, J., L. A. Solomon, and R. P. DeKoter. 2019. A role for ATP Citrate Lyase in cell cycle regulation during myeloid differentiation. In *Blood Cells, Molecules, and Diseases*. 82-90.
78. Zhang, L., Q. Lu, and C. Chang. 2020. Epigenetics in Health and Disease. *Adv Exp Med Biol* 1253: 3-55.
79. Dexheimer, P. J., and L. Cochella. 2020. MicroRNAs: From Mechanism to Organism. *Front Cell Dev Biol* 8: 409.
80. Zhang, R., Y. Jing, H. Zhang, Y. Niu, C. Liu, J. Wang, K. Zen, C. Y. Zhang, and D. Li. 2018. Comprehensive Evolutionary Analysis of the Major RNA-Induced Silencing Complex Members. *Sci Rep* 8: 14189.
81. Huang, C., M. Xu, and B. Zhu. 2013. Epigenetic inheritance mediated by histone lysine methylation: maintaining transcriptional states without the precise restoration of marks? *Philos Trans R Soc Lond B Biol Sci* 368: 20110332.
82. Heijmans, B. T., E. W. Tobi, A. D. Stein, H. Putter, G. J. Blauw, E. S. Susser, P. E. Slagboom, and L. H. Lumey. 2008. Persistent epigenetic differences associated with prenatal exposure to famine in humans. *Proc Natl Acad Sci U S A* 105: 17046-17049.
83. Greenberg, M. V. C., and D. Bourc'his. 2019. The diverse roles of DNA methylation in mammalian development and disease. *Nat Rev Mol Cell Biol* 20: 590-607.
84. Shvedunova, M., and A. Akhtar. 2022. Modulation of cellular processes by histone and non-histone protein acetylation. *Nat Rev Mol Cell Biol* 23: 329-349.
85. Fallah, M. S., D. Szarics, C. M. Robson, and J. H. Eubanks. 2020. Impaired Regulation of Histone Methylation and Acetylation Underlies Specific Neurodevelopmental Disorders. *Front Genet* 11: 613098.
86. Aoyama, K., N. Itokawa, M. Oshima, and A. Iwama. 2022. Epigenetic Memories in Hematopoietic Stem and Progenitor Cells. *Cells* 11.
87. Kaufmann, E., J. Sanz, J. L. Dunn, N. Khan, L. E. Mendonça, A. Pacis, F. Tzelepis, E. Pernet, A. Dumaine, J.-C. Grenier, F. Mailhot-Léonard, E. Ahmed, J. Belle, R. Besla, B. Mazer, I. L. King, A. Nijnik, C. S. Robbins, L. B. Barreiro, and M. Divangahi. 2018. BCG Educates Hematopoietic Stem Cells to Generate Protective Innate Immunity against Tuberculosis. *Cell* 172: 176-190.e119.
88. Cirovic, B., L. C. J. De Bree, L. Groh, B. A. Blok, J. Chan, W. J. F. M. Van Der Velden, M. E. J. Bremmers, R. Van Crevel, K. Händler, S. Picelli, J. Schulte-Schrepping, K. Klee,

M. Oosting, V. A. C. M. Koeken, J. Van Ingen, Y. Li, C. S. Benn, J. L. Schultze, L. A. B. Joosten, N. Curtis, M. G. Netea, and A. Schlitzer. 2020. BCG Vaccination in Humans Elicits Trained Immunity via the Hematopoietic Progenitor Compartment. *Cell Host & Microbe* 28: 322-334.e325.

89. Itokawa, N., M. Oshima, S. Koide, N. Takayama, W. Kuribayashi, Y. Nakajima-Takagi, K. Aoyama, S. Yamazaki, K. Yamaguchi, Y. Furukawa, K. Eto, and A. Iwama. 2022. Epigenetic traits inscribed in chromatin accessibility in aged hematopoietic stem cells. *Nat Commun* 13: 2691.
90. Shi, L., and B. P. Tu. 2015. Acetyl-CoA and the regulation of metabolism: mechanisms and consequences. *Curr Opin Cell Biol* 33: 125-131.
91. Reid, M. A., Z. Dai, and J. W. Locasale. 2017. The impact of cellular metabolism on chromatin dynamics and epigenetics. In *Nature Cell Biology*. Nature Publishing Group. 1298-1306.
92. Seibert, E., and T. S. Tracy. 2021. Fundamentals of Enzyme Kinetics: Michaelis-Menten and Non-Michaelis-Type (Atypical) Enzyme Kinetics. *Methods Mol Biol* 2342: 3-27.
93. Peng, M., N. Yin, S. Chhangawala, K. Xu, C. S. Leslie, and M. O. Li. 2016. Aerobic glycolysis promotes T helper 1 cell differentiation through an epigenetic mechanism. *Science* 354: 481-484.
94. Sperber, H., J. Mathieu, Y. Wang, A. Ferreccio, J. Hesson, Z. Xu, K. A. Fischer, A. Devi, D. Detraux, H. Gu, S. L. Battle, M. Showalter, C. Valensisi, J. H. Bielas, N. G. Ericson, L. Margaretha, A. M. Robitaille, D. Margineantu, O. Fiehn, D. Hockenbery, C. A. Blau, D. Raftery, A. A. Margolin, R. D. Hawkins, R. T. Moon, C. B. Ware, and H. Ruohola-Baker. 2015. The metabolome regulates the epigenetic landscape during naive-to-primed human embryonic stem cell transition. *Nat Cell Biol* 17: 1523-1535.
95. Umemoto, T., A. Johansson, S. A. I. Ahmad, M. Hashimoto, S. Kubota, K. Kikuchi, H. Odaka, T. Era, D. Kurotaki, G. Sashida, and T. Suda. 2022. ATP citrate lyase controls hematopoietic stem cell fate and supports bone marrow regeneration. *The EMBO Journal* 41.
96. Moussaieff, A., M. Rouleau, D. Kitsberg, M. Cohen, G. Levy, D. Barasch, A. Nemirovski, S. Shen-Orr, I. Laevsky, M. Amit, D. Bomze, B. Elena-Herrmann, T. Scherf, M. Nissim-Rafinia, S. Kempa, J. Itskovitz-Eldor, E. Meshorer, D. Aberdam, and Y. Nahmias. 2015. Glycolysis-Mediated Changes in Acetyl-CoA and Histone Acetylation Control the Early Differentiation of Embryonic Stem Cells. *Cell Metabolism* 21: 392-402.
97. Li, X., W. Yu, X. Qian, Y. Xia, Y. Zheng, J. H. Lee, W. Li, J. Lyu, G. Rao, X. Zhang, C. N. Qian, S. G. Rozen, T. Jiang, and Z. Lu. 2017. Nucleus-Translocated ACSS2 Promotes Gene Transcription for Lysosomal Biogenesis and Autophagy. *Mol Cell* 66: 684-697.e689.
98. Serio, R. N., C. Lu, S. S. Gross, and L. J. Gudas. 2019. Different Effects of Knockouts in ALDH2 and ACSS2 on Embryonic Stem Cell Differentiation. *Alcohol Clin Exp Res* 43: 1859-1871.
99. Du, X., and H. Hu. 2021. The Roles of 2-Hydroxyglutarate. *Front Cell Dev Biol* 9: 651317.
100. Kokubo, K., A. Onodera, M. Kiuchi, K. Tsuji, K. Hirahara, and T. Nakayama. 2022. Conventional and pathogenic Th2 cells in inflammation, tissue repair, and fibrosis. *Front Immunol* 13: 945063.
101. O'Connor, R. A., and S. M. Anderton. 2015. Inflammation-associated genes: risks and benefits to Foxp3+ regulatory T-cell function. *Immunology* 146: 194-205.
102. Lazarevic, V., L. H. Glimcher, and G. M. Lord. 2013. T-bet: a bridge between innate and adaptive immunity. *Nat Rev Immunol* 13: 777-789.
103. Jiang, Q., G. Yang, F. Xiao, J. Xie, S. Wang, L. Lu, and D. Cui. 2021. Role of Th22 Cells in the Pathogenesis of Autoimmune Diseases. *Front Immunol* 12: 688066.

104. Lee, G. R. 2018. The Balance of Th17 versus Treg Cells in Autoimmunity. *Int J Mol Sci* 19.
105. Philip, M., and A. Schietinger. 2022. CD8(+) T cell differentiation and dysfunction in cancer. *Nat Rev Immunol* 22: 209-223.
106. Fernández-Quintero, M. L., C. A. Seidler, and K. R. Liedl. 2020. T-Cell Receptor Variable β Domains Rigidify During Affinity Maturation. *Sci Rep* 10: 4472.
107. Shah, K., A. Al-Haidari, J. Sun, and J. U. Kazi. 2021. T cell receptor (TCR) signaling in health and disease. *Signal Transduct Target Ther* 6: 412.
108. Ngoenkam, J., W. W. Schamel, and S. Pongcharoen. 2018. Selected signalling proteins recruited to the T-cell receptor-CD3 complex. *Immunology* 153: 42-50.
109. Choi, Y., Y. Shi, C. L. Haymaker, A. Naing, G. Ciliberto, and J. Hajjar. 2020. T-cell agonists in cancer immunotherapy. *J Immunother Cancer* 8.
110. Ghaedi, M., C. A. Steer, I. Martinez-Gonzalez, T. Y. F. Halim, N. Abraham, and F. Takei. 2016. Common-Lymphoid-Progenitor-Independent Pathways of Innate and T Lymphocyte Development. *Cell Rep* 15: 471-480.
111. Robert, P. A., H. Kunze-Schumacher, V. Greiff, and A. Krueger. 2021. Modeling the Dynamics of T-Cell Development in the Thymus. *Entropy (Basel)* 23.
112. Robey, E. A., B. J. Fowlkes, J. W. Gordon, D. Kioussis, H. von Boehmer, F. Ramsdell, and R. Axel. 1991. Thymic selection in CD8 transgenic mice supports an instructive model for commitment to a CD4 or CD8 lineage. *Cell* 64: 99-107.
113. Karimi, M. M., Y. Guo, X. Cui, H. A. Pallikonda, V. Horková, Y. F. Wang, S. R. Gil, G. Rodriguez-Esteban, I. Robles-Rebollo, L. Bruno, R. Georgieva, B. Patel, J. Elliott, M. H. Dore, D. Dauphars, M. S. Krangel, B. Lenhard, H. Heyn, A. G. Fisher, O. Štěpánek, and M. Merkenschlager. 2021. The order and logic of CD4 versus CD8 lineage choice and differentiation in mouse thymus. *Nat Commun* 12: 99.
114. Wang, H. X., W. Pan, L. Zheng, X. P. Zhong, L. Tan, Z. Liang, J. He, P. Feng, Y. Zhao, and Y. R. Qiu. 2019. Thymic Epithelial Cells Contribute to Thymopoiesis and T Cell Development. *Front Immunol* 10: 3099.
115. Dzhagalov, I. L., K. G. Chen, P. Herzmark, and E. A. Robey. 2013. Elimination of self-reactive T cells in the thymus: a timeline for negative selection. *PLoS Biol* 11: e1001566.
116. Christie, S. M., C. Fijen, and E. Rothenberg. 2022. V(D)J Recombination: Recent Insights in Formation of the Recombinase Complex and Recruitment of DNA Repair Machinery. *Front Cell Dev Biol* 10: 886718.
117. Haen, S. P., M. W. Löffler, H. G. Rammensee, and P. Brossart. 2020. Towards new horizons: characterization, classification and implications of the tumour antigenic repertoire. *Nat Rev Clin Oncol* 17: 595-610.
118. Tsuji, T., K. H. Eng, J. Matsuzaki, S. Battaglia, J. B. Szender, A. Miliotto, S. Gnjatic, W. Bshara, C. D. Morrison, S. Lele, R. O. Emerson, J. Wang, S. Liu, H. Robins, A. A. Lugade, and K. Odunsi. 2020. Clonality and antigen-specific responses shape the prognostic effects of tumor-infiltrating T cells in ovarian cancer. *Oncotarget* 11: 2669-2683.
119. Aoki, H., S. Ueha, Y. Nakamura, S. Shichino, H. Nakajima, M. Shimomura, A. Sato, T. Nakatsura, T. Yoshino, and K. Matsushima. 2021. Greater extent of blood-tumor TCR repertoire overlap is associated with favorable clinical responses to PD-1 blockade. *Cancer Sci* 112: 2993-3004.
120. Stubbington, M. J. T., T. Lönnberg, V. Proserpio, S. Clare, A. O. Speak, G. Dougan, and S. A. Teichmann. 2016. T cell fate and clonality inference from single-cell transcriptomes. *Nat Methods* 13: 329-332.
121. Montagne, J. M., X. A. Zheng, I. Pinal-Fernandez, J. C. Milisenda, L. Christopher-Stine, T. E. Lloyd, A. L. Mammen, and H. B. Larman. 2020. Ultra-efficient sequencing of T Cell

receptor repertoires reveals shared responses in muscle from patients with Myositis. *EBioMedicine* 59: 102972.
122. Clarke, S. R., M. Barnden, C. Kurts, F. R. Carbone, J. F. Miller, and W. R. Heath. 2000. Characterization of the ovalbumin-specific TCR transgenic line OT-I: MHC elements for positive and negative selection. *Immunol Cell Biol* 78: 110-117.
123. Liu, Z., T. Poiret, Q. Meng, M. Rao, A. von Landenberg, E. Schoutrop, D. Valentini, E. Dodoo, I. Peredo-Harvey, and M. Maeurer. 2018. Epstein-Barr virus- and cytomegalovirus-specific immune response in patients with brain cancer. *J Transl Med* 16: 182.
124. Lanfermeijer, J., P. C. de Greef, M. Hendriks, M. Vos, J. van Beek, J. A. M. Borghans, and D. van Baarle. 2021. Age and CMV-Infection Jointly Affect the EBV-Specific CD8(+) T-Cell Repertoire. *Front Aging* 2: 665637.
125. Naidus, E., J. Bouquet, D. Y. Oh, T. J. Looney, H. Yang, L. Fong, N. E. Standifer, and L. Zhang. 2021. Early changes in the circulating T cells are associated with clinical outcomes after PD-L1 blockade by durvalumab in advanced NSCLC patients. *Cancer Immunol Immunother* 70: 2095-2102.
126. Gadot, M., M. Gal, P. Dobosz, Z. Dotan, J. Ramon, R. Berger, D. Avni, E. Fridman, and R. Leibowitz. 2021. Associations between T cell infiltration, T cell receptor clonality, histology and recurrence in renal cell carcinoma. *Clin Exp Immunol* 205: 160-168.
127. Li, H., A. Zhao, M. Li, L. Shi, Q. Han, and Z. Hou. 2022. Targeting T-cell metabolism to boost immune checkpoint inhibitor therapy. *Frontiers in Immunology* 13.
128. Amitrano, A. M., B. J. Berry, K. Lim, K. D. Kim, R. E. Waugh, A. P. Wojtovich, and M. Kim. 2021. Optical Control of CD8(+) T Cell Metabolism and Effector Functions. *Front Immunol* 12: 666231.
129. Gerner, M. C., L. Niederstaetter, L. Ziegler, A. Bileck, A. Slany, L. Janker, R. L. J. Schmidt, C. Gerner, G. Del Favero, and K. G. Schmetterer. 2019. Proteome Analysis Reveals Distinct Mitochondrial Functions Linked to Interferon Response Patterns in Activated CD4+ and CD8+ T Cells. *Front Pharmacol* 10: 727.
130. Liao, P., W. Wang, W. Wang, I. Kryczek, X. Li, Y. Bian, A. Sell, S. Wei, S. Grove, J. K. Johnson, P. D. Kennedy, M. Gijón, Y. M. Shah, and W. Zou. 2022. CD8(+) T cells and fatty acids orchestrate tumor ferroptosis and immunity via ACSL4. *Cancer Cell* 40: 365-378.e366.
131. Ma, X., E. Bi, Y. Lu, P. Su, C. Huang, L. Liu, Q. Wang, M. Yang, M. F. Kalady, J. Qian, A. Zhang, A. A. Gupte, D. J. Hamilton, C. Zheng, and Q. Yi. 2019. Cholesterol Induces CD8(+) T Cell Exhaustion in the Tumor Microenvironment. *Cell Metab* 30: 143-156.e145.
132. Yang, W., Y. Bai, Y. Xiong, J. Zhang, S. Chen, X. Zheng, X. Meng, L. Li, J. Wang, C. Xu, C. Yan, L. Wang, C. C. Chang, T. Y. Chang, T. Zhang, P. Zhou, B. L. Song, W. Liu, S. C. Sun, X. Liu, B. L. Li, and C. Xu. 2016. Potentiating the antitumour response of CD8(+) T cells by modulating cholesterol metabolism. *Nature* 531: 651-655.
133. Li, C., B. Zhu, Y. M. Son, Z. Wang, L. Jiang, M. Xiang, Z. Ye, K. E. Beckermann, Y. Wu, J. W. Jenkins, P. J. Siska, B. G. Vincent, Y. S. Prakash, T. Peikert, B. T. Edelson, R. Taneja, M. H. Kaplan, J. C. Rathmell, H. Dong, T. Hitosugi, and J. Sun. 2019. The Transcription Factor Bhlhe40 Programs Mitochondrial Regulation of Resident CD8(+) T Cell Fitness and Functionality. *Immunity* 51: 491-507.e497.
134. Patsoukis, N., K. Bardhan, P. Chatterjee, D. Sari, B. Liu, L. N. Bell, E. D. Karoly, G. J. Freeman, V. Petkova, P. Seth, L. Li, and V. A. Boussiotis. 2015. PD-1 alters T-cell metabolic reprogramming by inhibiting glycolysis and promoting lipolysis and fatty acid oxidation. *Nat Commun* 6: 6692.
135. Tkachev, V., S. Goodell, A. W. Opipari, L. Y. Hao, L. Franchi, G. D. Glick, J. L. Ferrara, and C. A. Byersdorfer. 2015. Programmed death-1 controls T cell survival by regulating oxidative metabolism. *J Immunol* 194: 5789-5800.

136. He, W., H. Zhang, F. Han, X. Chen, R. Lin, W. Wang, H. Qiu, Z. Zhuang, Q. Liao, W. Zhang, Q. Cai, Y. Cui, W. Jiang, H. Wang, and Z. Ke. 2017. CD155T/TIGIT Signaling Regulates CD8(+) T-cell Metabolism and Promotes Tumor Progression in Human Gastric Cancer. *Cancer Res* 77: 6375-6388.
137. Lee, M. J., S. J. Yun, B. Lee, E. Jeong, G. Yoon, K. Kim, and S. Park. 2020. Association of TIM-3 expression with glucose metabolism in Jurkat T cells. *BMC Immunol* 21: 48.
138. Kumagai, S., S. Koyama, K. Itahashi, T. Tanegashima, Y. T. Lin, Y. Togashi, T. Kamada, T. Irie, G. Okumura, H. Kono, D. Ito, R. Fujii, S. Watanabe, A. Sai, S. Fukuoka, E. Sugiyama, G. Watanabe, T. Owari, H. Nishinakamura, D. Sugiyama, Y. Maeda, A. Kawazoe, H. Yukami, K. Chida, Y. Ohara, T. Yoshida, Y. Shinno, Y. Takeyasu, M. Shirasawa, K. Nakama, K. Aokage, J. Suzuki, G. Ishii, T. Kuwata, N. Sakamoto, M. Kawazu, T. Ueno, T. Mori, N. Yamazaki, M. Tsuboi, Y. Yatabe, T. Kinoshita, T. Doi, K. Shitara, H. Mano, and H. Nishikawa. 2022. Lactic acid promotes PD-1 expression in regulatory T cells in highly glycolytic tumor microenvironments. *Cancer Cell* 40: 201-218.e209.
139. Liu, Y., X. Liang, W. Dong, Y. Fang, J. Lv, T. Zhang, R. Fiskesund, J. Xie, J. Liu, X. Yin, X. Jin, D. Chen, K. Tang, J. Ma, H. Zhang, J. Yu, J. Yan, H. Liang, S. Mo, F. Cheng, Y. Zhou, H. Zhang, J. Wang, J. Li, Y. Chen, B. Cui, Z. W. Hu, X. Cao, F. Xiao-Feng Qin, and B. Huang. 2018. Tumor-Repopulating Cells Induce PD-1 Expression in CD8(+) T Cells by Transferring Kynurenine and AhR Activation. *Cancer Cell* 33: 480-494.e487.
140. Mock, A., S. Zschäbitz, R. Kirsten, M. Scheffler, B. Wolf, C. Herold-Mende, R. Kramer, E. Busch, M. Jenzer, D. Jäger, and C. Grüllich. 2019. Serum very long-chain fatty acid-containing lipids predict response to immune checkpoint inhibitors in urological cancers. *Cancer Immunol Immunother* 68: 2005-2014.
141. Schmidt, N. M., P. A. C. Wing, M. O. Diniz, L. J. Pallett, L. Swadling, J. M. Harris, A. R. Burton, A. Jeffery-Smith, N. Zakeri, O. E. Amin, S. Kucykowicz, M. H. Heemskerk, B. Davidson, T. Meyer, J. Grove, H. J. Stauss, I. Pineda-Torra, C. Jolly, E. C. Jury, J. A. McKeating, and M. K. Maini. 2021. Targeting human Acyl-CoA:cholesterol acyltransferase as a dual viral and T cell metabolic checkpoint. *Nat Commun* 12: 2814.
142. Siu, L. L., H. Burris, D. T. Le, A. Hollebecque, N. Steeghs, J.-P. Delord, J. Hilton, B. Barnhart, E. Sega, K. Sanghavi, A. Klippel, C. Hedvat, E. Hilt, M. Donovan, A. Gipson, P. Basciano, J. Postelnek, Y. Zhao, R. P. Perez, and R. D. Carvajal. 2018. Abstract CT180: Preliminary phase 1 profile of BMS-986179, an anti-CD73 antibody, in combination with nivolumab in patients with advanced solid tumors. *Cancer Research* 78: CT180-CT180.
143. Deleuze, A., J. Saout, F. Dugay, B. Peyronnet, R. Mathieu, G. Verhoest, K. Bensalah, L. Crouzet, B. Laguerre, M. A. Belaud-Rotureau, N. Rioux-Leclercq, and S. F. Kammerer-Jacquet. 2020. Immunotherapy in Renal Cell Carcinoma: The Future Is Now. *Int J Mol Sci* 21.
144. Hoefflin, R., S. Harlander, S. Schäfer, P. Metzger, F. Kuo, D. Schönenberger, M. Adlesic, A. Peighambari, P. Seidel, C. Y. Chen, M. Consenza-Contreras, A. Jud, B. Lahrmann, N. Grabe, D. Heide, F. M. Uhl, T. A. Chan, J. Duyster, R. Zeiser, C. Schell, M. Heikenwalder, O. Schilling, A. A. Hakimi, M. Boerries, and I. J. Frew. 2020. HIF-1α and HIF-2α differently regulate tumour development and inflammation of clear cell renal cell carcinoma in mice. *Nat Commun* 11: 4111.
145. Takahashi, A., H. Sasaki, S. J. Kim, K. Tobisu, T. Kakizoe, T. Tsukamoto, Y. Kumamoto, T. Sugimura, and M. Terada. 1994. Markedly increased amounts of messenger RNAs for vascular endothelial growth factor and placenta growth factor in renal cell carcinoma associated with angiogenesis. *Cancer Res* 54: 4233-4237.
146. Ricketts, C. J., A. A. De Cubas, H. Fan, C. C. Smith, M. Lang, E. Reznik, R. Bowlby, E. A. Gibb, R. Akbani, R. Beroukhim, D. P. Bottaro, T. K. Choueiri, R. A. Gibbs, A. K.

Godwin, S. Haake, A. A. Hakimi, E. P. Henske, J. J. Hsieh, T. H. Ho, R. S. Kanchi, B. Krishnan, D. J. Kwiatkowski, W. Lui, M. J. Merino, G. B. Mills, J. Myers, M. L. Nickerson, V. E. Reuter, L. S. Schmidt, C. S. Shelley, H. Shen, B. Shuch, S. Signoretti, R. Srinivasan, P. Tamboli, G. Thomas, B. G. Vincent, C. D. Vocke, D. A. Wheeler, L. Yang, W. Y. Kim, A. G. Robertson, P. T. Spellman, W. K. Rathmell, and W. M. Linehan. 2018. The Cancer Genome Atlas Comprehensive Molecular Characterization of Renal Cell Carcinoma. *Cell Rep* 23: 3698.

147. Varela, I., P. Tarpey, K. Raine, D. Huang, C. K. Ong, P. Stephens, H. Davies, D. Jones, M. L. Lin, J. Teague, G. Bignell, A. Butler, J. Cho, G. L. Dalgliesh, D. Galappaththige, C. Greenman, C. Hardy, M. Jia, C. Latimer, K. W. Lau, J. Marshall, S. McLaren, A. Menzies, L. Mudie, L. Stebbings, D. A. Largaespada, L. F. Wessels, S. Richard, R. J. Kahnoski, J. Anema, D. A. Tuveson, P. A. Perez-Mancera, V. Mustonen, A. Fischer, D. J. Adams, A. Rust, W. Chan-on, C. Subimerb, K. Dykema, K. Furge, P. J. Campbell, B. T. Teh, M. R. Stratton, and P. A. Futreal. 2011. Exome sequencing identifies frequent mutation of the SWI/SNF complex gene PBRM1 in renal carcinoma. *Nature* 469: 539-542.
148. Thompson, R. H., H. Dong, C. M. Lohse, B. C. Leibovich, M. L. Blute, J. C. Cheville, and E. D. Kwon. 2007. PD-1 is expressed by tumor-infiltrating immune cells and is associated with poor outcome for patients with renal cell carcinoma. *Clin Cancer Res* 13: 1757-1761.
149. Serzan, M. T., and M. B. Atkins. 2021. Current and emerging therapies for first line treatment of metastatic clear cell renal cell carcinoma. *J Cancer Metastasis Treat* 7.
150. Iacovelli, R., F. Nolè, E. Verri, G. Renne, C. Paglino, M. Santoni, M. Cossu Rocca, P. Giglione, G. Aurilio, D. Cullurà, S. Cascinu, and C. Porta. 2016. Prognostic Role of PD-L1 Expression in Renal Cell Carcinoma. A Systematic Review and Meta-Analysis. *Target Oncol* 11: 143-148.
151. Leite, K. R., S. T. Reis, J. P. Junior, M. Zerati, O. Gomes Dde, L. H. Camara-Lopes, and M. Srougi. 2015. PD-L1 expression in renal cell carcinoma clear cell type is related to unfavorable prognosis. *Diagn Pathol* 10: 189.
152. Powles, T., E. R. Plimack, D. Soulières, T. Waddell, V. Stus, R. Gafanov, D. Nosov, F. Pouliot, B. Melichar, I. Vynnychenko, S. J. Azevedo, D. Borchiellini, R. S. McDermott, J. Bedke, S. Tamada, L. Yin, M. Chen, L. R. Molife, M. B. Atkins, and B. I. Rini. 2020. Pembrolizumab plus axitinib versus sunitinib monotherapy as first-line treatment of advanced renal cell carcinoma (KEYNOTE-426): extended follow-up from a randomised, open-label, phase 3 trial. *Lancet Oncol* 21: 1563-1573.
153. Kim, T. J., Y. H. Lee, and K. C. Koo. 2022. Current and future perspectives on CAR-T cell therapy for renal cell carcinoma: A comprehensive review. *Investigative and Clinical Urology* 63: 486.
154. Motzer, R. J., N. M. Tannir, D. F. McDermott, O. Arén Frontera, B. Melichar, T. K. Choueiri, E. R. Plimack, P. Barthélémy, C. Porta, S. George, T. Powles, F. Donskov, V. Neiman, C. K. Kollmannsberger, P. Salman, H. Gurney, R. Hawkins, A. Ravaud, M. O. Grimm, S. Bracarda, C. H. Barrios, Y. Tomita, D. Castellano, B. I. Rini, A. C. Chen, S. Mekan, M. B. McHenry, M. Wind-Rotolo, J. Doan, P. Sharma, H. J. Hammers, and B. Escudier. 2018. Nivolumab plus Ipilimumab versus Sunitinib in Advanced Renal-Cell Carcinoma. *N Engl J Med* 378: 1277-1290.
155. Tannir, N. M., S. Signoretti, T. K. Choueiri, D. F. McDermott, R. J. Motzer, A. Flaifel, J. C. Pignon, M. Ficial, O. A. Frontera, S. George, T. Powles, F. Donskov, M. R. Harrison, P. Barthélémy, S. S. Tykodi, J. Kocsis, A. Ravaud, J. R. Rodriguez-Cid, S. K. Pal, A. M. Murad, Y. Ishii, S. S. Saggi, M. B. McHenry, and B. I. Rini. 2021. Efficacy and Safety of Nivolumab Plus Ipilimumab versus Sunitinib in First-line Treatment of Patients with Advanced Sarcomatoid Renal Cell Carcinoma. *Clin Cancer Res* 27: 78-86.

156. Hudes, G., M. Carducci, P. Tomczak, J. Dutcher, R. Figlin, A. Kapoor, E. Staroslawska, J. Sosman, D. McDermott, I. Bodrogi, Z. Kovacevic, V. Lesovoy, I. G. Schmidt-Wolf, O. Barbarash, E. Gokmen, T. O'Toole, S. Lustgarten, L. Moore, and R. J. Motzer. 2007. Temsirolimus, interferon alfa, or both for advanced renal-cell carcinoma. *N Engl J Med* 356: 2271-2281.
157. Motzer, R. J., B. Escudier, P. Tomczak, T. E. Hutson, M. D. Michaelson, S. Negrier, S. Oudard, M. E. Gore, J. Tarazi, S. Hariharan, C. Chen, B. Rosbrook, S. Kim, and B. I. Rini. 2013. Axitinib versus sorafenib as second-line treatment for advanced renal cell carcinoma: overall survival analysis and updated results from a randomised phase 3 trial. *Lancet Oncol* 14: 552-562.
158. Rini, B. I., S. K. Pal, B. J. Escudier, M. B. Atkins, T. E. Hutson, C. Porta, E. Verzoni, M. N. Needle, and D. F. McDermott. 2020. Tivozanib versus sorafenib in patients with advanced renal cell carcinoma (TIVO-3): a phase 3, multicentre, randomised, controlled, open-label study. *Lancet Oncol* 21: 95-104.
159. Choueiri, T. K., R. J. Motzer, B. I. Rini, J. Haanen, M. T. Campbell, B. Venugopal, C. Kollmannsberger, G. Gravis-Mescam, M. Uemura, J. L. Lee, M. O. Grimm, H. Gurney, M. Schmidinger, J. Larkin, M. B. Atkins, S. K. Pal, J. Wang, M. Mariani, S. Krishnaswami, P. Cislo, A. Chudnovsky, C. Fowst, B. Huang, A. di Pietro, and L. Albiges. 2020. Updated efficacy results from the JAVELIN Renal 101 trial: first-line avelumab plus axitinib versus sunitinib in patients with advanced renal cell carcinoma. *Ann Oncol* 31: 1030-1039.
160. Cancer stat facts: kidney and renal pelvis cancer. In *Surveillance, Epidemiology, and End Results Program*. National Cancer Institute.
161. Jhaveri, K. D., and M. H. Rosner. 2018. Chimeric Antigen Receptor T Cell Therapy and the Kidney: What the Nephrologist Needs to Know. *Clin J Am Soc Nephrol* 13: 796-798.
162. Lamers, C. H., S. Sleijfer, S. van Steenbergen, P. van Elzakker, B. van Krimpen, C. Groot, A. Vulto, M. den Bakker, E. Oosterwijk, R. Debets, and J. W. Gratama. 2013. Treatment of metastatic renal cell carcinoma with CAIX CAR-engineered T cells: clinical evaluation and management of on-target toxicity. *Mol Ther* 21: 904-912.
163. Jensen, M. C., L. Popplewell, L. J. Cooper, D. DiGiusto, M. Kalos, J. R. Ostberg, and S. J. Forman. 2010. Antitransgene rejection responses contribute to attenuated persistence of adoptively transferred CD20/CD19-specific chimeric antigen receptor redirected T cells in humans. *Biol Blood Marrow Transplant* 16: 1245-1256.
164. Tang, F., C. Barbacioru, Y. Wang, E. Nordman, C. Lee, N. Xu, X. Wang, J. Bodeau, B. B. Tuch, A. Siddiqui, K. Lao, and M. A. Surani. 2009. mRNA-Seq whole-transcriptome analysis of a single cell. *Nat Methods* 6: 377-382.
165. Jovic, D., X. Liang, H. Zeng, L. Lin, F. Xu, and Y. Luo. 2022. Single-cell RNA sequencing technologies and applications: A brief overview. *Clinical and Translational Medicine* 12.
166. Lambrechts, D., E. Wauters, B. Boeckx, S. Aibar, D. Nittner, O. Burton, A. Bassez, H. Decaluwé, A. Pircher, K. Van den Eynde, B. Weynand, E. Verbeken, P. De Leyn, A. Liston, J. Vansteenkiste, P. Carmeliet, S. Aerts, and B. Thienpont. 2018. Phenotype molding of stromal cells in the lung tumor microenvironment. *Nat Med* 24: 1277-1289.
167. Osorio, D., and J. J. Cai. 2021. Systematic determination of the mitochondrial proportion in human and mice tissues for single-cell RNA-sequencing data quality control. *Bioinformatics* 37: 963-967.
168. Gladka, M. M., B. Molenaar, H. de Ruiter, S. van der Elst, H. Tsui, D. Versteeg, G. P. A. Lacraz, M. M. H. Huibers, A. van Oudenaarden, and E. van Rooij. 2018. Single-Cell Sequencing of the Healthy and Diseased Heart Reveals Cytoskeleton-Associated Protein 4 as a New Modulator of Fibroblasts Activation. *Circulation* 138: 166-180.

169. Huang, Q., Y. Liu, Y. Du, and L. X. Garmire. 2021. Evaluation of Cell Type Annotation R Packages on Single-cell RNA-seq Data. *Genomics Proteomics Bioinformatics* 19: 267-281.
170. Aibar, S., C. B. González-Blas, T. Moerman, V. A. Huynh-Thu, H. Imrichova, G. Hulselmans, F. Rambow, J. C. Marine, P. Geurts, J. Aerts, J. van den Oord, Z. K. Atak, J. Wouters, and S. Aerts. 2017. SCENIC: single-cell regulatory network inference and clustering. *Nat Methods* 14: 1083-1086.
171. Herring, C. A., A. Banerjee, E. T. McKinley, A. J. Simmons, J. Ping, J. T. Roland, J. L. Franklin, Q. Liu, M. J. Gerdes, R. J. Coffey, and K. S. Lau. 2018. Unsupervised Trajectory Analysis of Single-Cell RNA-Seq and Imaging Data Reveals Alternative Tuft Cell Origins in the Gut. *Cell Syst* 6: 37-51.e39.
172. Qiu, X., Q. Mao, Y. Tang, L. Wang, R. Chawla, H. A. Pliner, and C. Trapnell. 2017. Reversed graph embedding resolves complex single-cell trajectories. *Nat Methods* 14: 979-982.
173. Ranzoni, A. M., A. Tangherloni, I. Berest, S. G. Riva, B. Myers, P. M. Strzelecka, J. Xu, E. Panada, I. Mohorianu, J. B. Zaugg, and A. Cvejic. 2021. Integrative Single-Cell RNA-Seq and ATAC-Seq Analysis of Human Developmental Hematopoiesis. *Cell Stem Cell* 28: 472-487.e477.
174. Hu, Y., K. Huang, Q. An, G. Du, G. Hu, J. Xue, X. Zhu, C. Y. Wang, Z. Xue, and G. Fan. 2016. Simultaneous profiling of transcriptome and DNA methylome from a single cell. *Genome Biol* 17: 88.
175. Stoeckius, M., C. Hafemeister, W. Stephenson, B. Houck-Loomis, P. K. Chattopadhyay, H. Swerdlow, R. Satija, and P. Smibert. 2017. Simultaneous epitope and transcriptome measurement in single cells. *Nat Methods* 14: 865-868.
176. He, H., Z. Li, J. Lu, W. Qiang, S. Jiang, Y. Xu, W. Fu, X. Zhai, L. Zhou, M. Qian, and J. Du. 2022. Single-cell RNA-seq reveals clonal diversity and prognostic genes of relapsed multiple myeloma. *Clin Transl Med* 12: e757.
177. Setliff, I., A. R. Shiakolas, K. A. Pilewski, A. A. Murji, R. E. Mapengo, K. Janowska, S. Richardson, C. Oosthuysen, N. Raju, L. Ronsard, M. Kanekiyo, J. S. Qin, K. J. Kramer, A. R. Greenplate, W. J. McDonnell, B. S. Graham, M. Connors, D. Lingwood, P. Acharya, L. Morris, and I. S. Georgiev. 2019. High-Throughput Mapping of B Cell Receptor Sequences to Antigen Specificity. *Cell* 179: 1636-1646.e1615.
178. Hicks, S. C., F. W. Townes, M. Teng, and R. A. Irizarry. 2018. Missing data and technical variability in single-cell RNA-sequencing experiments. *Biostatistics* 19: 562-578.
179. Qiu, P. 2020. Embracing the dropouts in single-cell RNA-seq analysis. *Nat Commun* 11: 1169.
180. Giralt, S., L. Costa, J. Schriber, J. Dipersio, R. Maziarz, J. McCarty, P. Shaughnessy, E. Snyder, W. Bensinger, E. Copelan, C. Hosing, R. Negrin, F. B. Petersen, D. Rondelli, R. Soiffer, H. Leather, A. Pazzalia, and S. Devine. 2014. Optimizing autologous stem cell mobilization strategies to improve patient outcomes: consensus guidelines and recommendations. *Biol Blood Marrow Transplant* 20: 295-308.
181. Guo, Q., H. Kang, J. Wang, Y. Dong, R. Peng, H. Zhao, W. Wu, H. Guan, and F. Li. 2021. Inhibition of ACLY Leads to Suppression of Osteoclast Differentiation and Function Via Regulation of Histone Acetylation. *Journal of Bone and Mineral Research* 36: 2065-2080.
182. Sivanand, S., I. Viney, and K. E. Wellen. 2018. Spatiotemporal Control of Acetyl-CoA Metabolism in Chromatin Regulation. In *Trends in Biochemical Sciences*. Elsevier Ltd. 61-74.
183. Fukuda, H., A. Katsurada, and N. Iritani. 1992. Effects of nutrients and hormones on gene expression of ATP citrate-lyase in rat liver. *Eur J Biochem* 209: 217-222.

184. Jiang, L., Q. Wang, Y. Yu, F. Zhao, P. Huang, R. Zeng, R. Z. Qi, W. Li, and Y. Liu. 2009. Leptin contributes to the adaptive responses of mice to high-fat diet intake through suppressing the lipogenic pathway. *PLoS One* 4: e6884.
185. Zhang, L., W. Zhang, Z. Li, S. Lin, T. Zheng, B. Hao, Y. Hou, Y. Zhang, K. Wang, C. Qin, L. Yue, J. Jin, M. Li, and L. Fan. 2022. Mitochondria dysfunction in CD8+ T cells as an important contributing factor for cancer development and a potential target for cancer treatment: a review. *Journal of Experimental & Clinical Cancer Research* 41.
186. Korshunov, S. S., V. P. Skulachev, and A. A. Starkov. 1997. High protonic potential actuates a mechanism of production of reactive oxygen species in mitochondria. *FEBS Lett* 416: 15-18.
187. Gottlieb, E., S. M. Armour, M. H. Harris, and C. B. Thompson. 2003. Mitochondrial membrane potential regulates matrix configuration and cytochrome c release during apoptosis. *Cell Death Differ* 10: 709-717.
188. Greenwood, D. L., H. E. Ramsey, P. T. T. Nguyen, A. R. Patterson, K. Voss, J. E. Bader, A. Sugiura, Z. A. Bacigalupa, S. Schaefer, X. Ye, D. O. Dahunsi, M. Z. Madden, K. E. Wellen, M. R. Savona, P. B. Ferrell, and J. C. Rathmell. 2022. Acly Deficiency Enhances Myelopoiesis through Acetyl Coenzyme A and Metabolic-Epigenetic Cross-Talk. *Immunohorizons* 6: 837-850.
189. Ito, K., and K. Ito. 2018. Hematopoietic stem cell fate through metabolic control. In *Experimental hematology*. Exp Hematol. 1-11.
190. Mortada, I., and R. Mortada. 2018. Epigenetic changes in mesenchymal stem cells differentiation. In *European journal of medical genetics*. Eur J Med Genet. 114-118.
191. Verzi, M. P., and R. A. Shivdasani. 2020. Epigenetic regulation of intestinal stem cell differentiation. In *American journal of physiology. Gastrointestinal and liver physiology*. Am J Physiol Gastrointest Liver Physiol. G189-G196.
192. Gerosa, R. C., S. Boettcher, L. V. Kovtonyuk, A. Hausmann, W. D. Hardt, J. Hidalgo, C. Nombela-Arrieta, and M. G. Manz. 2021. CXCL12-abundant reticular cells are the major source of IL-6 upon LPS stimulation and thereby regulate hematopoiesis. *Blood Adv* 5: 5002-5015.
193. Ho, T. T., M. R. Warr, E. R. Adelman, O. M. Lansinger, J. Flach, E. V. Verovskaya, M. E. Figueroa, and E. Passegué. 2017. Autophagy maintains the metabolism and function of young and old stem cells. *Nature* 543: 205-210.
194. Trowbridge, J. J., J. W. Snow, J. Kim, and S. H. Orkin. 2009. DNA Methyltransferase 1 Is Essential for and Uniquely Regulates Hematopoietic Stem and Progenitor Cells. *Cell Stem Cell* 5: 442-449.
195. Santillan, D. A., C. M. Theisler, A. S. Ryan, R. Popovic, T. Stuart, M. M. Zhou, S. Alkan, and N. J. Zeleznik-Le. 2006. Bromodomain and histone acetyltransferase domain specificities control mixed lineage leukemia phenotype. *Cancer Res* 66: 10032-10039.
196. Senyuk, V., K. K. Sinha, S. Chakraborty, S. Buonamici, and G. Nucifora. 2003. P/CAF and GCN5 acetylate the AML1/MDS1/EVI1 fusion oncoprotein. *Biochem Biophys Res Commun* 307: 980-986.
197. Rokudai, S., Y. Aikawa, Y. Tagata, N. Tsuchida, Y. Taya, and I. Kitabayashi. 2009. Monocytic Leukemia Zinc Finger (MOZ) Interacts with p53 to Induce p21 Expression and Cell-cycle Arrest. *Journal of Biological Chemistry* 284: 237-244.
198. SRERE, P. A. 1959. The citrate cleavage enzyme. I. Distribution and purification. In *The Journal of biological chemistry*. Â© 1959 ASBMB. Currently published by Elsevier Inc; originally published by American Society for Biochemistry and Molecular Biology. 2544-2547.
199. Zhao, S., A. Torres, Ryan, S. Trefely, M. Wallace, Joyce, A. Carrer, A. Sengupta, Sydney, Y.-M. Kuo, Alexander, N. Meurs, John, Ian, Aalim, Christian, Nathaniel, Andrew,

and Kathryn. 2016. ATP-Citrate Lyase Controls a Glucose-to-Acetate Metabolic Switch. *Cell Reports* 17: 1037-1052.
200. Balmer, M. L., E. H. Ma, G. R. Bantug, J. Grählert, S. Pfister, T. Glatter, A. Jauch, S. Dimeloe, E. Slack, P. Dehio, M. A. Krzyzaniak, C. G. King, A. V. Burgener, M. Fischer, L. Develioglu, R. Belle, M. Recher, W. V. Bonilla, A. J. Macpherson, S. Hapfelmeier, R. G. Jones, and C. Hess. 2016. Memory CD8+ T Cells Require Increased Concentrations of Acetate Induced by Stress for Optimal Function. In *Immunity*. Cell Press. 1312-1324.
201. Vaughn, N., and D. Haviland. 2020. Acly promotes metabolic reprogramming and induction of IRF4 during early CD8 + T cell activation. In *Cytometry. Part A : the journal of the International Society for Analytical Cytology*. Cytometry A.
202. Dziennis, S., R. A. Van Etten, H. L. Pahl, D. L. Morris, T. L. Rothstein, C. M. Blosch, R. M. Perlmutter, and D. G. Tenen. 1995. The CD11b promoter directs high-level expression of reporter genes in macrophages in transgenic mice. *Blood* 85: 319-329.
203. Hickstein, D. D., J. Ozols, S. A. Williams, J. U. Baenziger, R. M. Locksley, and G. J. Roth. 1987. Isolation and characterization of the receptor on human neutrophils that mediates cellular adherence. *J Biol Chem* 262: 5576-5580.
204. Schmid, M. C., S. Q. Khan, M. M. Kaneda, P. Pathria, R. Shepard, T. L. Louis, S. Anand, G. Woo, C. Leem, M. H. Faridi, T. Geraghty, A. Rajagopalan, S. Gupta, M. Ahmed, R. I. Vazquez-Padron, D. A. Cheresh, V. Gupta, and J. A. Varner. 2018. Integrin CD11b activation drives anti-tumor innate immunity. *Nat Commun* 9: 5379.
205. Pearce, N. J., J. W. Yates, T. A. Berkhout, B. Jackson, D. Tew, H. Boyd, P. Camilleri, P. Sweeney, A. D. Gribble, A. Shaw, and P. H. Groot. 1998. The role of ATP citrate-lyase in the metabolic regulation of plasma lipids. Hypolipidaemic effects of SB-204990, a lactone prodrug of the potent ATP citrate-lyase inhibitor SB-201076. *Biochem J* 334 (Pt 1): 113-119.
206. Wei, X., J. Shi, Q. Lin, X. Ma, Y. Pang, H. Mao, R. Li, W. Lu, Y. Wang, and P. Liu. 2021. Targeting ACLY Attenuates Tumor Growth and Acquired Cisplatin Resistance in Ovarian Cancer by Inhibiting the PI3K-AKT Pathway and Activating the AMPK-ROS Pathway. *Front Oncol* 11: 642229.
207. Lüscher-Firzlaff, J., N. Chatain, C. C. Kuo, T. Braunschweig, A. Bochyńska, A. Ullius, B. Denecke, I. G. Costa, S. Koschmieder, and B. Lüscher. 2019. Hematopoietic stem and progenitor cell proliferation and differentiation requires the trithorax protein Ash2l. *Sci Rep* 9: 8262.
208. Iemura, A., M. Tsai, A. Ando, B. K. Wershil, and S. J. Galli. 1994. The c-kit ligand, stem cell factor, promotes mast cell survival by suppressing apoptosis. *Am J Pathol* 144: 321-328.
209. Pluznik, D. H., and L. Sachs. 1965. The cloning of normal "mast" cells in tissue culture. *J Cell Physiol* 66: 319-324.
210. Aran, D., A. P. Looney, L. Liu, E. Wu, V. Fong, A. Hsu, S. Chak, R. P. Naikawadi, P. J. Wolters, A. R. Abate, A. J. Butte, and M. Bhattacharya. 2019. Reference-based analysis of lung single-cell sequencing reveals a transitional profibrotic macrophage. In *Nature Immunology 2019 20:2*. Nature Publishing Group. 163-172.
211. Heng, T. S. P., M. W. Painter, K. Elpek, V. Lukacs-Kornek, N. Mauermann, S. J. Turley, D. Koller, F. S. Kim, A. J. Wagers, N. Asinovski, S. Davis, M. Fassett, M. Feuerer, D. H. D. Gray, S. Haxhinasto, J. A. Hill, G. Hyatt, C. Laplace, K. Leatherbee, D. Mathis, C. Benoist, R. Jianu, D. H. Laidlaw, J. A. Best, J. Knell, A. W. Goldrath, J. Jarjoura, J. C. Sun, Y. Zhu, L. L. Lanier, A. Ergun, Z. Li, J. J. Collins, S. A. Shinton, R. R. Hardy, R. Friedline, K. Sylvia, and J. Kang. 2008. The Immunological Genome Project: networks of gene expression in immune cells. *Nature Immunology* 9: 1091-1094.
212. Muench, D. E., A. Olsson, K. Ferchen, G. Pham, R. A. Serafin, S. Chutipongtanate, P. Dwivedi, B. Song, S. Hay, K. Chetal, L. R. Trump-Durbin, J. Mookerjee-Basu, K. Zhang,

J. C. Yu, C. Lutzko, K. C. Myers, K. L. Nazor, K. D. Greis, D. J. Kappes, S. S. Way, N. Salomonis, and H. L. Grimes. 2020. Mouse models of neutropenia reveal progenitor-stage-specific defects. *Nature* 582: 109-114.

213. Yashiro, T., M. Yamamoto, S. Araumi, M. Hara, K. Yogo, K. Uchida, K. Kasakura, and C. Nishiyama. 2021. PU.1 and IRF8 Modulate Activation of NLRP3 Inflammasome via Regulating Its Expression in Human Macrophages. *Front Immunol* 12: 649572.
214. Kikuchi, K., M. Iida, N. Ikeda, S. Moriyama, M. Hamada, S. Takahashi, H. Kitamura, T. Watanabe, Y. Hasegawa, K. Hase, T. Fukuhara, H. Sato, E. H. Kobayashi, T. Suzuki, M. Yamamoto, M. Tanaka, and K. Asano. 2018. Macrophages Switch Their Phenotype by Regulating Maf Expression during Different Phases of Inflammation. *The Journal of Immunology* 201: 635-651.
215. Cuevas, V. D., L. Anta, R. Samaniego, E. Orta-Zavalza, J. Vladimir De La Rosa, G. Baujat, Á. Domínguez-Soto, P. Sánchez-Mateos, M. M. Escribese, A. Castrillo, V. Cormier-Daire, M. A. Vega, and Á. L. Corbí. 2017. MAFB Determines Human Macrophage Anti-Inflammatory Polarization: Relevance for the Pathogenic Mechanisms Operating in Multicentric Carpotarsal Osteolysis. *The Journal of Immunology* 198: 2070-2081.
216. Granja, J. M., M. R. Corces, S. E. Pierce, S. T. Bagdatli, H. Choudhry, H. Y. Chang, and W. J. Greenleaf. 2021. ArchR is a scalable software package for integrative single-cell chromatin accessibility analysis. In *Nature genetics*. Nat Genet. 403-411.
217. Liguori, M., E. Digifico, A. Vacchini, R. Avigni, F. S. Colombo, E. M. Borroni, F. M. Farina, S. Milanesi, A. Castagna, L. Mannarino, I. Craparotta, S. Marchini, E. Erba, N. Panini, M. Tamborini, V. Rimoldi, P. Allavena, and C. Belgiovine. 2021. The soluble glycoprotein NMB (GPNMB) produced by macrophages induces cancer stemness and metastasis via CD44 and IL-33. *Cellular & Molecular Immunology* 18: 711-722.
218. Zhou, L., H. Zhuo, H. Ouyang, Y. Liu, F. Yuan, L. Sun, F. Liu, and H. Liu. 2017. Glycoprotein non-metastatic melanoma protein b (Gpnmb) is highly expressed in macrophages of acute injured kidney and promotes M2 macrophages polarization. *Cell Immunol* 316: 53-60.
219. Gombart, A. F., S. H. Kwok, K. L. Anderson, Y. Yamaguchi, B. E. Torbett, and H. P. Koeffler. 2003. Regulation of neutrophil and eosinophil secondary granule gene expression by transcription factors C/EBP epsilon and PU.1. *Blood* 101: 3265-3273.
220. Wang, W., X. Xia, L. Mao, and S. Wang. 2019. The CCAAT/Enhancer-Binding Protein Family: Its Roles in MDSC Expansion and Function. *Front Immunol* 10: 1804.
221. Shyamsunder, P., M. Shanmugasundaram, A. Mayakonda, P. Dakle, W. W. Teoh, L. Han, D. Kanojia, M. C. Lim, M. Fullwood, O. An, H. Yang, J. Shi, M. Z. Hossain, V. Madan, and H. P. Koeffler. 2019. Identification of a novel enhancer of CEBPE essential for granulocytic differentiation. In *Blood*. Blood. 2507-2517.
222. Osada, S., H. Yamamoto, T. Nishihara, and M. Imagawa. 1996. DNA binding specificity of the CCAAT/enhancer-binding protein transcription factor family. *J Biol Chem* 271: 3891-3896.
223. Bitto, A., N. Tatom, T. Krivak, P. Grotz, and M. Kaeberlein. 2021. Evidence that C/EBP-β LAP Increases Fat Metabolism and Protects Against Diet-Induced Obesity in Response to mTOR Inhibition. *Frontiers in Aging* 2.
224. Olofsson, L. E., M. Orho-Melander, L. William-Olsson, K. Sjöholm, L. Sjöström, L. Groop, B. Carlsson, L. M. Carlsson, and B. Olsson. 2008. CCAAT/enhancer binding protein alpha (C/EBPalpha) in adipose tissue regulates genes in lipid and glucose metabolism and a genetic variation in C/EBPalpha is associated with serum levels of triglycerides. *J Clin Endocrinol Metab* 93: 4880-4886.
225. Puleston, D. 2015. Detection of Mitochondrial Mass, Damage, and Reactive Oxygen Species by Flow Cytometry. *Cold Spring Harb Protoc* 2015: pdb.prot086298.

226. Huang, Z., M. Zhang, A. A. Plec, S. J. Estill, L. Cai, J. J. Repa, S. L. McKnight, and B. P. Tu. 2018. ACSS2 promotes systemic fat storage and utilization through selective regulation of genes involved in lipid metabolism. *Proc Natl Acad Sci U S A* 115: E9499-e9506.
227. Gbotosho, O. T., M. G. Kapetanaki, M. Ross, S. Ghosh, F. Weidert, G. C. Bullock, S. Watkins, S. F. Ofori-Acquah, and G. J. Kato. 2020. Nrf2 deficiency in mice attenuates erythropoietic stress-related macrophage hypercellularity. *Exp Hematol* 84: 19-28.e14.
228. Chiba, A., N. Kawabata, M. Yamaguchi, S. Tokonami, and I. Kashiwakura. 2020. Regulation of Antioxidant Stress-Responsive Transcription Factor Nrf2 Target Gene in the Reduction of Radiation Damage by the Thrombocytopenia Drug Romiplostim. *Biol Pharm Bull* 43: 1876-1883.
229. Tsai, J. J., J. A. Dudakov, K. Takahashi, J. H. Shieh, E. Velardi, A. M. Holland, N. V. Singer, M. L. West, O. M. Smith, L. F. Young, Y. Shono, A. Ghosh, A. M. Hanash, H. T. Tran, M. A. Moore, and M. R. van den Brink. 2013. Nrf2 regulates haematopoietic stem cell function. *Nat Cell Biol* 15: 309-316.
230. Sun, J., S. Aluvila, R. Kotaria, J. A. Mayor, D. E. Walters, and R. S. Kaplan. 2010. Mitochondrial and Plasma Membrane Citrate Transporters: Discovery of Selective Inhibitors and Application to Structure/Function Analysis. *Mol Cell Pharmacol* 2: 101-110.
231. Cabal-Hierro, L., P. van Galen, M. A. Prado, K. J. Higby, K. Togami, C. T. Mowery, J. A. Paulo, Y. Xie, P. Cejas, T. Furusawa, M. Bustin, H. W. Long, D. B. Sykes, S. P. Gygi, D. Finley, B. E. Bernstein, and A. A. Lane. 2020. Chromatin accessibility promotes hematopoietic and leukemia stem cell activity. *Nat Commun* 11: 1406.
232. Sun, X. J., N. Man, Y. Tan, S. D. Nimer, and L. Wang. 2015. The Role of Histone Acetyltransferases in Normal and Malignant Hematopoiesis. In *Frontiers in oncology*. Front Oncol.
233. Baardman, J., S. G. S. Verberk, S. van der Velden, M. J. J. Gijbels, C. P. P. A. van Roomen, J. C. Sluimer, J. Y. Broos, G. R. Griffith, K. H. M. Prange, M. van Weeghel, S. Lakbir, D. Molenaar, E. Meinster, A. E. Neele, G. Kooij, H. E. de Vries, E. Lutgens, K. E. Wellen, M. P. J. de Winther, and J. Van den Bossche. 2020. Macrophage ATP citrate lyase deficiency stabilizes atherosclerotic plaques. In *Nature Communications 2020 11:1*. Nature Publishing Group. 1-15.
234. Wang, J., W. Ye, X. Yan, Q. Guo, Q. Ma, F. Lin, J. Huang, and J. Jin. 2019. Low expression of ACLY associates with favorable prognosis in acute myeloid leukemia. *J Transl Med* 17: 149.
235. Bradley, T. R., and D. Metcalf. 1966. The growth of mouse bone marrow cells in vitro. *Aust J Exp Biol Med Sci* 44: 287-299.
236. Nakahata, T., S. S. Spicer, J. R. Cantey, and M. Ogawa. 1982. Clonal assay of mouse mast cell colonies in methylcellulose culture. *Blood* 60: 352-361.
237. Ogawa, M., R. T. Parmley, H. L. Bank, and S. S. Spicer. 1976. Human marrow erythropoiesis in culture. I. Characterization of methylcellulose colony assay. *Blood* 48: 407-417.
238. Wang, T., B. Glover, G. Hadwiger, C. A. Miller, O. di Martino, and J. S. Welch. 2019. Smc3 is required for mouse embryonic and adult hematopoiesis. *Exp Hematol* 70: 70-84.e76.
239. Velier, M., A. L. Chateau, C. Malenfant, S. Ouffai, B. Calmels, C. Chabannon, and C. Lemarié. 2019. Validation of a semi automatic device to standardize quantification of Colony-Forming Unit (CFU) on hematopoietic stem cell products. *Cytotherapy* 21: 820-823.
240. Miller, C. L., and B. Lai. 2005. Human and mouse hematopoietic colony-forming cell assays. *Methods Mol Biol* 290: 71-89.

241. Sarma, N. J., A. Takeda, and N. R. Yaseen. 2010. Colony forming cell (CFC) assay for human hematopoietic cells. *J Vis Exp*.
242. Cluntun, A. A., H. Huang, L. Dai, X. Liu, Y. Zhao, and J. W. Locasale. 2015. The rate of glycolysis quantitatively mediates specific histone acetylation sites. *Cancer Metab* 3: 10.
243. Sidoli, S., S. Trefely, B. A. Garcia, and A. Carrer. 2019. Integrated Analysis of Acetyl-CoA and Histone Modification via Mass Spectrometry to Investigate Metabolically Driven Acetylation. *Methods Mol Biol* 1928: 125-147.
244. Zhang, T., X. Niu, L. Liao, E. A. Cho, and H. Yang. 2013. The contributions of HIF-target genes to tumor growth in RCC. *PLoS One* 8: e80544.
245. Xu, W., X. Jiang, C. Guan, and M. Gu. 2020. The prognostic and predictive value of tumor infiltrating Macrophage and Neutrophil in patient with clear cell renal cell carcinoma: Tumor infiltrating lymphocytes in renal cell carcinoma. *Medicine (Baltimore)* 99: e23181.
246. Borcherding, N., A. Vishwakarma, A. P. Voigt, A. Bellizzi, J. Kaplan, K. Nepple, A. K. Salem, R. W. Jenkins, Y. Zakharia, and W. Zhang. 2021. Mapping the immune environment in clear cell renal carcinoma by single-cell genomics. *Communications Biology* 4.
247. Xu, J. X., V. E. Maher, L. Zhang, S. Tang, R. Sridhara, A. Ibrahim, G. Kim, and R. Pazdur. 2017. FDA Approval Summary: Nivolumab in Advanced Renal Cell Carcinoma After Anti-Angiogenic Therapy and Exploratory Predictive Biomarker Analysis. *Oncologist* 22: 311-317.
248. Yang, J. C., M. Hughes, U. Kammula, R. Royal, R. M. Sherry, S. L. Topalian, K. B. Suri, C. Levy, T. Allen, S. Mavroukakis, I. Lowy, D. E. White, and S. A. Rosenberg. 2007. Ipilimumab (anti-CTLA4 antibody) causes regression of metastatic renal cell cancer associated with enteritis and hypophysitis. *J Immunother* 30: 825-830.
249. Sheng, I. Y., and M. C. Ornstein. 2020. Ipilimumab and Nivolumab as First-Line Treatment of Patients with Renal Cell Carcinoma: The Evidence to Date. *Cancer Manag Res* 12: 4871-4881.
250. Geissler, K., P. Fornara, C. Lautenschläger, H. J. Holzhausen, B. Seliger, and D. Riemann. 2015. Immune signature of tumor infiltrating immune cells in renal cancer. *Oncoimmunology* 4: e985082.
251. Su, S., S. Akbarinejad, and L. Shahriyari. 2021. Immune classification of clear cell renal cell carcinoma. *Sci Rep* 11: 4338.
252. Xu, Y., A. J. Morales, A. M. H. Towlerton, S. Akilesh, C. P. Miller, S. S. Tykodi, and E. H. Warren. 2022. Integrated TCR repertoire analysis and single-cell transcriptomic profiling of tumor-infiltrating T cells in renal cell carcinoma identifies shared and tumor-restricted expanded clones with unique phenotypes. *Front Oncol* 12: 952252.
253. Scharping, N. E., A. V. Menk, R. S. Moreci, R. D. Whetstone, R. E. Dadey, S. C. Watkins, R. L. Ferris, and G. M. Delgoffe. 2016. The Tumor Microenvironment Represses T Cell Mitochondrial Biogenesis to Drive Intratumoral T Cell Metabolic Insufficiency and Dysfunction. *Immunity* 45: 374-388.
254. Sukumar, M., J. Liu, G. U. Mehta, S. J. Patel, R. Roychoudhuri, J. G. Crompton, C. A. Klebanoff, Y. Ji, P. Li, Z. Yu, G. D. Whitehill, D. Clever, R. L. Eil, D. C. Palmer, S. Mitra, M. Rao, K. Keyvanfar, D. S. Schrump, E. Wang, F. M. Marincola, L. Gattinoni, W. J. Leonard, P. Muranski, T. Finkel, and N. P. Restifo. 2016. Mitochondrial Membrane Potential Identifies Cells with Enhanced Stemness for Cellular Therapy. *Cell Metab* 23: 63-76.
255. Li, C., Y. P. Phoon, K. Karlinsey, Y. F. Tian, S. Thapaliya, A. Thongkum, L. Qu, A. J. Matz, M. Cameron, C. Cameron, A. Menoret, P. Funchain, J. M. Song, C. M. Diaz-Montero, B. Tamilselvan, J. B. Golden, M. Cartwright, A. Rodriguez, C. Bonin, A. Vella,

B. Zhou, and B. R. Gastman. 2022. A high OXPHOS CD8 T cell subset is predictive of immunotherapy resistance in melanoma patients. *J Exp Med* 219.
256. Siska, P. J., K. E. Beckermann, F. M. Mason, G. Andrejeva, A. R. Greenplate, A. B. Sendor, Y. J. Chiang, A. L. Corona, L. F. Gemta, B. G. Vincent, R. C. Wang, B. Kim, J. Hong, C. L. Chen, T. N. Bullock, J. M. Irish, W. K. Rathmell, and J. C. Rathmell. 2017. Mitochondrial dysregulation and glycolytic insufficiency functionally impair CD8 T cells infiltrating human renal cell carcinoma. *JCI Insight* 2.
257. Diggins, K. E., A. R. Greenplate, N. Leelatian, C. E. Wogsland, and J. M. Irish. 2017. Characterizing cell subsets using marker enrichment modeling. *Nat Methods* 14: 275-278.
258. Barone, S. M., A. G. Paul, L. M. Muehling, J. A. Lannigan, W. W. Kwok, R. B. Turner, J. A. Woodfolk, and J. M. Irish. 2021. Unsupervised machine learning reveals key immune cell subsets in COVID-19, rhinovirus infection, and cancer therapy. *eLife* 10.
259. Wei, Y. Y., J. Fan, M. X. Shan, D. D. Yin, L. L. Wang, W. Ye, and W. Zhao. 2022. TIGIT marks exhausted T cells and serves as a target for immune restoration in patients with chronic HBV infection. *Am J Transl Res* 14: 942-954.
260. Cretenet, G., I. Clerc, M. Matias, S. Loisel, M. Craveiro, L. Oburoglu, S. Kinet, C. Mongellaz, V. Dardalhon, and N. Taylor. 2016. Cell surface Glut1 levels distinguish human CD4 and CD8 T lymphocyte subsets with distinct effector functions. *Sci Rep* 6: 24129.
261. Brown, Z. J., Q. Fu, C. Ma, M. Kruhlak, H. Zhang, J. Luo, B. Heinrich, S. J. Yu, Q. Zhang, A. Wilson, Z. D. Shi, R. Swenson, and T. F. Greten. 2018. Carnitine palmitoyltransferase gene upregulation by linoleic acid induces CD4(+) T cell apoptosis promoting HCC development. *Cell Death Dis* 9: 620.
262. Yang, Y., L. Cheng, X. Deng, H. Yu, and L. Chao. 2018. Expression of GRIM-19 in unexplained recurrent spontaneous abortion and possible pathogenesis. *Mol Hum Reprod* 24: 366-374.
263. Hou, X., G. Wang, W. Fan, X. Chen, C. Mo, Y. Wang, W. Gong, X. Wen, H. Chen, D. He, L. Mo, S. Jiang, M. Ou, H. Guo, and H. Liu. 2021. T-cell receptor repertoires as potential diagnostic markers for patients with COVID-19. *Int J Infect Dis* 113: 308-317.
264. Mark, M., S. Reich-Zeliger, E. Greenstein, D. Reshef, A. Madi, B. Chain, and N. Friedman. 2022. A hierarchy of selection pressures determines the organization of the T cell receptor repertoire. *Front Immunol* 13: 939394.
265. Xie, X., T. Venit, N. Drou, and P. Percipalle. 2018. In Mitochondria ?-Actin Regulates mtDNA Transcription and Is Required for Mitochondrial Quality Control. *iScience* 3: 226-237.
266. Paulsen, M., S. Valentin, B. Mathew, S. Adam-Klages, U. Bertsch, I. Lavrik, P. H. Krammer, D. Kabelitz, and O. Janssen. 2011. Modulation of CD4+ T-cell activation by CD95 co-stimulation. *Cell Death Differ* 18: 619-631.
267. Kurtulus, S., K. Sakuishi, S. F. Ngiow, N. Joller, D. J. Tan, M. W. Teng, M. J. Smyth, V. K. Kuchroo, and A. C. Anderson. 2015. TIGIT predominantly regulates the immune response via regulatory T cells. *J Clin Invest* 125: 4053-4062.
268. McKenna, E., A. U. Mhaonaigh, R. Wubben, A. Dwivedi, T. Hurley, L. A. Kelly, N. J. Stevenson, M. A. Little, and E. J. Molloy. 2021. Neutrophils: Need for Standardized Nomenclature. *Front Immunol* 12: 602963.
269. Huang, B., R. Liu, P. Wang, Z. Yuan, J. Yang, H. Xiong, N. Zhang, Q. Huang, X. Fu, W. Sun, and L. Li. 2020. CD8(+)CD57(+) T cells exhibit distinct features in human non-small cell lung cancer. *J Immunother Cancer* 8.
270. Phetsouphanh, C., D. Aldridge, E. Marchi, C. M. L. Munier, J. Meyerowitz, L. Murray, C. Van Vuuren, D. Goedhals, S. Fidler, A. Kelleher, P. Klenerman, and J. Frater. 2019.

Maintenance of Functional CD57+ Cytolytic CD4+ T Cells in HIV+ Elite Controllers. *Front Immunol* 10: 1844.
271. Tiberti, S., C. Catozzi, O. Croci, M. Ballerini, D. Cagnina, C. Soriani, C. Scirgolea, Z. Gong, J. He, A. D. Macandog, A. Nabinejad, C. B. Nava Lauson, A. Quinte, G. Bertalot, W. L. Petz, S. P. Ravenda, V. Licursi, P. Paci, M. Rasponi, L. Rotta, N. Fazio, G. Ren, U. Fumagalli-Romario, M. H. Schaefer, S. Campaner, E. Lugli, L. Nezi, and T. Manzo. 2022. GZMK(high) CD8(+) T effector memory cells are associated with CD15(high) neutrophil abundance in non-metastatic colorectal tumors and predict poor clinical outcome. *Nat Commun* 13: 6752.
272. Bertrand, F., J. Rochotte, C. Colacios, A. Montfort, A. F. Tilkin-Mariamé, C. Touriol, P. Rochaix, I. Lajoie-Mazenc, N. Andrieu-Abadie, T. Levade, H. Benoist, and B. Ségui. 2015. Blocking Tumor Necrosis Factor α Enhances CD8 T-cell-Dependent Immunity in Experimental Melanoma. *Cancer Res* 75: 2619-2628.
273. Mogilenko, D. A., O. Shpynov, P. S. Andhey, L. Arthur, A. Swain, E. Esaulova, S. Brioschi, I. Shchukina, M. Kerndl, M. Bambouskova, Z. Yao, A. Laha, K. Zaitsev, S. Burdess, S. Gillfilan, S. A. Stewart, M. Colonna, and M. N. Artyomov. 2021. Comprehensive Profiling of an Aging Immune System Reveals Clonal GZMK(+) CD8(+) T Cells as Conserved Hallmark of Inflammaging. *Immunity* 54: 99-115.e112.
274. Zhang, J. A., X. Y. Zhou, D. Huang, C. Luan, H. Gu, M. Ju, and K. Chen. 2020. Development of an Immune-Related Gene Signature for Prognosis in Melanoma. *Front Oncol* 10: 602555.
275. Pauken, K. E., O. Shahid, K. A. Lagattuta, K. M. Mahuron, J. M. Luber, M. M. Lowe, L. Huang, C. Delaney, J. M. Long, M. E. Fung, K. Newcomer, K. K. Tsai, M. Chow, S. Guinn, J. R. Kuchroo, K. P. Burke, J. M. Schenkel, M. D. Rosenblum, A. I. Daud, A. H. Sharpe, and M. Singer. 2021. Single-cell analyses identify circulating anti-tumor CD8 T cells and markers for their enrichment. *Journal of Experimental Medicine* 218.
276. Satija, R., J. A. Farrell, D. Gennert, A. F. Schier, and A. Regev. 2015. Spatial reconstruction of single-cell gene expression data. In *Nature biotechnology*. Nat Biotechnol. 495-502.
277. Stuart, T., A. Butler, P. Hoffman, C. Hafemeister, E. Papalexi, W. M. Mauck, 3rd, Y. Hao, M. Stoeckius, P. Smibert, and R. Satija. 2019. Comprehensive Integration of Single-Cell Data. *Cell* 177: 1888-1902 e1821.
278. Auguie, B. 2017. gridExtra: Miscellaneous Functions for "Grid" Graphics.
279. Wickham, H. 2016. *Elegant Graphics for Data Analysis*. Springer-Verlag.
280. Ren, K., and K. Russell. 2021. formattable: Create 'Formattable' Data Structures.
281. Pedersen, T. L. 2020. pathwork: The Composer of Plots.
282. Wickham, H., R. Francois, L. Henry, and K. Müller. 2021. dplyr: A Grammar of Data Manipulation.
283. Hafemeister, C., and R. Satija. 2019. Normalization and variance stabilization of single-cell RNA-seq data using regularized negative binomial regression. *Genome Biology* 20.
284. Lawrence, M., W. Huber, H. Pagès, P. Aboyoun, M. Carlson, R. Gentleman, M. T. Morgan, and V. J. Carey. 2013. Software for Computing and Annotating Genomic Ranges. *PLoS Computational Biology* 9: e1003118.
285. Ushey, K., J. Allaire, and Y. Tang. 2021. reticulate: Interface to 'Python'.
286. Hoffman, P., and R. Satija. 2018. loomR: An R interface for loom files.
287. McCarthy, D. J., K. R. Campbell, A. T. L. Lun, and Q. F. Wills. 2017. Scater: pre-processing, quality control, normalization and visualization of single-cell RNA-seq data in R. *Bioinformatics*: btw777.
288. Kolde, R. 2019. pheatmap: Pretty Heatmaps.
289. Risso, D., and M. Cole. 2020. scRNAseq: Collection of Public Single-Cell RNA-Seq Datasets.

290. Wickham, H. 2019. stringr: Simple, Consistent Wrappers for Common String Operations.
291. Wickham, H. 2011. The Split-Apply-Combine Strategy for Data Analysis. *Journal of Statistical Software* 40: 1 - 29.
292. Wickham, H., and D. Seidel. 2020. scales: Scale Functions for Visualization.
293. Wickham, H., J. Hester, and W. Chang. 2021. devtools: Tools to Make Developing R Packages Easier.
294. Eddelbuettel, D., and R. Francois. 2011. Rcpp: Seamless R and C++ Integration. *Journal of Statistical Software* 40: 1 - 18.
295. Eddelbuettel, D. 2013. *Seamless R and C++ Integration with Rcpp*. Springer.
296. Eddelbuettel, D., and J. J. Balamuta. 2018. Extending R with C++: A Brief Introduction to Rcpp. *The American Statistician* 72: 28-36.
297. Korsunsky, I., A. Nathan, N. Millard, and S. Raychaudhuri. 2020. presto: Fast Functions for Differential Expression using Wilcox and AUC.
298. Dolgaley, I. 2021. msigdbr: MSigDB Gene Sets for Multiple Organisms in a Tidy Data Format.
299. Korotkevich, G., V. Sukhov, N. Budin, B. Shpak, M. N. Artyomov, and A. Sergushichev. 2016. Fast gene set enrichment analysis. Cold Spring Harbor Laboratory.
300. Morgan, M. T., V. Obenchain, J. Hester, and H. Pagès. 2020. SummarizedExperiment: SummarizedExperiment container.
301. Schep, A. 2020. chromVARmotifs: Stores motifs as PWMatrixList objects.
302. Liao, F. H., J. W. Shui, E. W. Hsing, W. Y. Hsiao, Y. C. Lin, Y. C. Chan, T. H. Tan, and C. Y. Huang. 2014. Protein phosphatase 4 is an essential positive regulator for Treg development, function, and protective gut immunity. In *Cell & Bioscience*. BioMed Central. 25.
303. Lai, J., S. Jiang, L. Shuai, Y. Zhang, R. Xia, Q. Chen, and L. Bai. 2021. Comparison of the biological and functional characteristics of mesenchymal stem cells from intrahepatic and identical bone marrow. *Stem Cell Research* 55: 102477.
304. Jasaszwili, M., T. Wojciechowicz, M. Z. Strowski, K. W. Nowak, and M. Skrzypski. 2021. The effects of neuronostatin on proliferation and differentiation of rat primary preadipocytes and 3T3-L1 cells. *Biochimica et Biophysica Acta (BBA) - Molecular and Cell Biology of Lipids* 1866: 159018.
305. Benchamana, A., H. Mori, O. A. Macdougald, and S. Soodvilai. 2019. Regulation of adipocyte differentiation and metabolism by lansoprazole. *Life Sciences* 239: 116897.
306. Team, I. 2022. Immunarch Version 0.8.0: an R package for painless bioinformatics analysis of T-cell and B-cell immune repertoires. *Zenodo*.
307. Kramer, K. J., E. M. Wilfong, K. Voss, S. M. Barone, A. R. Shiakolas, N. Raju, C. E. Roe, N. Suryadevara, L. M. Walker, S. C. Wall, A. Paulo, S. Schaefer, D. Dahunsi, C. S. Westlake, J. E. Crowe, Jr., R. H. Carnahan, J. C. Rathmell, R. H. Bonami, I. S. Georgiev, and J. M. Irish. 2022. Single-cell profiling of the antigen-specific response to BNT162b2 SARS-CoV-2 RNA vaccine. *Nat Commun* 13: 3466.
308. Irish, J. M., J. H. Myklebust, A. A. Alizadeh, R. Houot, J. P. Sharman, D. K. Czerwinski, G. P. Nolan, and R. Levy. 2010. B-cell signaling networks reveal a negative prognostic human lymphoma cell subset that emerges during tumor progression. *Proc Natl Acad Sci U S A* 107: 12747-12754.
309. Becker, R. A., J. M. Chambers, and A. R. Wilks. 1988. *The New S Language: A Programming Environment for Data Analysis and Graphics*. Wadsworth & Brooks/Cole Advanced Books & Software.